Schweizerische Eidgenossenschaft
Confédération suisse
Confederazione Svizzera
Confederaziun svizra

Federal Department of the Environment, Transport,
Energy and Communications DETEC

Swiss Federal Office of Energy SFOE
Energy Research and Cleantech

Final report dated 29.2.2020

Semi-autonomous DC-microgrid for industrial sites with predicted precise smooth power profile for very high penetration of renewable energy (>50% of total consumption)

Source: ©HES-SO 2020

Date: 29.2.2020

Location: Bern

Publisher:
Swiss Federal Office of Energy SFOE
Energy Research and Cleantech
CH-3003 Bern
www.bfe.admin.ch

Co-financing:

Energy Sion Region ESR
Rue de l'Industrie 43
1951 Sion
https://www.esr.ch/fr/

Force Motrice Valaisanne FMV
Rue de la Dixence 9
CH-1951 Sion
https://www.fmv.ch/de/

EOS Holding
Chemin de Mornex 6
CH-1003 Lausanne
http://eosholding.ch/fr/

Fondation The Ark
Route de Rawyl 47
CH-1950 Sion
https://www.theark.ch/fr/

Subsidy recipients:
HESSO Valais-Wallis, ISI, Route de Rawil 47, CH-1950 Sion
www.hevs.ch

Imperix SA, Rue de la Dixence 10, 1950 Sion

Studer Innotec SA, Rue des Casernes 57, 1950 Sion

EPFL/STI /IMT, Rue de la Maladière 71B, 2002 Neuchatel

EPFL / LMER /ISIC, Rue de l'Industrie 17, 1951 Sion

HEIG-Vd, IESE Route de Cheseaux 1, 1401 Yverdon-les-Bains

HES-SO Genève, HEPIA, Rue de la Prairie 4, 1202 Genève

Institut de recherche Icare, eEnergy Center, Technopole, 3960 Sierre

Authors:
Christoph Ellert, Dominique Roggo, Thomas Sterren, Didier Blatter, HESSO Valais-Wallis, ISI, christoph.ellert@hevs.ch
Thebti Mohamed Bechir, Elena-Lavinia Niederhäuser, HEIA-Fr, MohamedBechir.Thebti@hefr.ch
Jordan Holweger, EPFL/STI/IMT, jordan.holweger@epfl.ch
Gaetan Wuilloud, Christopher Finelli, Institut icare, wuilloud@icare.ch
Simon Delalay, Imperix SA, simon.delalay@imperix.ch
Alan Lauraux, Stéphane Genoud, HESSO Valais, HEG, alan.lauraux@hevs.ch

SFOE project coordinators:
Jerôme Rampazzo, replaced by
Karin Soederstroem, Karin.Soederstroem@bfe.admin.ch

SFOE contract number: SI/501512-01

The authors bear the entire responsibility for the content of this report and for the conclusions drawn therefrom.

Zusammenfassung

Während dieses Demonstrationsprojektes wurde ein funktionierendes DC-microgrid mit allen relevanten Funktionalitäten, wie sie für Anwendungen im industriellen Umfeld sowohl qualitativ als auch quantitativ erforderlich sind, aufgebaut. Eine Vielzahl solcher DC-microgrids könnte eine netzfreundliche Integration stark variabler erneuerbarer Energiequellen (z.B. Photovoltaik) bis zu einem Anteil der erneuerbaren Energie von über 50% des jährlichen Gesamtenergieverbrauchs vereinfachen und damit den Ausbau der Übertragungsnetze weniger dringlich bzw. überflüssig machen. Die potentiellen Vorteile von DC-microgrids in technischer als auch in wirtschaftlicher Hinsicht werden diskutiert.

Für den Aufbau dieses Demonstrators wurden alle notwendigen Komponenten überwiegend selbst entwickelt, die kommerziellen Komponenten funktionell angepasst, sowie die Regelalgorithmen und Kommunikationsschnittstellen implementiert. Aufbauend darauf wurden Möglichkeiten einer Kommerzialisierung ermittelt und initiiert. Das DC-microgrid ist funktionell seit 2015, die Entwicklungen und Erweiterungen wurden am laufenden Demonstrator vorgenommen. Dadurch konnte die Zuverlässigkeit getestet, sowie typische Fehlerquellen und passende Abhilfen identifiziert werden. Besonderes Letzteres ist für zukünftige Umsetzungen im industriellen Umfeld wichtig, um eine fehlerfreie oder -tolerante Funktion zu gewährleisten.

Résumé

Pendant ce projet de démonstration un micro-réseau en courant continu fonctionnel a été réalisé. Ce dernier intègre quantitativement et qualitativement toutes les fonctionnalités nécessaires à un environnement industriel. Une multitude de micro-réseaux en courant continu de ce type pourrait, selon nos calculs, faciliter l'intégration de sources d'énergie renouvelables très variables (par exemple, le photovoltaïque) dans le réseau de distribution, jusqu'à une part d'énergie renouvelable supérieure à 50% de la consommation annuelle totale d'énergie. Cela pourrais rendre l'expansion des réseaux de transport moins urgente voire superflue. La faisabilité ainsi que les avantages potentiels d'un micro-réseau à courant continu, tant sur le plan technique qu'économique, sont discutés.

Pour la mise en place de ce démonstrateur, tous les composants nécessaires ont été développés ou adaptés et les algorithmes de contrôle et les interfaces de communication entre les équipements ont été implémentés. Sur cette base, des possibilités de commercialisation ont été identifiées et lancées. Le microgrid DC est opérationnel depuis 2015, les développements et extensions ont été réalisés pour le démonstrateur actuel. Ainsi, la fiabilité a pu être testée et les sources d'erreurs typiques et les remèdes appropriés ont pu être identifiés. Ce dernier point est particulièrement important pour les applications futures dans un environnement industriel afin de garantir un fonctionnement sans erreur ou tolérant aux défauts de fonctionnement.

Summary

During this demonstration project a permanently operational DC microgrid has been installed with all relevant functionalities required for qualitatively and quantitatively equivalent applications in an industrial environment. A multitude of such DC-microgrids could make a grid-friendly integration of highly variable renewable energy sources (e.g. photovoltaics) easier for a share of renewable energy of more than 50% of the total annual energy consumption and thus potentially making the expansion of

the transmission grids less urgent or superfluous. The potential advantages of a DC-microgrid in technical as well as in economic respect are discussed.

For the implementation of this demonstrator, all necessary components were developed or adapted in their functionality, and the control algorithms and communication interfaces were implemented. Based on this, possibilities for commercialization were identified and initiated. The DC-microgrid has been functional since 2015; the developments and extensions were carried out on the current demonstrator. Thus, the reliability could be tested and typical error sources and suitable remedies identified. The latter is particularly important for future implementations in an industrial environment in order to guarantee error-free or error-tolerant function.

Main findings

- The first demonstrator of a DC-microgrid in Switzerland, which includes all relevant components for efficient sector coupling (electricity, thermal energy, gas and mobility) on a power scale relevant for industrial applications, is permanently operational.
- The technical challenge for the realization of a low voltage DC microgrid is to create a robust controller for the DC bus voltage and an energy management system with multiple prosumers since both depend on the configuration and specific requirements of the application site.
- Simulations with various scenarios show that DC-microgrids could become economically viable with cost reduction of batteries and the introduction of dynamic electricity tariff.
- Our simulations suggest that the introduction of a multitude of microgrids reduces the required regulation power of the distribution grid operator and thus the operational costs.

Contents

Abbreviations

IEC	International Electrotechnical Commission®, Geneva, Switzerland
DC	Direct current, Gleichstrom, courant continu
AC	Alternating current, Wechselstrom
VF	Variable frequency
EMC	Electromagnetic compatibility
EMS	Energy management system
PV	Photovoltaic
LV	Low voltage (in our context all voltages below 1000 Volt)
DGO, DNM	Distribution grid operator or distribution network manager
AFE	Active front end
PEM	Proton exchange membrane = polymer electrolyte membrane
DB	Database
H2	Hydrogen
MPP	Maximum power point
SOC	State of charge (percentage of the nominal capacity of a battery)
SCADA	Supervisory Control and Data Acquisition
c-Si	Cristalline silicon
IBC	Inter-digited back contact cells
HJT	Hetero-junction solar cell
MTBF	Mean time between failures
kW_p	kilowatt-peak, which is the commonly used unit for nominally installed solar power, not to be confused with really generated power at a certain instant of time.
TRL	Technology Readiness Level
STC	Standard Test Conditions: temperature = 25°C, solar spectrum 1.5 AM (air mass), solar irradiance = 1000 W/m^2
ROI	Return of Investment

1 Introduction

1.1 Background information and current situation

The DC-technology is still not well known in the community of the grid operators, since the AC 50 Hz or 60 Hz is evidently dominating the transfer and distribution grids. It is unlikely that this situation will change since the established distribution infrastructure is installed and functioning. However, as the title of the project implies, the DC-microgrids have their advantages in industrial applications where integration of renewable power sources, local storage and the need for efficient variable frequency driven motors will be combined. This is mainly driven by the deployment of decentralized power generation, which poses more and more challenges on the stabilization of the grid infrastructure. A comprehensive introduction and summary of the situation at the time of the start of the project is given in the Technology Report of the IEC in reference [IEC2017].

The DC-technology itself is possible due to the advancement of the power electronics which in turn is made possible by the rise of the silicon switching capabilities in the last decades. The application of the DC-technology in turn is present in localized or even independent (“islanded”) electric environments, like electric cars, battle ships, datacentres, etc. where an introduction of AC voltage supply will be of no benefit. It is important to remember, that batteries as local power supplies or storage elements, various consumers (computers, LEDs) and variable frequency driven motors (as they are the majority in mobility applications) are either directly DC-driven or need at least an intermediate DC-voltage for their operation. To this DC-world fits perfectly the PV generator, which provides power at DC-outputs of several hundred volts as well. Thus, the step from independent localized DC-networks in mobility applications to stationary DC-microgrids in industrial environments, which are dominated by DC-consumers (as datacentres) or by VF-driven motors (as in industrial machinery) with integrated PV-generators seems promising for reducing conversion losses and simplifying grid architecture.

The challenges of realizing such a DC-microgrid are:

a) The DC-technology is relatively unknown for distribution grid operator (DGO) and industrial districts, which tend to innovate in terms of energy distribution within their area of operation.

b) Even though individual DC/DC converters are abundant on the market, the proper configuration and the identification of appropriate DC/DC-converters and all required elements is time consuming, since no standard solutions are available yet comparable to the highly standardized AC-technology at 50 (or 60) Hz, see reference [IEC2017].

c) The maturity of the DC-technology is less advanced than for AC-networks, while the requirements for the stability and availability of the electricity distribution within a manufacturing environment are extremely high since blackouts are very costly and must absolutely be avoided.

1.2 Purpose of the project

In view of the opportunities and advantages of the DC-technology on the one hand, and the technical challenges on the other hand, this project aimed at solving some of the latter. Therefore, the aim is to implement an operational DC-microgrid in Switzerland, to serve as a starting point to make this technology better known while providing a flexible platform for operating and testing particular configurations of prosumers in reality before installing the system on a potential site.

While a bare simulation in which unforeseen events never occur, such a test platform which operates continuously over several years is able to demonstrate the potential of the technology and its composing elements for future users.

Because the economic relevance of the technology depends strongly on the market conditions, a part of the project aimed to show the influence of future electricity cost and availability on the return on investment of this technology. Taking into account that the evolution of the electric energy infrastructure and the electricity tariffs are slow to change, this calculation has to look at least 10 years ahead. Finally, the topological effect of a future distribution grid composed of microgrid is also discussed. While this latter section also apply as well to AC-microgrids, the main part of this project refers directly to the DC-technology.

1.3 Objectives

The following objectives were pursued during the project:

1. Setup and operation of a semi-autonomous microgrid, suitable for an industrial production site, based on DC-bus technology which serves as power link between the renewable power generation (here: photovoltaics), local energy storage and consumption of energy, including the link to power-to-gas via electrolysis, while still being linked to the AC-distribution grid.
2. Development of the required power electronics and system components in order to allow full permanent operation and long-term performance evaluation of the DC-microgrid.
3. Development of the required algorithms for power control and an energy management system (EMS) for the microgrid, using a predictive algorithm based on meteorological and load forecasting. The voltage control on a fast time scale within milliseconds assures the stability of the DC-bus system, e.g. that the numerous mono- and bidirectional converters work smoothly together, avoiding voltage oscillations or current loops. The energy management will be decoupled from the voltage control due to a different operating time scale.
4. Smoothing the power exchange (injection and consumption) between the semi-autonomous microgrid and the distribution grid, with (a) 48h-in advance forecast of the time profile of the power exchange, and (b) within a tolerance of 1% between forecasted and real power exchange.
5. Simulation of a superimposed distribution grid consisting of a multitude of such individual semi-autonomous microgrids, based on the assumptions and operational outcome of the demonstrator systems of this project.
6. Economic evaluation of the proposed topology for the semi-autonomous DC-microgrid and the superimposed distribution grid.

2 Description of facility

The DC-microgrid consists of a heterogeneous PV-generator, various storage elements and consumers. The components of the entire system shown in Figure 1 are distributed over several floors in various buildings of the engineering campus of the HESSO Valais in Sion. The total distance spanned by the 700 V DC-power link amounts to more than hundred meters, thus representing a geometrical size, which is relevant for any future application of a DC-microgrid. The DC-voltage of 700 Volt has been chosen such that it is compatible with an upcoming DC-bus voltage standard presently under development in Europe, see section 6 in reference [IEC2017]. Essentially, the DC-bus voltage must allow easy voltage conversion between DC and AC standards, since the main applications of the technology are expected to be in industrial environments in the future, where the AC distribution grid will be nearby.

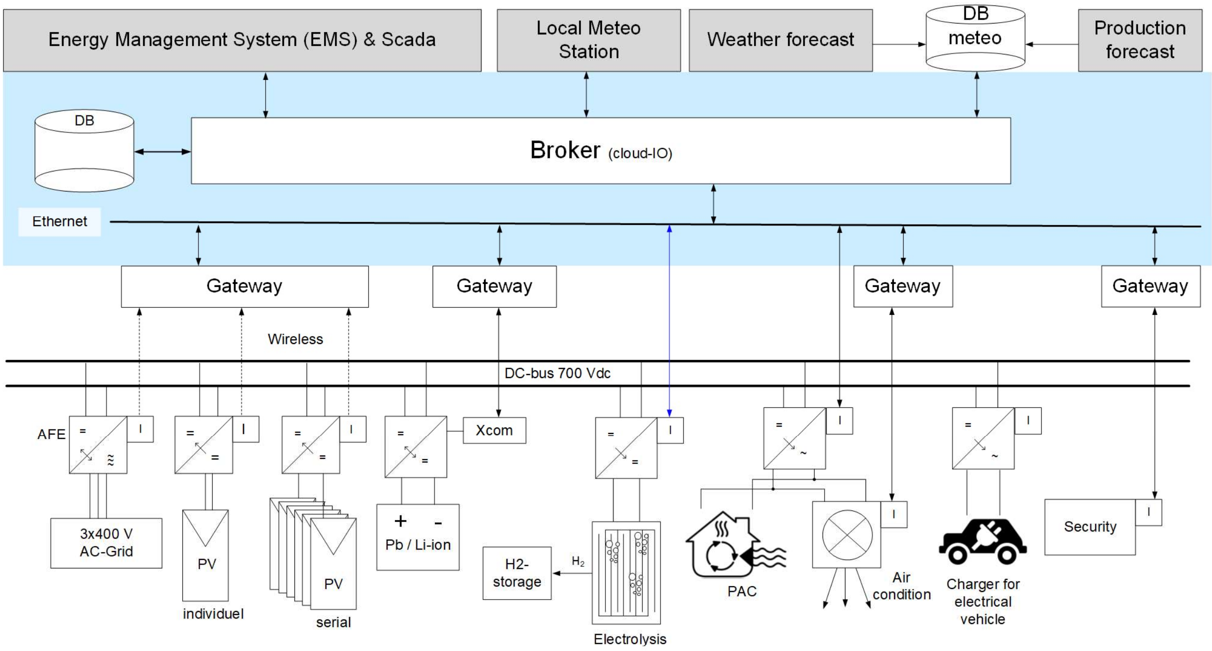

Figure 1: Schematic representation of the DC-microgrid demonstrator implemented at the HESSO Valais. The numerous components are organized in three functional layers: (i) the hardware (consumers, power generation, energy storage elements) on the lower edge of the figure, with their corresponding voltage converter, which establishes the link to the 700V DC-bus (black double line in the centre). (ii) the ICT-system (above the DC-bus), consisting of various gateways and the broker cloud-IO, which guarantees a smooth (wireless or wire based) data exchange between the hardware elements, the data bases and the EMS. (iii) the EMS and the remote elements on the top row, which are entirely device independent.

A coarse description of the facility is given here while details are provided in annex A and section 3. Energy can enter the microgrid either from the PV-generator or via the DC/AC interface, generally referred to as active front end (AFE). Short-term energy storage is possible by integrating various battery systems, based either on Lithium ion or on lead-acid technology. Long-term energy storage is integrated via DC/DC power conversion for driving a PEM electrolyser. The generated renewable hydrogen can be stored in form of metal-hydrides. Various consumers act as loads on the DC-bus: a charging station for electric vehicles, a standard air conditioning system of 1.2 kW electrical power, a heat pump of about 2 kW electric power, and an innovative device for time shifting the heat flow via a thermal energy storage system based on phase change materials. The main consumer of electricity in this device is the ventilation system of about 500 Watt.

All mentioned hardware applications require appropriate converters, compatible with their respective characteristics on the appliance side as well as to the DC-bus specifications in order to inject or extract power from the DC-bus. These converters were developed according to the requirements (both, in terms of power and communication capabilities) during the project, see details in annex B.

The data exchange between the components and the central energy management system (EMS) is standardized by means of gateways as indicated in *Figure 1*. A proprietary data broker system, developed at the HESSO Valais named cloud-IO permits any EMS reading and writing independent of the type of equipment connected to the system. This standardization will allow in the future connecting any type of hardware to the grid as well as programming any type of energy balancing or EMS that may be implemented to be tested, while only the cloud-IO exchange permission must be attributed.

The control system must fulfill various objectives and has thus been handled in two different ways, which will be described in the sections below. In short, a separation in two distinct levels has been required from the very beginning to ensure safe operation even at moments of lost data connection between the hardware and the centralized EMS. The fast acting (order of milliseconds) local power electronics regulation of the converters ensures the voltage stability while the slow long term regulation tasks on the order of several seconds, minutes or hours for energy balance of the batteries is done by the EMS. A principle description of the ICT system has been published in [ICDCM2017].

The data history of all devices is logged into a database. Another database stores the meteorological data from the weather forecast of Meteoswiss. The local meteo station on the roof is used to know precisely the local weather conditions. A leakage current supervision, measuring the differential current between the positive and the negative pole of the DC-bus, has been installed at various positions within the microgrid as a first measure of a safety concept.

3 Procedures and methodology

The project consists of three subsequent and thematically connected blocks. The major part of the project comprises technical development of power electronics components, communication, voltage and regulation and energy management system with the aim to build an operational and permanently running DC-microgrid capable of demonstrating the features of the DC-technology and determining bottlenecks for further development. Based on the experience gained the advantages of the microgrid technology for the distribution grid operator were analyzed. Eventually these advantages were the background for various hypothesis, which formed the basis for an overall economic analysis of the impact such a technology could have on the owner of the microgrid as well as on tariff structure and the distribution grid operator.

Figure 1 illustrates the components and the structure of the entire operational DC-microgrid at the HESSO-Valais in Sion at the school of engineering (HEI). The DC-microgrid has been developed as an organic upgrade of the previously existing smaller DC-bus system. The development of these components formed a major task of the project before they could be integrated into the microgrid. The entirely functional microgrid could only be realized with all components present, connected and operational.

Since a main feature of this project has been the operating mode of the EMS where a specific power forecast is announced for the interface between the DC-microgrid and the AC-grid (i.e. the AFE), the behavior of the bidirectional converters for the batteries and the DC/AC interface must be defined beforehand. The description of the EMS in the following sections will refer to two distinct operating modes:

Mode 1: the AFE controls and stabilizes the DC-bus voltage, whereas the bidirectional converters of all batteries receive an order from the EMS for charging or discharging, respectively. All other converters, either for PV-generation or for the consumers fulfill their task as long as the bus voltage is within the required operational window.

Mode 2: several of the bidirectional converters of the batteries regulate the DC-bus voltage. Thus, the AFE receives and executes a bidirectional power exchange program from the EMS. This mode is required for achieving the project goals with a 1% tolerance on the power forecast to the AC-grid. Again, PV and consumers push or pull the power they need into or from the DC-power link.

3.1 Power electronics, battery storage system & communication

Voltage converters for the producing, storing and consuming elements were mostly developed in house or by the participating partners of the project. Table 1 lists the converters required for the operation of the DC-microgrid at HESSO Valais and at the EPFL PV-lab in Neuchatel. For the consumer system and the EV-charger, the variable frequency drive, transformer and filter were purchased from commercial suppliers and modified for the desired purpose. All converters measure the DC bus voltage at their position and can react properly in case the DC-power link breaks down or is switched off. Since every converter has a certain capacity at the interface to the DC-bus, the power link carries a total capacity of several microfarad. Any converter which will be connected or disconnected to the DC-power link must therefore be equipped with a so-called precharge-box, which assures precharging of this internal capacity of the device under consideration, such that not too high currents are drawn via the bus under rapid connection of the operational DC-power link.

Converter function	origin	power [kW]	number	Features
AFE - gen.1	HESSO Valais	10	2	bidirectional, grid generating, since 2015, installed at EPFL PV-lab
AFE - gen.2	HESSO Valais	15	1	bidirectional, grid generating, program executing, bipolar
Battery converter VS120-35	Studer-Innotec	7	7	bidirectional, gridgenerating or gridfeeding
Serial PV converter	HEIG-Vd	8	1	with MPPT, pre-charge included,
individual PV - gen.2	IMPERIX	0.4	21	MPPT, small footprint, 24 - 60 V PV input
individual PV - gen.1	HESSO Valais	0.35	30	MPPT, high efficiency, 20 - 45 V PV input
		0.35	23	pilot series (2015), 20 - 45 V PV input
individual PV	HESSO Valais	0.35	3	pre-pilot series, 120 V PV input
Electrolyzer	HESSO Valais	0.6	1	current regulation for electrolyzer stack, modular, 2 step-downconversion, 1. step using VS120-35
DC-AC consumer	HESSO Valais	5.5	1	filter, galvanic separation, based on Emerson drive
EV-charging	HESSO Valais	21	1	filter, galvanic separation, adapted to commercial EV charger
Pre-charge box	HESSO Valais	n.a.	15	pre-charging of DC-capacity on connection, supervision, safety

Table 1: Summary of all power electronics developed and used for operation on the DC-microgrid at HESSO Valais and EPFL-PV lab Neuchatel.

3.1.1 Battery storage system and gateways

Different types of batteries are connected to the DC-bus: (1) lead-acid batteries, which are often used for solar storage applications in remote locations, where reliability and cost are valued higher than storage density or "modernity"; (2) Lithium batteries of various suppliers, (3) in the future other types (e.g. salt-batteries).

Année installation	Fabricant / type	Technologie	Capacité kWh	Nombre	Utilisable kWh
2017	Leclanché / Apollion Cube	NMC	6.3	4	20.16
	Powersafe / SBS 900	Pb	43.2	1	21.6
2019	Leclanché / Apollion Cube	NMC	6.3	1	5.04
	BMZ / ESS X	NCA	10.06	2	16.1
	BYD / B-Box Pro 10	LiFePO4	10.24	2	20.48
2019	**TOTAL**				**83.38**

Table 2: Overview of the installed battery storage system with the year of installation in our DC-microgrid, the supplier and the key characteristic specifying the performance.

The total battery storage capacity has been upgraded throughout the project. *Figure 2* and *Table 2* summarize the latest extension of the battery system summing up to more than 80 kWh useable energy storage capacity. Seven bi-directional DC/DC converters VS120-35 of Studer-Innotec of 7 kW have been installed, e.g. a storage power of nearly 50 kW is available on the DC-microgrid. While a selectable number of the battery converters with their corresponding battery can be dedicated to control the DC-bus voltage, the others assure energy balancing between day and night.

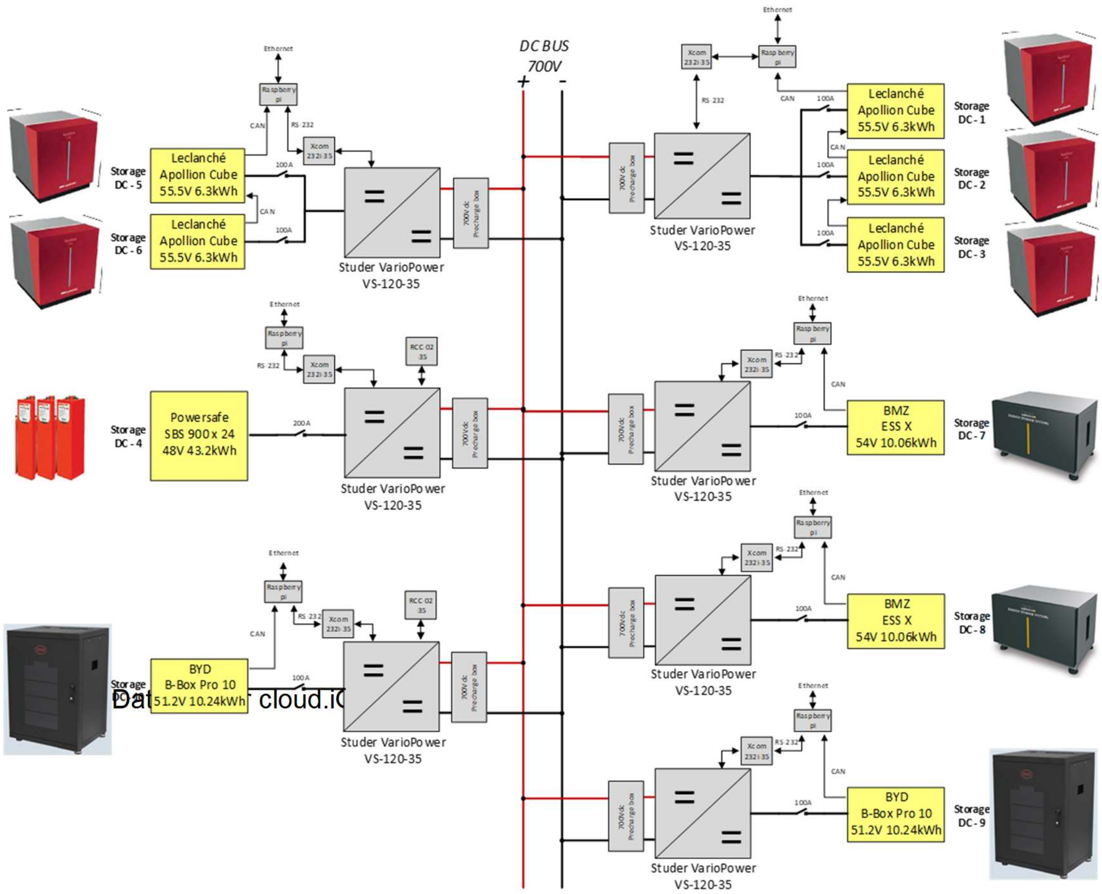

Figure 2: Overview of the entire battery storage system linked to the DC-bus. Table 2 summarizes the available storage capacity.

Since each type of battery has its particular characteristics and data protocol, as defined by the supplier, the gateway provides the data transfer between the DC/DC converter, the BMS (battery management system) and the broker cloud.iO (see Figure 3). In addition, the gateway keeps the batteries in the operation mode and SOC range as required for safety reasons or recommended by the respective supplier for longest lifetime. For example, in a situation where the EMS emits a command reducing the SOC below a critical value (for example SOC 20%), the gateway overrides this command by assuring the safety requirements for the Lithium battery. For the lead batteries, other requirement apply, in addition to the fact that lead batteries are not supplied with a proprietary BMS. Therefore, the gateway assures the proper boost charging and floating cycles as required for longest lifetime by the suppliers for example for electrode reconditioning.

The data exchange system (or broker) cloud-IO, developed previously at the HESSO Valais, assures smooth communication between all components attached to the DC-bus and the EMS, *Figure 1*. This choice was favored compared to an individual data exchange from each element to the EMS allowing implementing different EMS which are device independent and can therefore be programmed by any supplier. Thus, all data are centrally stored and are independent from the EMS-program, which may be open for any developer, as long as he has access to the data broker. However, it requires a gateway for each device connected to the DC-microgrid, which converts the communication protocol of the respective device into the standard of the cloud-IO system.

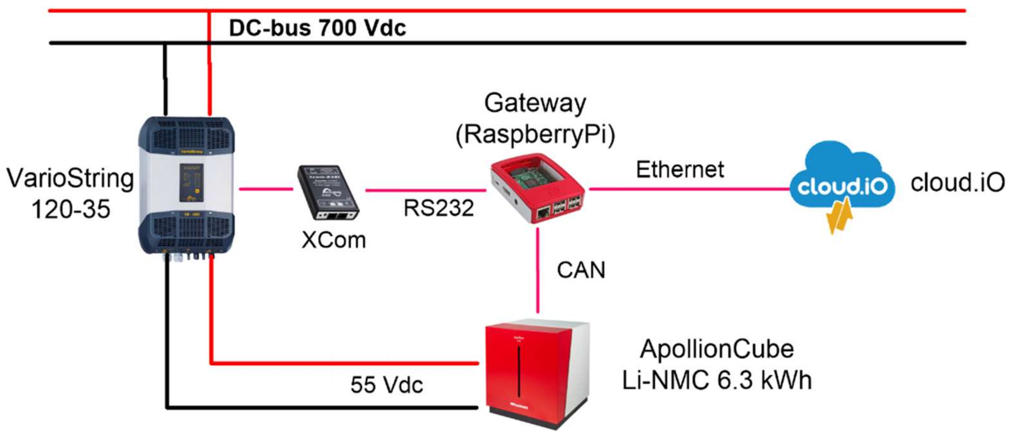

Figure 3: sketch of the communication system GibsCom (gateway software), developed for linking the DC/DC battery converter and its proprietary internal communication bus (CAN) to the cloud-IO system.

The power electronics of the converter systems as well as the data communication system, developed for the implementation and permanent operation of the DC-microgrid, are described in 11.

3.2 Energy management system (EMS)

In this section, we describe the objectives of the EMS and two key building blocks, which are the algorithm of the PV-production forecast and the predictive algorithm used to generate the 48 h ahead power program at the interface between the DC-microgrid and the AC distribution grid. The data communication (see cloud-IO in annex 11.9) within the microgrid is implemented such that the EMS can be programmed entirely device independent. This allows simplifying future compatibility with any additional application or device, and could even allow a complete EMS change. This latter is shown as two independent EMS were implemented during the project and, depending on the requirements, a switch between the two can be made.

To achieve the project objectives listed in section 2, the EMS has to fulfill different objectives:

1. Generate forecasts for the PV-production and for the load consumption for at least 48 hours ahead.
2. Determine a forecast for the DC/AC balance for the next 48 h in accordance with a chosen maximum allowed power exchange and provide this forecast to the AC-distribution grid operator. This could allow reducing the fees for the maximum power connection of the end user to the distribution grid.
3. Determine an optimized forecast (trajectory) for the power and SOC of the batteries always 48 h in advance using the forecast algorithm for the PV-production and a consumption forecast.

4. Control the real SOC of the batteries, such that the microgrid can always rely on sufficient energy reserve and maintain the real DC/AC-balance within a tolerance of 1% relative to the forecast, (objective 2).
5. Reduce (smoothening) the strong fluctuations of the PV-power source compared to an unlimited and strongly fluctuating DC-AC balance of a directly AC-connected PV-plant. The fluctuations are quantified by the time derivate $\frac{dP}{dt}$(transient) of the power exchange with the AC-grid.

3.2.1 Forecast of the PV-power generation

The forecast of the PV power generation is based on an algorithm developed throughout a preceding project by the eEnergy center, Sierre. The underlying algorithm was adapted and the parameters adjusted to the characteristics of the PV-generator of the DC-microgrid. The PV-forecast is generated and stored into a database. The EMS has access to this database via cloud-iO and can integrate the PV-generation forecast into the steering of the SOC of the batteries and for the DC/AC balance.

The algorithm uses PV-production history, local weather forecasts and actual measurements to predict PV power generation. The temperature and solar irradiance are key features for the prediction (see *Figure 4*, lower diagram). These data are dumped into a time-series database by an importation process, which is not part of the algorithm itself. The predictions are then versioned in the same database, for easy retrieval of past predictions. Two different weather forecasts from Meteoswiss have been used: cosmo2, corresponding to 33h in advance and cosmo7, corresponding to 72h in advance. Since the predictions we make are up to 48h in the future, we need the long-term weather forecast (e.g. cosmo7 72 hours in advance) even if it is supposed to be less accurate than the short-term (cosmo2) forecast. The difference between these two are visible in the lower panel of *Figure 4*. Note, that in the PV-production history, the nominal installed PV-power of the DC-microgrid changed several times, since during the system upgrade solar panels were added while others became deficient. This issue was solved by normalizing the PV-production history against its nominal power at each instant of time.

The prediction process is expressed as a regression problem using the above features in the machine learning approach. An algorithm called Random Forest (see reference [Breiman2001]) is used to map

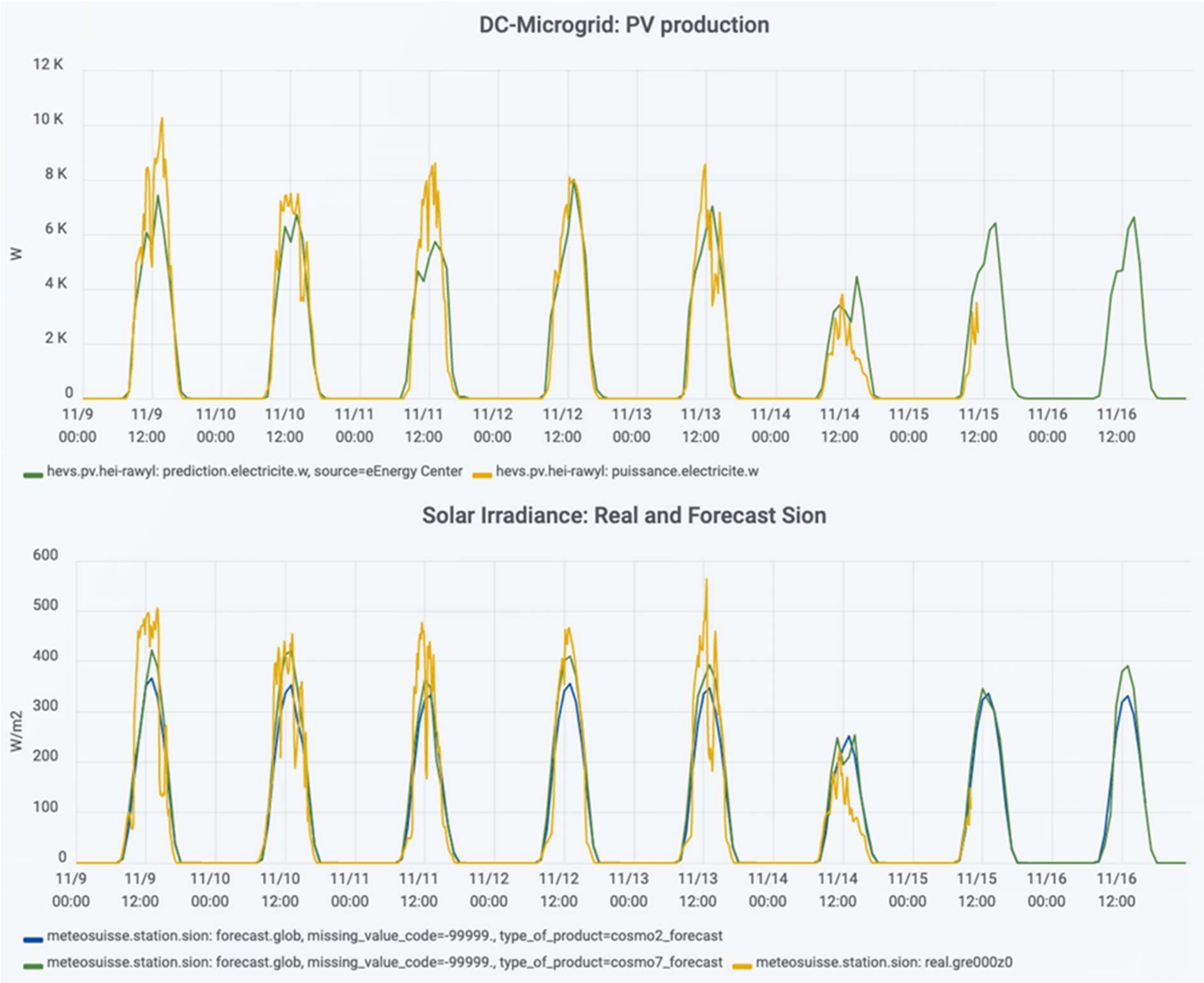

Figure 4: Result of the prediction algorithm as calculated at noon on November 15th. Above: actual PV-production (in orange) and its corresponding prediction (in green). Below: solar irradiance: real (orange), short-term (cosmo-2, green) and long-term (cosmo-7, blue) forecasts from Meteoswiss. As of noon, November 15th, there are no measured data for PV-production or solar irradiance after that instant of time.

the predicted PV-production as a function of the weather features discussed above, as well as some temporal features. Random Forest consists in growing several decision trees randomly and averaging their corresponding predictions over the set of trees, namely: the forest.

The results show an averaged error of 30%, which is determined as mean absolute deviation percentage PMAD evaluated over the entire year 2019

$$PMAD = \frac{\sum_{k=1}^{N} |Y_{predicted} - Y_{real}|}{\sum_{k=1}^{N} |Y_{real}|}.$$

Where $Y_{predicted}$ is the predicted production by our algorithm and Y_{real} the real production as measured. This error is lager than the typical mean error of about 25%, obtained for the day ahead production forecasts, which are regularly performed by the eEnergy Center for 60 PV-plants of ESR. There are principally two reasons: first the data history used to create the models is smaller than for the other PV-production, secondly as mentioned above, the setup's nominal power has changed several time during the last years. Therefore, throughout the next years, this error will decrease due to a more extended data history and a stabilisation of the nominal power. A detailed discussion about the error and the various contributions can be found in reference [IEEEIMIS]. Comparing to the literature, we note that the here described variation fits well to the range of precision, which is typically claimed for the PV production forecast results of other groups, which may range from as low as 5% and up to 35%. However, a direct comparison cannot easily be done, since the meteorological conditions in the mentioned reference were very different from ours, as they were performed in other climatic regions and as the mathematical procedure to quantify the error is often very different.

The error of the PV-forecast can show strong variations throughout the year, since the difficulty and thus the quality of the prediction depends on the meteorological conditions. For example on cloudy days, the deviation of the forecast is larger than during a clear day with blue sky the entire day. Further studies need to consider this for improvement of the forecast algorithm.

3.2.2 EMS regulation algorithm

Different EMS were implemented and tested. A simplified SCADA is integrated into each EMS, while the open source analytics and monitoring software GRAFANA (see [grafana]) displays all required data for supervision and debugging in a detailed and efficient way.

Because of the different time scale requirements, the fast voltage regulation and the slow energy management are decoupled. Three different control systems for the DC-bus voltage have been used throughout this project: the original AFE, already operational at the beginning of the project in 2017, needed to be replaced by a more powerful and versatile AFE. The new AFE has been developed and is adapted to the particular and extended requirements of this DC-microgrid. It allows for example, the realisation of a real bipolar DC-bus, an extended voltage range or the acceptance of an external current command. Both AFE have assured the control of the bus voltage in mode 1 where the AFE is controlling the DC Bus voltage.

The new AFE allowed for the development of a second type of voltage regulation method, labelled mode 2, where one or several of the bidirectional DC/DC converters[1] VS120-35 for all battery systems control the DC-bus voltage. Since the total power acceptance of the voltage-regulating converter must be at least as high as the maximum total surplus power (production minus consumption) on the DC-bus three of the battery converters must operate smoothly together. This voltage regulation is achieved using the “droop control” method of the VS120-35 from Studer-Innotec. Therein, a small deviation of the effective bus voltage from the set point is accepted. The current injected by the regulating bidirectional converter can be defined linearly with a negative slope as function of the bus-voltage. The remaining bidirectional battery converters were kept in a command mode receiving a power program from the EMS to follow the energy management tasks by charging or discharging the batteries according to the power needs as well as the available and required energy reserves. The results for the regulation performance in mode 1 and mode 2 are shown separately in the following.

<u>Mode 1 regulation</u>

In mode 1 the AFE, controls the desired DC Bus voltage to 700Vdc. The power flow through the AFE circulates automatically according to the regulation aim:

- production is greater than consumption → power is fed into the AC-grid.

- consumption is greater than production → power is extracted from the AC-grid.

[1] supplied by Studer-Innotec

Mode 2 regulation

In mode 2, several (presently two, the number can be adapted according to needs) of the bidirectional battery converters of 7 kW power are regulating the DC-bus voltage to 710 Volt assuring stable operation of the DC-bus. Due to the droop control logic, the DC-voltage varies – depending on the load or PV-power generation between 710V +/- 10V. The batteries connected to the controlling bidirectional converters are termed *regulating batteries*. Their real capacity and instantaneous SOC must be sufficient to absorb or release rapid variations (within milliseconds) in PV-generation or consumption. Therefore, their nominal working point is chosen to be at SOC = 60%.

The remaining batteries of the entire battery storage system (BSS) are termed *storage batteries*. Their power trajectory follows the forecast curve calculated by the EMS. When production or consumption variations occur, they have to absorb or supply power to the DC bus on long time scales of minutes to hours.

3.2.3 Integration of power forecast

As indicated in the section describing the energy management algorithms above, the capacity of the regulation batteries is linked to the time interval with which a BSS can smoothen peaks in either consumption or PV-generation. The aim of the project is not necessarily to decouple entirely the microgrid from the AC-distribution grid but to smooth strong variations of either PV-generation or consumption that cause increased regulation difficulties for the DGO. In order to optimize battery costs, as they do not produce value but shift energy in time according to a more suitable usage schedule, the installed storage capacity C_{batt} can be calculated as follow:

$$C_{batt} = P_{PV} \cdot \Delta t$$

With Δt being the time interval over which the battery should absorb (or deliver) the maximum PV-power. An intelligent algorithm should therefore be able to predict whether the batteries should have spare capacity in both direction. Thus, the predictive algorithm for the energy management system should incorporate a PV-production forecast as reliable as possible using thus an appropriate weather forecast.

3.2.4 Predictive algorithm

A genetic algorithm determines the optimal parameters for the next 48 hours allowing the EMS to predict the right control parameters for the system, i.e. the power for all bidirectional converters (AFE and battery converters).

The input parameters taken into account by the optimization algorithm are:

a. The predicted consumption for all consumers for the next 48 hours
b. The predicted consumption for all producers for the next 48 hours
c. Total maximal capacity of all battery storage systems (BSS)
d. Total residual capacity of all BSS at present
e. Lower and upper SOC bound for every BSS available to the optimization algorithm
f. Minimal and maximal power provided by all battery storage systems together
g. Minimal and maximal power provided by the AFE

The algorithm calculates the reference power for the BSS's (i.e. BSS trajectory) and for the AFE (i.e. AFE trajectory) for the next 48 hours with an interval of 15 minutes, which leads to 192 values for each trajectory (48h / 15min = 192), see *Figure 5*.

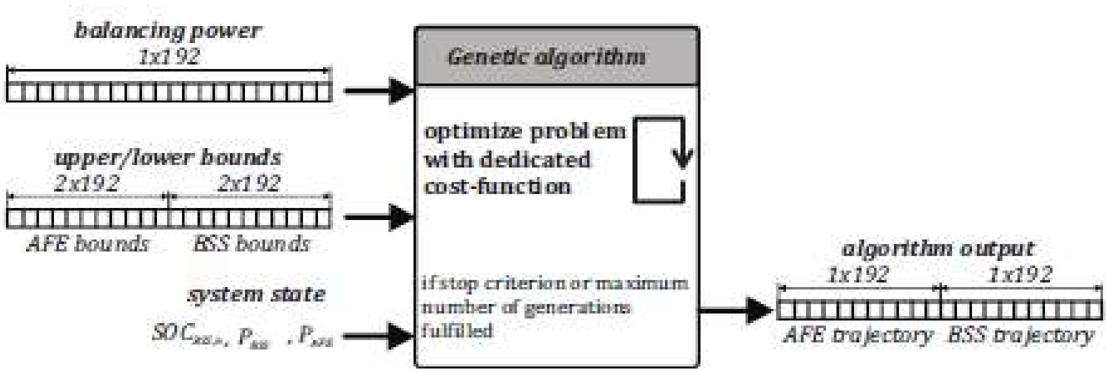

Figure 5: A genetic algorithm determines the trajectories for the next 48hours for both the AFE and the battery storage system.

During optimization (iterations), a genetic algorithm is checking the fitness ("quality" or "cost") of each potential future trajectory with a fitness-function (often called cost-function in general optimization theory). Trajectories with better suitability (i.e. "fitness") will get a higher chance to be chosen for the next iteration. Finally, the trajectory with best convergence (see description of the fitness function below) will determine the power values for the next 48 hours.

The fit-function checks the following constraints and penalises them with different weights:

a.	Penalty on DC-Microgrid power peaks	Weight: Maximum
b.	Penalty to SOC over or underflows	Weight: Marginal
c.	Penalty on fast power variations	Weight: Normal
d.	Penalty on exceeding power limits of AFE	Weight: Normal
e.	Penalty on power peaks exchanged with grid	Weight: Very high
f.	Penalty on self-consumption violation	Weight: High
g.	Penalty for too high power on BSS	Weight: Marginal

The fitness function C_{tot} tells the predictive algorithm if a solution is better than another. The optimization process tries to find the global minimum of the fitness function, written here as the total cost function, being the sum of the individual costs:

$$C_{tot} = \lambda_{bal}C_{bal} + \lambda_{AFE}C_{AFE} + \lambda_{BSS}C_{BSS} + \lambda_{p}C_{peak} + \lambda_{v,AFE}C_{v,AFE} + \lambda_{v,BSS}C_{v,BSS} + \lambda_{SOCmax}C_{SOCmax} + \lambda_{SOCmin}C_{SOCmin}$$

These individual costs are described in the following paragraph. With the weighting coefficients λ the user can adjust the weight of each individual part of the fitness function according to the needs.

3.2.4.1. Achieve power balance

Production and load predictions are available thanks to forecasting. One goal of the optimization process is to balance injected and consumed power on the DC microgrid with the available devices. For each of the k = 192 discrete time-steps the following power balanced is calculated and deviation from balance is penalized.

$$P_{BSS}^{k} + P_{AFE}^{k} + P_{PV}^{pred,k} + P_{load}^{pred,k} = 0, \qquad \forall k \in \Phi^{k}$$

Power flowing in the microgrid is considered as positive and power flowing out of the microgrid is considered as negative. P^{nom} is the nominal power of the AFE. The contribution to the cost function for the power balance at the interface to the distribution grid is therefore

$$C_{bal} = \sum_{k=1}^{192} \left(\frac{P_{BSS}^{k} + P_{AFE}^{k} + P_{PV}^{pred,k} + P_{load}^{pred,k}}{P^{norm}} \right)^{2}$$

A high weighting is given to this part in the fitness function as it is the most important optimization goal.

3.2.4.2. Optimize auto-consumption

A further goal of the optimization is to maximize the auto-consumption coefficient. This is achieved by attributing to the grid exchange energy a higher cost than the stored energy.

$$C_{AFE} = \sum_{k=1}^{192} \frac{|P_{AFE}^{k}|}{P_{AFE}^{max}} \; ; \qquad C_{BSS} = \sum_{k=1}^{192} \frac{|P_{BSS}^{k}|}{P_{BSS}^{max}} \; ; \qquad \lambda_{AFE} > \lambda_{BSS}$$

This difference in cost per kWh will guide the algorithm to use the distribution grid as little as possible. This is equivalent to increase the auto-consumption coefficient.

3.2.4.3. Permit peak-shaving

The maximum power exchanged with the distribution grid must be as small as possible. This is achieved by penalizing the highest power peak of the AFE trajectory.

$$C_{peak} = \max_{k} \left(\frac{P_{AFE}^{k}}{P^{norm}} \right)$$

3.2.4.4. Reduce power variations

An optimal trajectory should be smooth and should not show fast power variations, i.e. have small time derivatives of the bidirectional power exchange. Thus, all power changes from one time-step to the next are penalized:

$$C_{v,AFE} = \sum_{k=1}^{192} \left(\frac{|P_{AFE}^{k} - P_{AFE}^{k-1}|}{P^{norm}} \right)^{2}, \qquad C_{v,BSS} = \sum_{k=1}^{192} \left(\frac{|P_{BSS}^{k} - P_{BSS}^{k-1}|}{P^{norm}} \right)^{2}$$

3.2.4.5. Upper and lower limits on SOC

The batteries must be kept within the upper and lower SOC limits, therefore a penalty is added to maintain $SOC_{max} = 100\%$ and SOC_{min}. We operate with a minimum allowed SOC for lithium of 20% and for lead-gel batteries of 50%.

$$C_{SOCmax} = \sum_{k=1}^{192} (SOC(k) - SOC_{max})^{2} \; ; \qquad C_{SOCmin} = \sum_{k=1}^{192} (SOC(k) - SOC_{min})^{2}$$

To work properly, the power difference from one time-step to the next hast to be normalized to some common reference P^{norm}. This reference is computed at the problem initialization based on the needed peak-to-peak balancing power. With this normalization, the power variation part of the fitness function works properly for very different algorithm inputs and balancing scenarios.

The EMS executes the optimization algorithm every 6 hours. The genetic algorithm needs presently about 20 minutes to converge to the optimal power trajectories for the AFE and BSS for the next 48 hours, see an example in *Figure 6*.

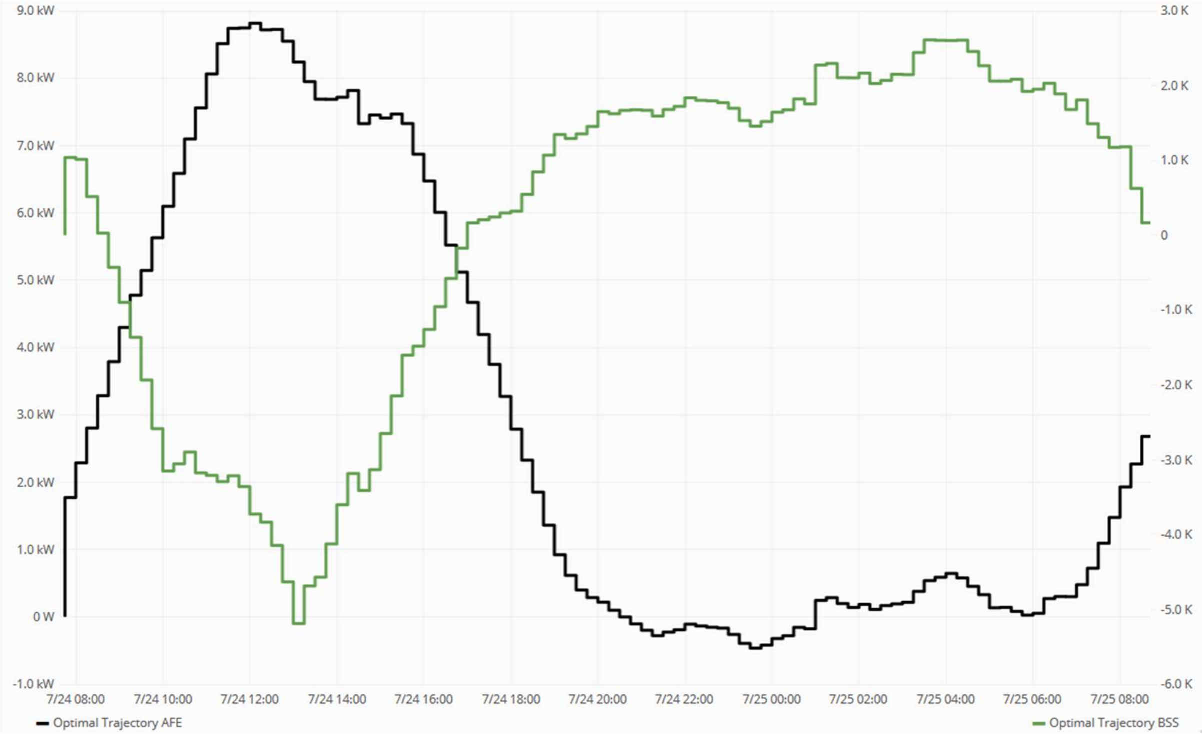

Figure 6: Example of optimized trajectories for the AFE and battery storage system (BSS) as output of the optimization algorithm.

3.3 Implementation & operation of DC-microgrid

In this sections we describe the two DC-systems developed during this project. One DC-bus system was installed at the PV-Lab of EPFL in Neuchatel and an entire DC-microgrid at the HESSO Valais. While the former was designed to study the behavior of the developed DC/DC converters for individual PV-modules, the latter incorporates all features required for proper functioning of a microgrid.

3.3.1 Installation at EPFL/PV-lab (Neuchatel)

The DC-bus installation at EPFL/PV-lab is operating independently from the one at HESSO Valais in Sion. Therefore, it is ideally suited to provide an independent view on the performance of the PV-

Figure 7: PV installation connected to the DC-bus system at EPFL-PV-lab, Neuchâtel.

generator operating with a DC-bus control. The PV-performances have been evaluated using the restricted number of converters available until winter 2017/18, see poster publication PV-Tagung, Bern 2018 [PV-Bern2018]. The 18 new converters delivered to PV-lab in June 2019 could be installed during summer 2019 and are presently under evaluation. In order to obtain significant statistics at least 6 month or better an entire year of data collection is required. A publication of these data is therefore expected in spring or summer 2020. An overview of the performance assessment methodology and some preliminary results are presented in the following paragraph.

The DC-bus installation (shown in Figure 7) in Neuchâtel consists of 22 connected modules representing a broad overview of the current and future main PV module technologies. The available module types are summarized in Table 3. Three modules were end of summer 2019 disconnected due to work on the roof. All modules are connected either via HES-made DC/DC converter or the Imperix converter to the DC-bus. The analysis period ranges from January 2017 up to October 2019.

id	Module Type	Manufacturer	Technology	Nominal Power (W)
String02	JAP6-60-260/3BB	JA SOLAR	multi c-Si	260
String06	Micromorph	Oerlikon	micromorph	125
String07	Zellen SWCT HJT	Meyer Burger	HJT	294
String10	Ma100T1	Mitsubishi	thin film	100
String11	VBHN240SJ25	PANASONIC	HJT	240
String12	VBHN240SJ25	PANASONIC	HJT	240
String13	VBHN240SJ25	PANASONIC	HJT	240
String14	SPR-X20-327-BLK	SUNPOWER	IBC	327
String15	SPR-245NE-WHT-D	SUNPOWER	IBC	245
String16	SPR-X21-345	SUNPOWER	IBC	345
String17	SPR-X21-345	SUNPOWER	IBC	345
String18	SPR-X21-345	SUNPOWER	IBC	345
String19	SPR-X21-345	SUNPOWER	IBC	345
String20	Yingli Panda YL265C-30b	YINGLI	mono c-Si	265
String21	LG SOLAR MONO LG300N1C	LG	mono c-Si	300
String22	LG SOLAR MONO LG300N1C	LG	mono c-Si	300
String23	LG SOLAR MONO LG300N1C	LG	mono c-Si	300
String24	YL255P-29B	YINGLI	multi c-Si	255
String25	Yingli Panda YL265C-30b	YINGLI	mono c-Si	265
String26	JAP6-60-260/3BB	JA SOLAR	multi c-Si	260
String27	LG SOLAR MONO LG300N1C	LG	mono c-Si	300
String28	JA SOLAR MONO JAM6(R) 60-275	JA SOLAR	mono c-Si	275

Table 3: *Characteristics and technology of the 22 PV-modules connected to the DC-bus system on the site at EPFL-PV-lab in Neuchâtel. c-Si corresponds to crystalline silicon, IBC corresponds to Inter-digited back contact cells, HJT is hetero-junction solar cell.*

3.3.2 Upgrade of PV-power at HESSO Valais

The DC-microgrid at the HESSO Valais has been operational throughout the entire duration of the project. This constant supervision is helpful to assure that the system is functioning as desired. Upgrades were made on the operating system with downtimes required to exchange part or entire components when ready for installation. A major upgrade was the switch from the original AFE (installed in 2015) to the new AFE in summer 2019. The implementation and testing of the EMS in the “mode 2” (batteries are controlling the voltage level of the DC-bus) could only be made after this switch. A second major step was the integration of the first storage and consumer elements into the DC-link, which marks the transition from a mere DC-bus operated PV-plant to a real DC-microgrid.

During the project, gradually, the battery power has been increased, the PV-power upgraded, the electrolysis system and several consumers (air conditioning, coolstock, EV-charger) have been integrated. For safety reasons a supervision system of the failure current which trips at the standard 30 mA level as in the AC-case has been purchased and integrated. As the former AFE did not allow a proper measurement of the isolation resistance, a supervision of the isolation resistance relative to ground was discarded after testing various options. This may however, become again an option for other AFE topologies.

At the beginning of the project in January 2017, the PV-generator on the roof comprised 44 PV-modules, all of which with individual power converters (reference [Steiner2013]) connected to the DC-bus. The installed PV-power has been upgraded throughout the project in order to reach the present value of 21.3 kW_p. see *Figure 8*. Sixty PV-modules are now connected to the DC-bus with individual DC/DC converters. Eighteen PV-modules are connected as a string to the serial DC/DC converter, developed at HEIG-Vd, see annexe A, the others are connected to individual DC/DC converters either from Imperix or the HES-design, see *Figure 9*.

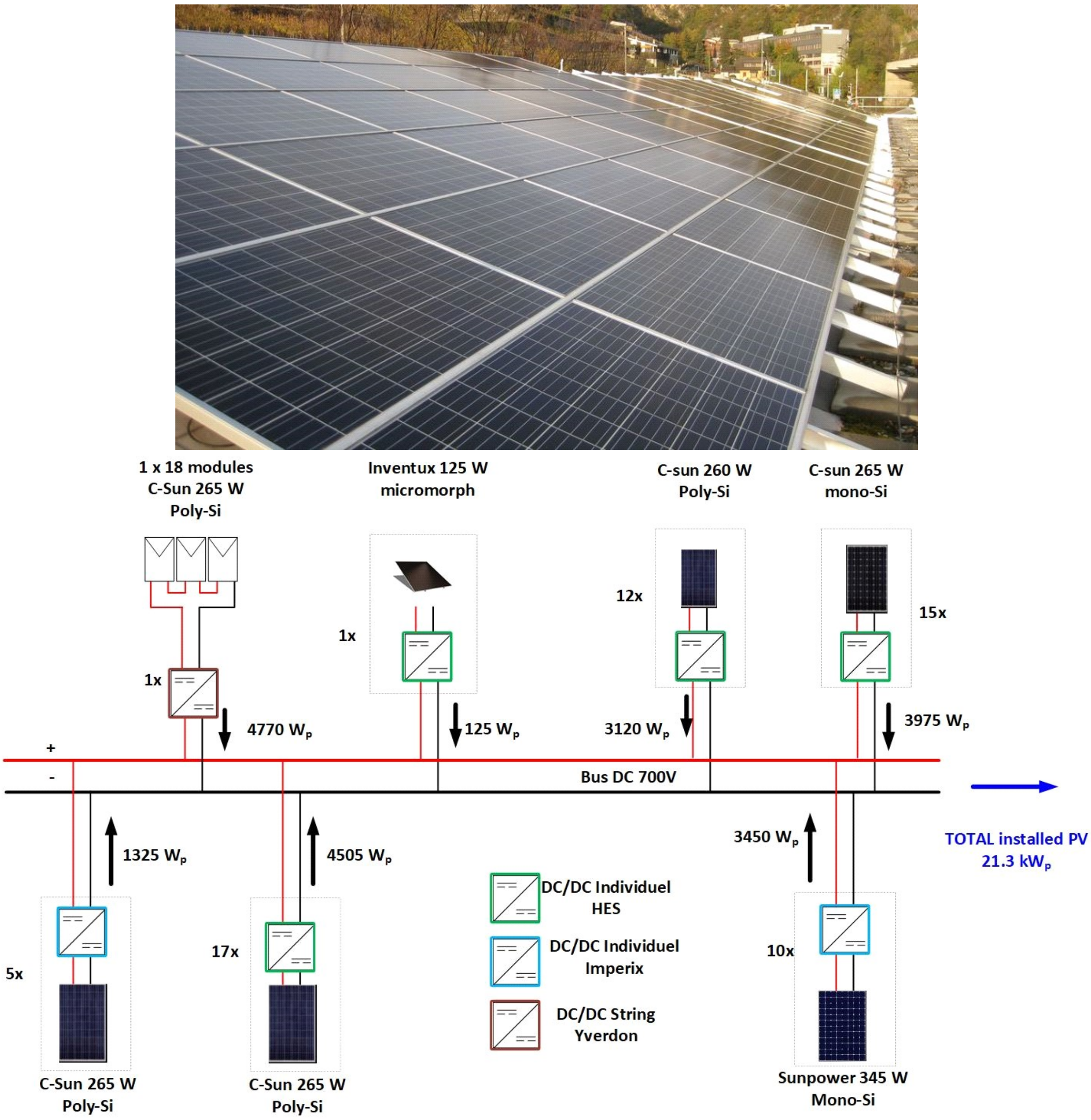

Figure 8: above: view of the PV-installation at the HESSO Valais with entire upgrade to 21 kWp. In front the block 42 most recently installed modules, 18 of which are connected in one serial string to one converter, the other 24 are linked to individual DC/DC converters. Below: connection schematics of the type of converter or PV technology, respectively.

Figure 9: above: all DC/DC converters installed during the upgrade, the large converter for an entire string is installed at the very right end of the line, lower than the others. Below: The new DC/DC converters designed by Imperix (e.g. the small boxes, second and 5th in the row, counted from the left) during this project show a clear gain in size compared to the larger DC/DC converters of the previous generation (the 4 larger boxes).

3.4 Evaluation & optimization

The evaluation of the system was permanently ongoing, which allowed an optimization of the regulation software under operating conditions. After integration of the hardware components, including the implementation of their respective communication interface (gateway), the last system component to be developed has been the EMS in the operational mode 2. The latter is required for the tight operation window of +/-1% for the power exchange between DC-microgrid and the AC distribution grid. Note that in particular due to the availability of the cloud-IO and Grafana software, all data collected within the DC-microgrid can be accessed by any of the partners, under the conditions that they are granted full or limited access rights to the cloud-IO broker. This made it easy for the developer in the remote locations to supervise the behaviour of their respective device in order to check for error message, undesired properties and to find directly remedies without requiring the transfer of large data sets from Sion to the respective collaborating partner. This will become a key element for future potential implementations of DC-microgrids on industrial sites (see section 6. Outlook).

Failure tracking & analysis

The reliability of the DC-microgrid has been evaluated quantitatively according to measurement metrics generally used in industry for quality insurance. Quality insurance is a critical topic for new products. At the beginning of a product lifetime, quality usually is low and quality engineers struggle to reach values close to 100%. Usually, highly sophisticated methods like 6sigma which are the key elements in well established industry branches like the automobile or semiconductor industry are a complete overkill in an early stage product phase, since relative uptime of a machine or relative number of goods passing quality tests are more likely in the 80 or 90% range instead of going beyond 99%. Therefore, at the beginning it is more relevant to identify the most relevant failures of a system since not all failures are similarly relevant. In order to distinguish between more or less relevant failures we have chosen to establish a failure tracking table, where each failure is listed and described. This table allows, based on the number of occurrences and the consequences of an error, to determine whether a failure is highly relevant and has to be addressed entirely or may be handled on a day-to-day basis.

First, it is important to receive as quickly as possible a message notifying the responsible engineer if anything on the DC-microgrid broke down. The Grafana software has the advantage not only to displays all data available in the databases in a coherent manner but also allows setting alarm points according to some logic which may be defined by the user, for example if the bus voltage drops below a certain critical value. Various alarms can thus be defined and automatic actions may be taken. For our permanently operating microgrid, we defined the following parameters, in order to quantify the reliability of the DC-microgrid:

- Number of failures N_{fail} during a chosen evaluation period
- Uptime, in percent of a chosen evaluation period
- Mean time between failures: $MTBF = \frac{uptime}{(N_{fail}+1)}$
- Downtime, which is essentially the complement of the uptime and thus has not been displayed separately

For the appreciation of the above-defined values, it is required to consider the corresponding evaluation period. The results are shown in section 4.2

3.5 Evaluation of the technical impact on the distribution grid

A simulation of a distribution grid, consisting of a multitude of individually operated DC-microgrid has been performed in order to demonstrate the technical benefits of the regulation mechanisms implemented for the distribution grid operator under simplifying hypothesis. Since this is an entirely hypothetic concept, we defined three different scenarios to compare the impact of the microgrid topology on the behaviour of the distribution grid:

Scenario 1: 5% of the clients of the distribution grid operator produce half of their electricity needs per year locally. This is approximately the situation in Switzerland in 2018.

Scenario 2: About 60% of the clients in a distribution grid produce 50% of their electricity needs per year locally. It means considering that about 30% of the electricity would be generated with strongly fluctuating renewable sources. For Switzerland, this scenario is far from the present situation. However, such situations are abroad already a reality today as seen for limited periods in Germany during 2019 where this situation was reached or even surpassed.

Scenario 3: 90% of all participants produce 50% of their electricity needs per year locally. It means considering that about 45% of the electricity would be generated with strongly fluctuating renewable sources, which in Switzerland is a big leap in the future, given the current slow installation rate of solar power generators.

The purpose of the simulation is to study, from the point of view of distribution grid operator (DGO), the consequences of having several microgrids connected to the grid. The simulation compares the two situations with and without using the microgrid regulation scheme as proposed here. Since each microgrid owner produces only half of the energy by its own PV-plant, the distribution grid operator to satisfy the energy balance provides the missing 50% of electric energy:

$$E_{consumption} = E_{Production} + E_{DGO}$$

Technical and economic advantages of having a microgrid that respects the consumption profile from the grid (announced to the DGO 48 hours before) with a difference lower than 1% for each time step of 15 min are highlighted.

If a consumer is exploiting a microgrid, he has to respect the following conditions, equivalent to the aims of DC-microgrid demonstrator developed in this project:

1. To announce its consumption profile $E_{forecast}(t_i)$ for all time steps t_i $(i = 1, \ldots, 192)$ 48h in advance to the DGO.
2. To have a difference on the real consumed energy $E_{real}(t_i)$ lower or equal to 1% ($|\Delta E_r| \leq 1\%$) for each time interval of 15 minutes.
3. Manage the consumption with the different elements of the microgrid such that the real consumption profile $E_{real}(t)$ of the customer will look like a slowly varying function in time, i.e. does not show rapid power fluctuations

To quantify if a user respects his consumption forecast $P_{forecast}(t)$ for the next 48 hours, the "relative Delta" ΔE_r is used as an indicator and computed as follows. The forecasted energy is given by integrating the consumption forecast with a time step of 15 minutes:

$$E_{forecast}(t_i) = \int_{t_i}^{t_{i+1}} P_{forecast}(t)\, dt$$

$$t_{i+1} - t_i = 900s = 15min$$

The same computation can be done on the real consumption of the user:

$$E_{real}(t_i) = \int_{ti}^{t_{i+1}} P_{real}(t)\, dt$$

Each time step of 15 minutes gives one value for $E_{forecast}$ and E_{real}. The relative deviation $\Delta E_r(t_i)$ of the consumed energy to the forecast energy (called "relative Delta" below) is determined for each time step t_i by

$$\Delta E_r(t_i) = \frac{E_{forecast} - E_{real}}{E_{real}} \cdot 100\ \%$$

More details of this evaluation are given in the corresponding appendix B.

3.6 Economic evaluation

For the economic evaluation, we assumed a future without nuclear power plants and with very little or no ribbon power generation. Coal power plants will fade out in Germany starting from 2028 to reach zero by 2038[2]. Therefore, only hydroelectric, PV and wind power plants will be operational in the following simulations. While for Switzerland this is a reasonable assumption because of the large available hydropower capacity, this may be more difficult to establish on a European level since hydropower is there less abundant. We discard explicitly the option to import electricity from European level, since this would shift the problem of missing power (energy) at certain times only to the European level without solving it. Note, that we project to replace roughly 40% of nuclear electricity by PV in Switzerland, whereas import of electricity amounted in recent years to one order of magnitude less [BFE2019].

3.6.1 Technical configuration of a hypothetical industrial site

The profitability of the DC microgrid for an industrial site is analysed based on the following assumptions:

a. The annual total power consumption of the industrial site operating with common AC-power distribution as shown in *Figure 10* is 4.3 GWh. The consumption follows a real load curve measured at a pharmaceutical company in Switzerland which was 2 MW during office hours, and 1 MW the rest of the time, including weekends. We scaled this reference power profile such that the total energy consumption equals that of our hypothetical site. The AC site serves as reference for calculating the time of return on investment for the battery and solar panel installation on the DC site. The total consumption of the site is set so that it can vary to take into account the potential energy savings on the DC motor part, when the site is operated using a DC-microgrid for electricity distribution.

b. A photovoltaic plant of 2.5 MW_p installed power, with a lifetime of 30 years as shown in *Figure 11*. The PV production profile is based on actual measurements at the DC-microgrid of the HESSO Valais.

c. Battery storage system of a total storage capacity of 7 MWh, a capability of charge and discharge with charging time of 1 hour, i.e. 7 MW of power, and a lifetime of 15 years. Thus, a replacement of the battery after 15 years will exactly double the total investment costs of the battery.

d. Assuming a DC-microgrid for power distribution on the industrial site as shown in *Figure 11*, 95% of the energy goes to consumers that are directly linked to the DC-bus. The remaining 5% is directly received from the AC-grid, since even in a long-term future scenario not all AC consumers will have vanished entirely. In more detail, the total consumption of the site can be broken down into four equipment categories:

    - Motor driven equipment for mechanical movements (robots, conveyor belts, lifting equipment, etc.), which are all linked to DC, consume 70% of the total energy [DC-Industrie]. This equipment may even work in a reverse mode for energy recovery, via bidirectional DC/DC converters, thus allowing for additional energy savings.

    - Heating, ventilation and air conditioning may be connected directly to DC, since they are motor driven. This equipment however, cannot work in reverse mode, since it converts electric energy into thermal energy. We assume 10% of the total energy consumption for this class of equipment.

[2] According to the plans of the Germany ministry of economy [BMWi2019].

- Other equipment (i.e. lighting, office equipment, etc.) which may as well be directly connected to DC and instead of AC, we estimate to 15% of total energy consumption.
- Equipment remaining on AC of 5% of total energy consumption.

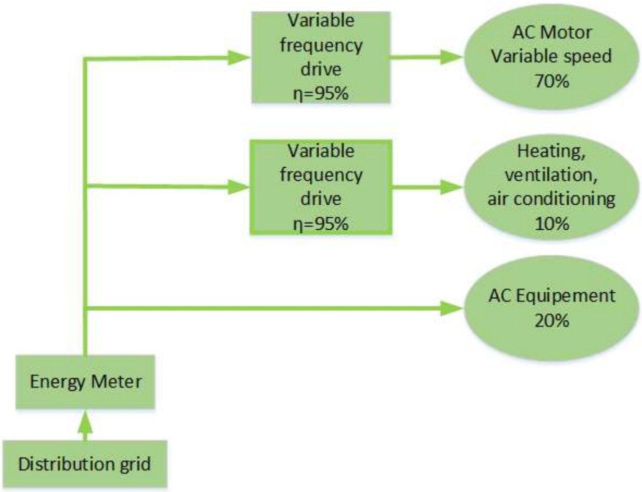

Figure 10: Composition of the hypothetical industrial site, as it operates with AC electric power distribution, which serves as reference for the assessment. We assume that 70% of the total electrical energy is consumed by motor driven equipment, which may vary in speed according to the operational needs of the respective factory; 10% of the energy goes into driving heating, ventilation and air conditioning and 20% are consumed by standard office AC-equipment like lighting, telephone, computers or others.

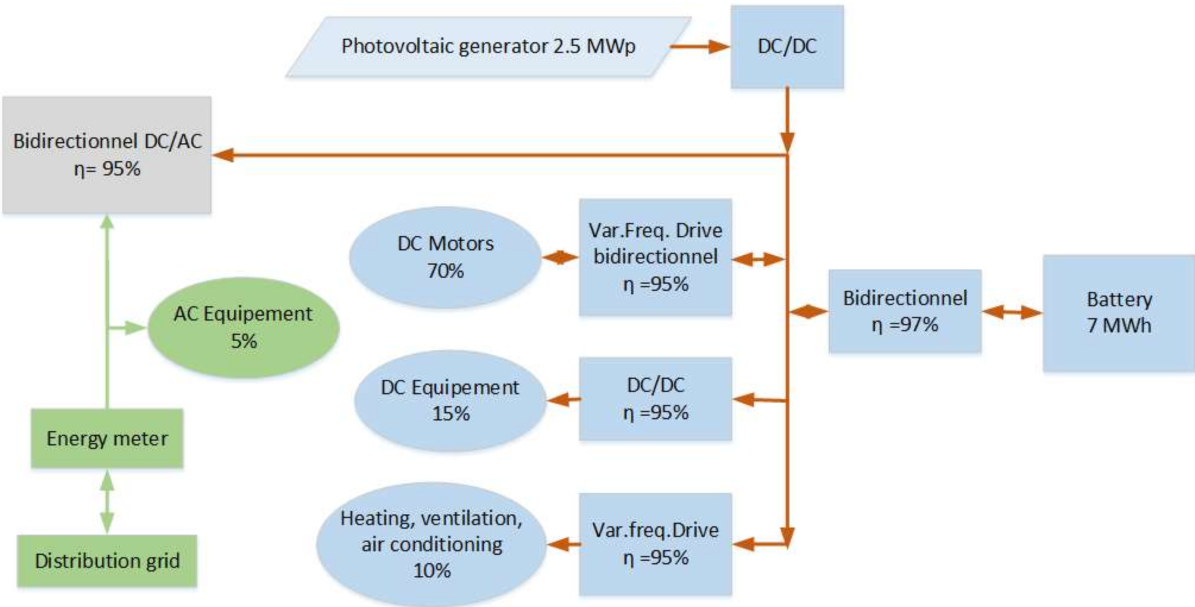

Figure 11: The described industrial site, now equipped with a DC-microgrid, PV generator and battery storage. Efficiencies η of the DC/DC or DC/AC converters, fraction of the energy consumption (in percent of total consumption) of the various types of consumer groups, are given as described in the text. The arrows indicate whether the power flow may be mono- or bidirectional.

3.6.2 Assumptions of energy tariff and investment costs

Three scenarios for the electricity price will be compared in the assessment, for both, the sales of energy from the DGO to the end customer and for the reinjection:

1. **Scenario 2018**: Electricity prices of Services Industriels de Genève (SIG) valid for 2018 (reference [SIG2018]) for sales of electricity by SIG to the end user, repurchase price of reinjected electricity and power tax. Peak hours are from 7am to 10pm on weekdays and from 5pm to 10pm on weekends. The power tax of SIG in 2018 is 7.93 CHF/kW per month for the maximum of consumed power. The maximum "power" is determined by dividing the total energy consumed per quarter of an hour divided by this time interval. However, in our simulation we calculate only for every hour, thus we increase the maximum power by 2% since averaging per quarter of an hour yields higher power peaks than an hourly averaged measurement.

Tarifs in CHF/MWh		Sales price	Reinjection
Summer	Peak hours	151.7	57.5
	Low hours	104.4	43.3
Winter	Peak hours	159.2	83.0
	Low hours	109.3	59.7

Table 4: Electricity prices in CHF/MWh of SIG for the sales and reinjecting electricity for 2018.

2. **Scenario 2050: Fixed electricity price** increased by 30% compared to 2018 conditions.
3. **Scenario 2050: Dynamic electricity price** in 2050: we generate a dynamic pricing first, based on various assumptions as described below.

For each of these scenarios, the variation of three parameters is studied:

I. Variation of the installation costs of the photovoltaic generator. We assume a moderate cost reduction over the next 30 years (until 2050) in three steps from 1100 CHF/kWc to 740 CHF/kW_p, since PV technology has already experienced a strong cost reduction due to the economy of scale over the last 2 decades.

II. Variation of installation costs for the battery storage system. We assume a cost reduction from presently 500 CHF/kWh down to 50 CHF/kWh in 2050, since batteries have just started to become a mass product and a strong cost down development may be expected [BNEF2019], [NatureEn2017].

III. We assume that about 20% of the total energy consumption may be saved due to energy recovery for deceleration of moving equipment or more efficiently operating motors when driven by variable frequency drives [IEA2011].

Additional hypothesis are required for the simulation such as:

- The installation costs of DC and AC converters are the same, assuming that mass production for DC-converters has been reached as in the AC converters nowadays. This assumption is justified, since from the technical point of view, DC converters should not be more complex (rather less) than AC-converters.
- Interest rate is 1.5%, with refunding over the lifetime, which increases PV-cost by 25% and battery costs by 12%.

The quantitative output of the evaluation is the time of return on investment, given in years for each of these variants with the variation of the different parameters I. to III. If not otherwise stated all the energy data per time interval are given as kWh per hour and are shown over an entire year.

3.6.3 Dynamic electricity pricing

We construct the dynamic price tariff **Scenario 2050** based on the following assumptions:

I. The same national hydropower and wind power capacity as in 2018 are maintained;
II. Installed PV capacity is multiplied by 18 to a total of 39 GW_p;
III. Nuclear and thermoelectric generation are equal to zero;
IV. No import or export is taken into account because the import site will in any case be the DGO's network, which will itself be controlled from abroad, if necessary.
V. The total hourly production must equal the consumption. For the time profile of the consumption, we use the 2018 electricity consumption profile and apply a weighing factor to achieve this equality.

Construction of power profile

For fulfilling the fifth assumption in the list above, we use the following input and methods. Hourly production data for nuclear, solar and hydroelectric power are taken from reference [entsoe2019]. The data differentiate for hydro-electric generation between the run-of-river part, the pump-turbine part and the accumulation part. Since the data are incomplete (e.g., for run-of-river generation with a total of 1.5 TWh instead of the 16.9 TWh given by [SFOE2018]). We used a weighting factor to obtain the total energy corresponding to the SFOE data. We used an installed total solar power for 2018 of 2.173 GWp, with a yearly production of 1.94 TWh.

Determination of PV-generation potential

By extrapolating the solar installation rate since 2011 until 2050, the total installed solar power in Switzerland could increase by a factor of five as shown in Figure 12. However, we assume a factor of 18, expecting advances in PV-technology, which influence profitability, deployment rate and growing awareness of the urgency to increase renewable energies. In particular, such an increase is required to be coherent with our aim of “strong penetration” of PV beyond 50% of total consumed energy per year.

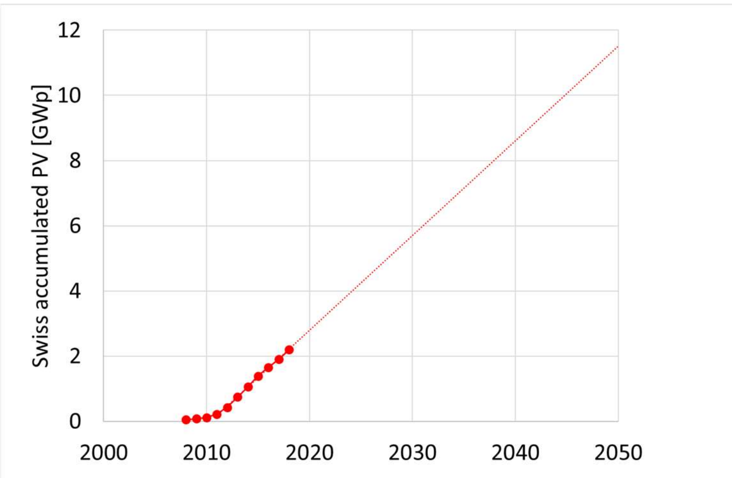

Figure 12: Evolution of accumulated installed PV power in Switzerland in recent years with a linear extrapolation of the installed power, yielding a total accumulated power of 11.5 GW_p in 2050. Data points are from reference [EE-Markt2018]

We construct a dynamic price $\Phi(t)$ based on the following assumptions:

1. Consumption profile of 2018 is weighted such the annual total equals production, i.e. 75.4 TWh.
2. The power profile of Swiss annual electricity consumption is the same as in 2018.
3. The mix of Swiss electricity production is modified according to the assumptions described at the top of this subsection and with the totals given in *Table 5*. This means that the electricity production is ensured in equal parts between PV and hydroelectric (i.e., wind is nearly negligible), with a total of 75.4 TWh per year, corresponding to an increase of about 11% compared to 2018. This increase seems reasonable, given that a large increase in electric transportation and heat pumps is expected.
4. Estimated average electricity price in 2050, according to *Figure 13*. The average curve was chosen, for 250 CHF/MWh, representing a 32% increase in the 2011 price (or an increase of about 30% compared to the 2018 price).
5. We chose an annual average price of the dynamic price fixed at $\overline{\phi} = 250$ CHF/MWh.
6. The minimum price is set to -50 CHF/MWh for historical reasons.
7. Daily smoothing between night and day is always achieved, since the battery equalizes the power drawn from the network over the 24 hours of the day.

Energy production	2018 [TWh]	2050 [TWh]
Hydro-electric	37.4	36.4
Nuclear	24.8	0
Solar	1.9	38.9
Konv.thermic & other renewables	3.7	0
Wind	0.1	0.1
Total production = consumption	67.5	75.4

Table 5: Assumed annual electricity production in 2050. For comparison, in 2018 the total (net) electricity production in Switzerland was 67.5 TW as taken from [SFOE2018]

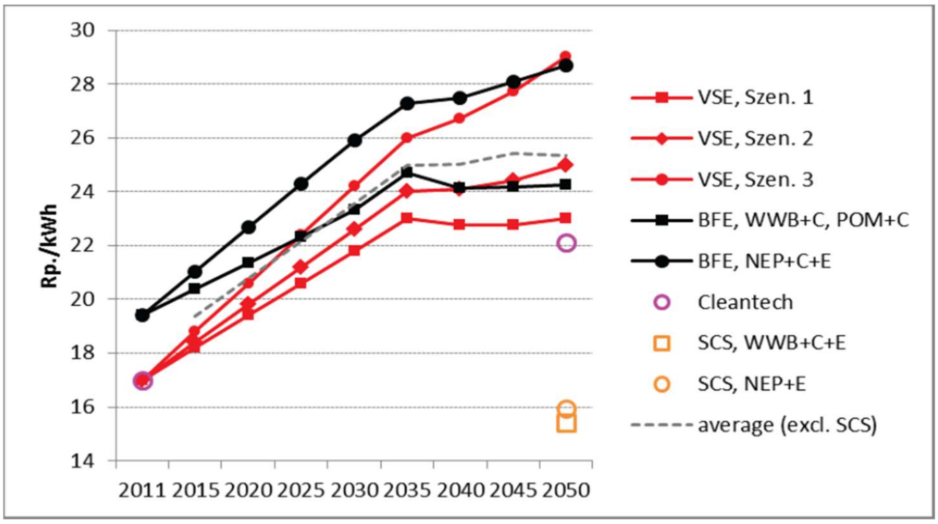

Figure 13: Scenarios of the price evolution for electricity until 2050. Reference [kWhCost].

The dynamic price Φ(t) is calculated as a function of the difference ∆E between production $E_p(t)$ and consumption $E_c(t)$ for each hour t. We adjust the dynamic price to obtain the assumed minimum price and the desired average price. Using these definitions, the calculations are defined as follows. A weighting energy σ= 26256 MWh is determined to obtain the desired minimum price:

a. $\Delta E(t) = E_p(t) - E_c(t)$
b. $\Phi(\mathrm{t}) = \overline{\phi} \cdot (1 - \frac{\Delta E(t)}{\sigma})$

As a result, we obtained a maximum price of 336 CHF/MWh.

The minimum price -50 CHF/MWh has been fixed, since historically the electricity prices, which were lower than this value, turned out to be due to errors in forecasts and lack of experience of the market with stochastically varying energy production, and market participants “hope” that it does not occur again. This hypothesis should be discussed as well in upcoming more detailed analysis on the influence of dynamic pricing.

By assumption, the electricity reinjection rate is based on the price of the sale of electricity with a fixed difference of ∆ϕ=70.3 CHF/MWh (if, for example, the price of the purchase of electricity on 1 January at midnight is 307.3 CHF/MWH, the reinjection price will be 237 CHF/MWh). This ∆ϕ =70.3 CHF/MWh comes from the average of the differences (between purchase and reinjection prices) of the four SIG tariffs, given in *Table 4*. It is necessary to discuss whether such a fixed difference is reasonable in the future, but in this paper, it has been assumed that this difference is only dependant of the transportation fee on the grid of this energy.

Figure 14 and *Figure 15* present two weeks, one during the winter in January and one during summer in July, to illustrate the resulting calculated dynamic prices. In January, the dynamic price is usually higher than the average price, because production is permanently insufficient to satisfy consumption. At this point, it is reasonable to trust the market rules, because an inequality between production and consumption is technically impossible. In reality, potential electricity suppliers will either install more means of production or use more storage to cover these gaps between consumption and production.

The same argument must be stressed for the situation in summer, *Figure 15*, where the dynamic price is permanently lower than the average annual price during the day. During the day, this is a consequence of highly abundant solar power. Solar production is subject to strong variation between night (PV power = 0) and day. As a result, the price varies greatly between the predefined minimum negative value and a slight overrun of the average annual price during the night.

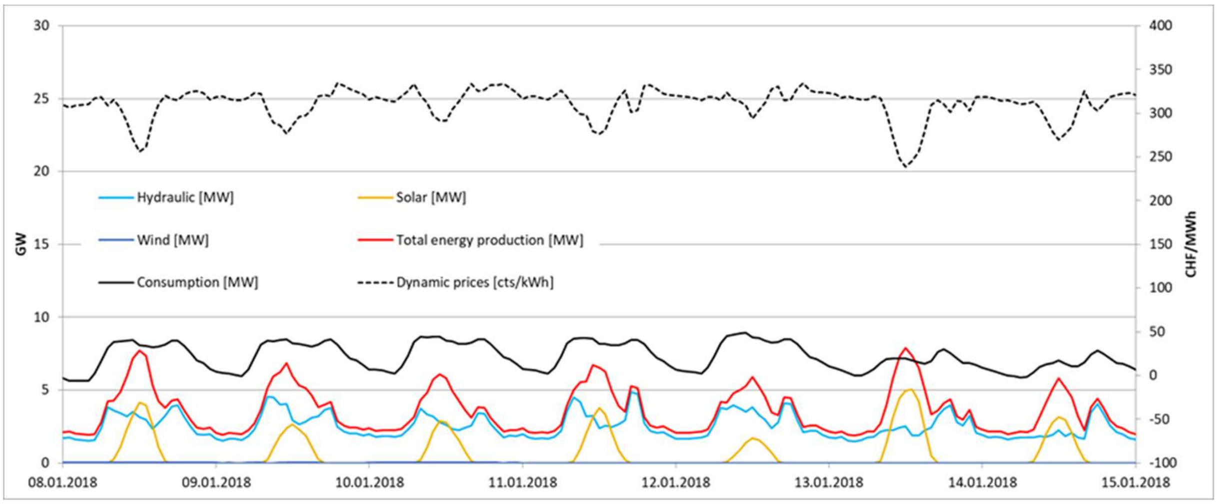

Figure 14: Dynamic electricity prices for a week in ***winter*** *2050, obtained with the algorithm and assumptions described in the text.*

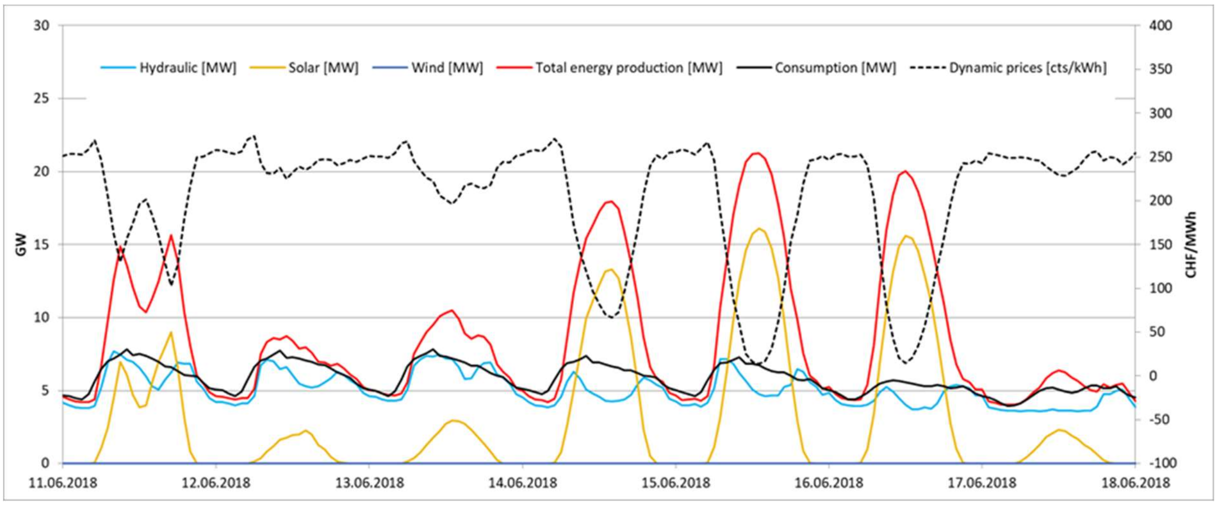

Figure 15: Dynamic electricity prices for a week in ***summer*** *2050, obtained with the algorithm and assumptions described in the text.*

4 Results and discussion

The achievements are described in the following sections following the project objectives that are listed in section 1.3.

4.1 Installation and operation of the DC-microgrid demonstrator

The demonstrator of the DC-microgrid is up and running on a permanent basis. This permanent operation is indispensable for continuous progress on performance by elimination of everyday problems, which occur not frequently but limit the reliability due to a too short MTBF. In addition, this demonstration is an ideal show-case for potential future end users in real industrial field or more general commercial applications.

As demonstrated through the example shown in section 4.4 and 4.5 which concern of the regulation algorithm and the evaluation of the reliability of the DC-microgrid, the entire power regulation is operational. This algorithm can work only properly with all hardware components connected to the power link (i.e. the 700 V DC-bus) as well as to the data interfaces.

4.2 Development of power electronics

The required power electronics were developed as described in section 3 and in the annex A, additional information can be found in [Capponi2018] and [Morey2019]. These developments were a major goal of the project, as a proper evaluation of the DC-microgrid demonstrator requires the full system operation in order to demonstrate the technology to interested users. While most of the converters were not available on the market at the beginning of the project, the situation has changed since then and a certain part of components can now be purchased. However, it will always be required to verify and test the compliance of specifications with the requirements of the DC-microgrid. The voltage level compliance as well the regulation characteristics and communication protocols must be suitable. The importance of this key topic should not be underestimated as soon as it comes to installation of microgrids on real test sites outside of a protected laboratory environment. The technical readiness level of this hardware will be determining.

It is worthwhile to comment on the choice of the DC-bus operating voltage. The choice of a +/-350 V DC-bus voltage has been made already at the very early stage of the development. The choice of the most suited standard (“nominal”) voltage of the DC-bus depends on the following basic considerations. The bus voltage must be at least large enough to allow injection into the AC grid at any time. Here a 700V DC-bus voltage can be considered in a bipolar configuration i.e. +/-350V.

1. The peak voltage on the AC side is $U_{AC-peak} = \sqrt{2} \times U_{rms} = 1.41 * 230\,V = 325\,V$. Thus for switching the DC-bus voltage of on pole onto any of the three phases L1, L2 or L3 the DC-pole must at least provide this value.
2. However, since the AC-standards allow a tolerance interval of +/-10 % around the peak voltage, instead of 325V the AC peak voltage may rise to 325 V + 32.5 V = 357.5 V. Thus, the half DC voltage must allow for this AC tolerance, e.g. be at least of this value.
3. In addition, there will be switching losses in any power electronics circuit and voltage drops on impedances. For these voltage losses, a safety margin of 20V was taken and it means that the DC-bus should have a voltage of 357.5 V + 20V = 377.5 V on each pole.

In total, doubling the two half-voltages to the total bus voltage we reach:

$$Ubus = 2 \times \sqrt{2} \times (U_{AC-pe} \quad + 10\%) + \text{margin} = 2 \times \sqrt{2} \times (230\text{Vac} + 23\text{Vac}) + \text{margin} = 718.5\text{Vdc} + \text{marge} \approx 758.5\ \text{Vdc}$$

Therefore, the international standard will probably be set around +/-380 V to allow sufficient margin for converter losses. Note that after upgrading to the new AFE an increase of our bus voltage from 700 V to 710 V was required to avoid shut downs due to voltage limitations.

4.2.1 Safety & EMC

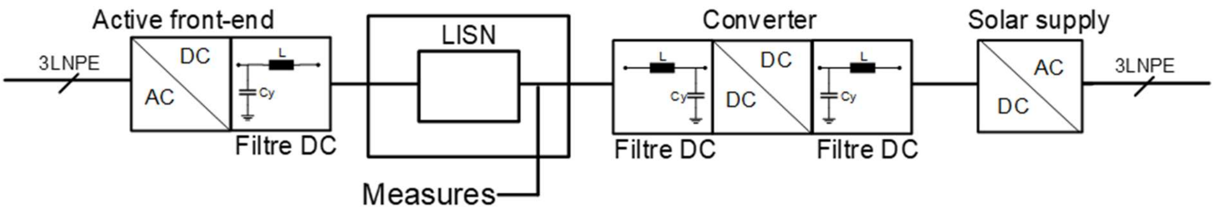

Figure 16: Measurement configuration for the EMC measurements with and without filtering the higher harmonics, created by the AFE and the serial PV-converter build at HEIG-Vd.

The description of the installed current sensors, supervising the leakage current to ground, is given in annexe A, see *Figure 59*. In addition to human safety, the machine safety must be assured, which is commonly referred to as electromagnetic compatibility EMC. EMC measurements have been carried out on the DC-bus, with the first prototype of the serial DC/DC converter connected, see *Figure 16*. The measurements were done in two different configurations: between the DC-bus as a whole and ground, usually referred to as common mode, and between the positive and negative pole of the DC-bus, called differential mode.

Since the various converters produce higher harmonics themselves, it was found necessary to install a filter for their reduction. Here we analyse in particular the harmonics created by the AFE and the converter for an entire PV-string, since they have the highest power, and are thus expected to create the strongest EMC perturbations. The results of common mode and differential mode with and without filter are shown in *Figure 17* and Figure 18. These results show, that even though we work on DC-lines, the consideration of EMC cannot be neglected. The application of filters seems necessary and for future applications, the DC/AC and/or DC/DC converters need to be checked for their EMC-performance.

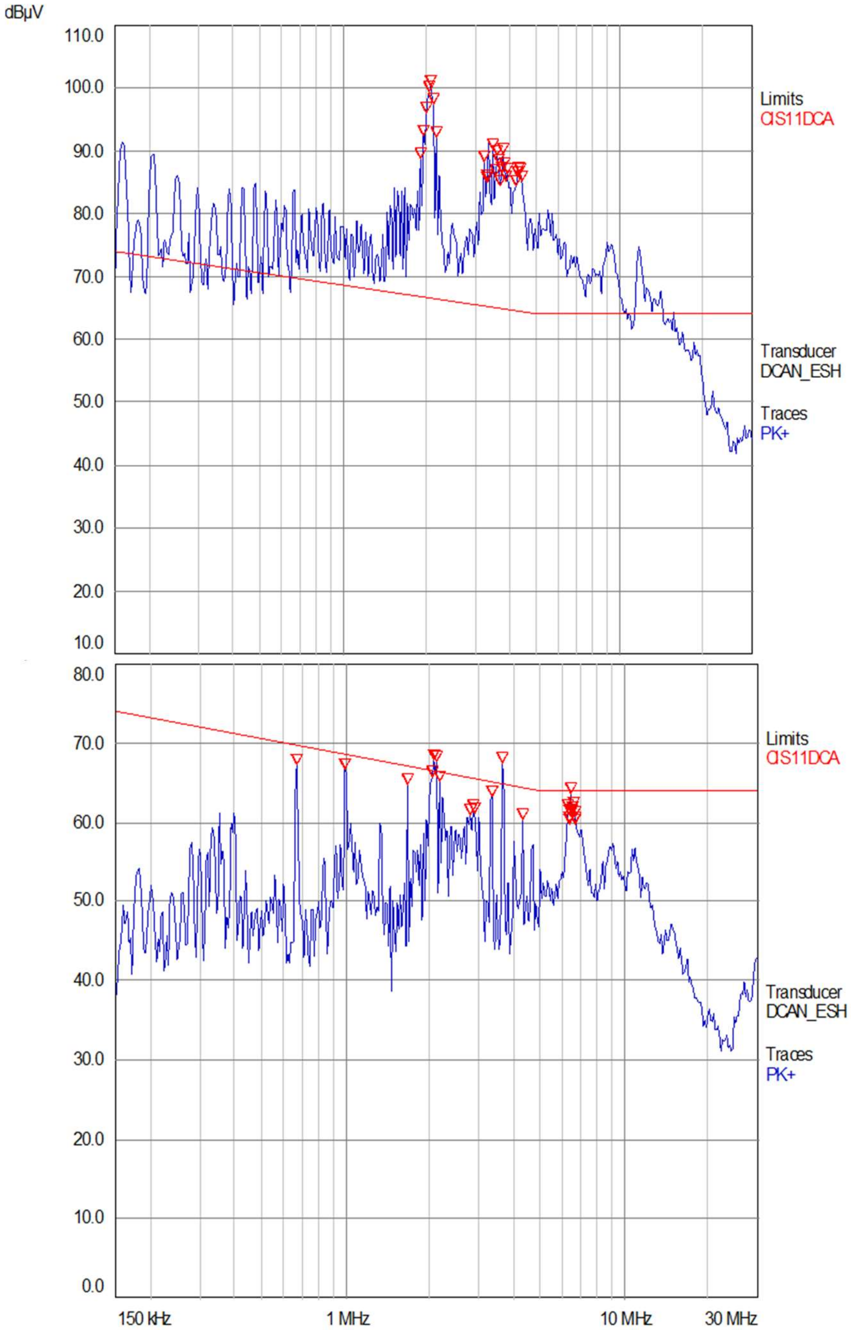

Figure 17: EMC measurements in ***common*** *mode (relative to ground) without (above) and with filter (below), with AFE and string PV-converter.*

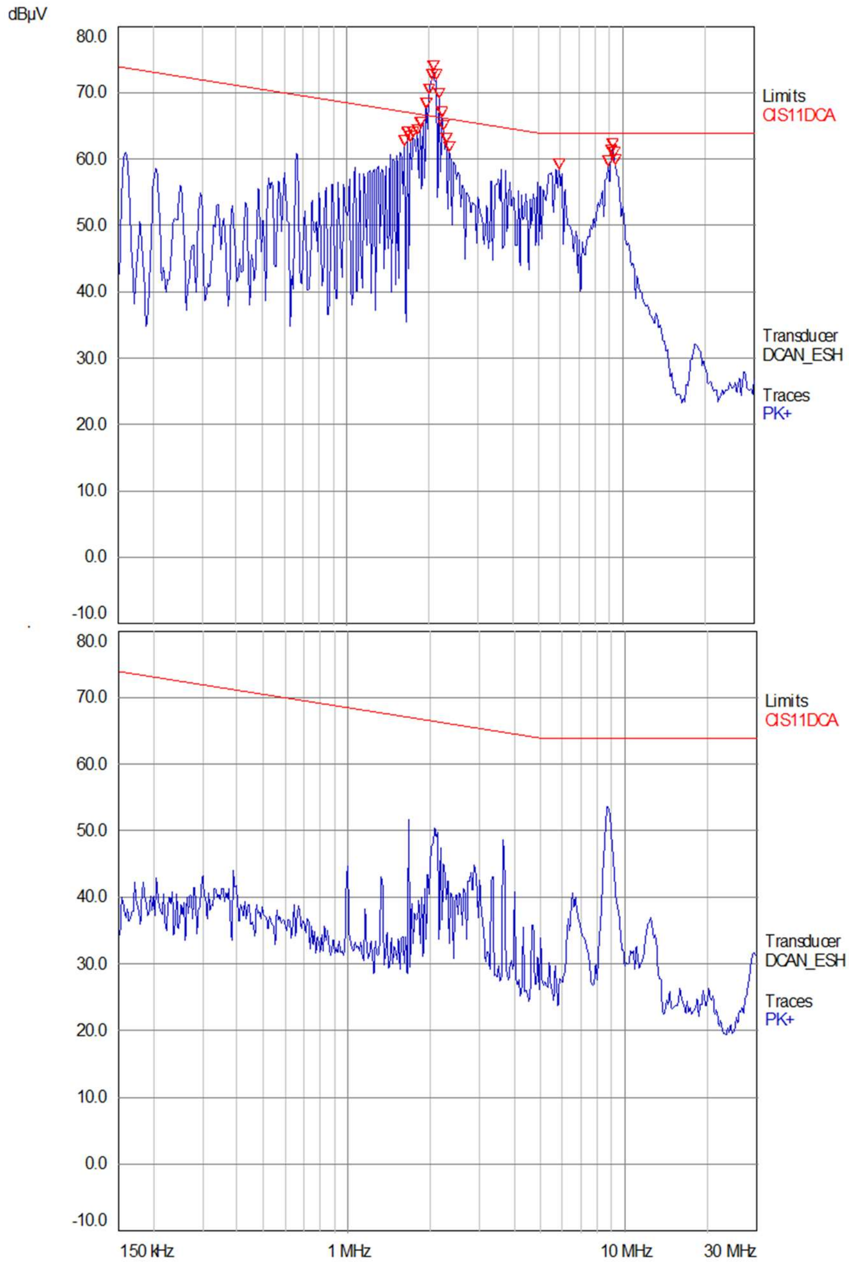

Figure 18: *EMC measurements in* ***differential*** *mode (between + and – pole of the DC-bus) without (above) and with filter (below), with AFE and string PV-converter.*

4.3 Evaluation of DC-converters for individual PV-modules

The independent DC-bus system installed at EPFL in Neuchatel (described in section 3.3.1) allowed an independent evaluation of the performances of the DC/DC converters from Imperix and HESSO Valais. PV-Lab Neuchatel operates a PV plant with 22 modules (not connected simultaneously) and analyses its operation since January 2017. Thanks to a lab-grade monitoring set-up, we installed twin modules on both the DC-bus and the monitoring set-up. In this way, we are able to compare the performance of both modules independently. Prior to the installation of these modules, they were characterized in standard test condition in order to ensure the correctness of future calculations. The performance of the PV modules coupled to the DC bus is evaluated by comparing their relative power output at any time t with the relative power output of the same modules on a dedicated installation referred as PV-monitoring

$$Relative\ power\ output = P_t/P_{stc}$$

Where P_t denotes the power of a given module at time t, and P_{stc} represents the nominal output power of that module under STC. The monitoring installation performs maximum power-point tracking and an I-V characteristic curve every three minutes. It allows then to compare at every-time the power output of the modules that are on both installations. Although the modules are the same, their power output under 1-sun condition might deviate from the nominal power, as shown in *Figure 19*.

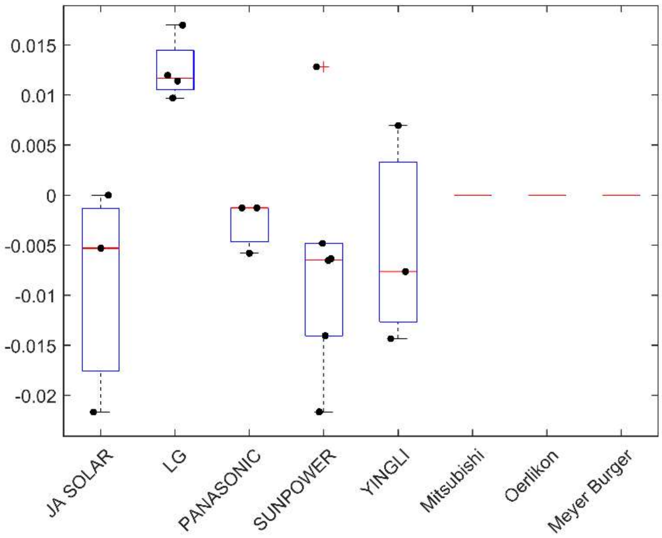

Figure 19 Relative difference between the maximum power as measured and the nominal power (grouped by manufacturer). The module types named Mitsubishi, Oerlikon and Meyer Burger are not commercially available. Therefore, no specifications are publically available.

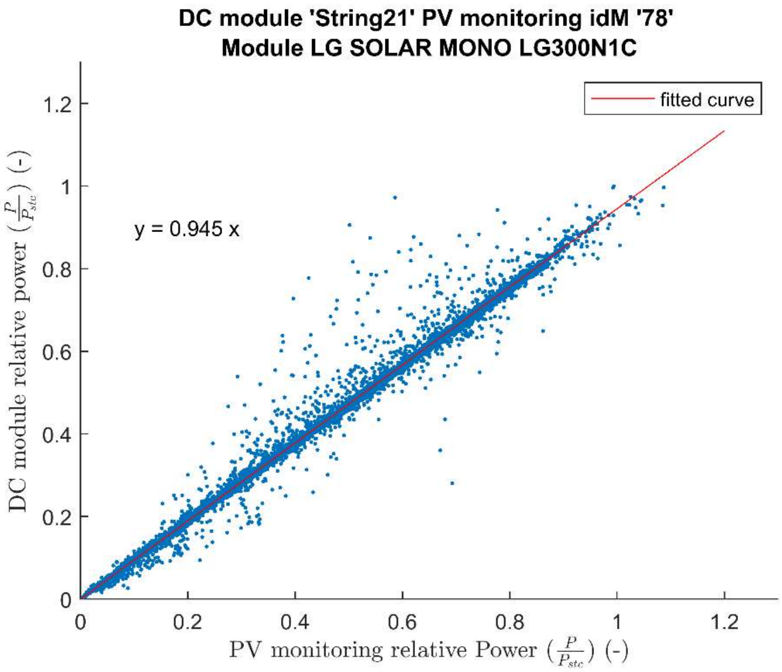

Figure 20 Relative power output of one PV-module connected via a DC/DC converter on the DC-bus vs the relative power output of the same module on the PV monitoring set-up.

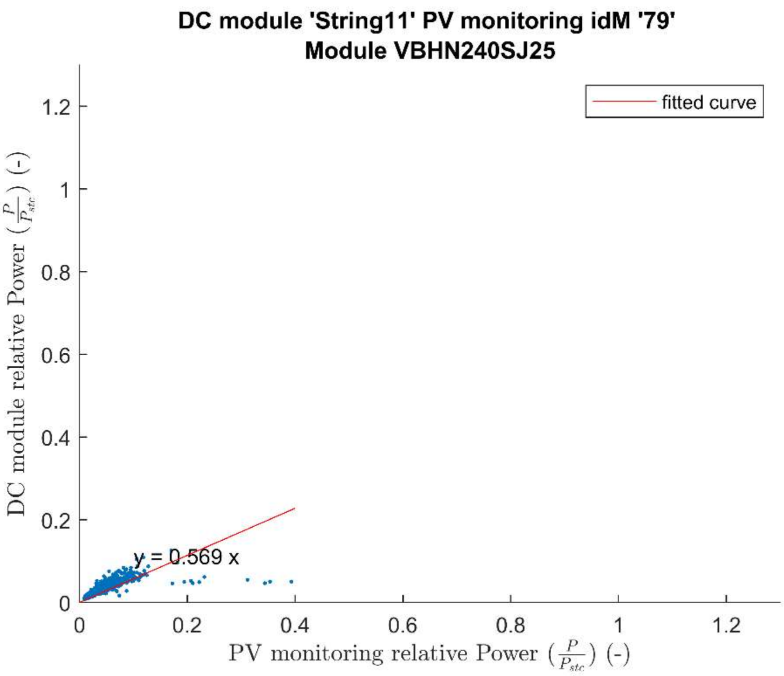

Figure 21 Relative power of a DC module with much less performance, the details for String 11 are given in Table 3*.*

This method allows comparing the modules on both installations as pictured in Figure 20. For sake of comparison, a filter was applied to select the points when no shadow is present as shadow can be different from module to module. In *Figure 20*, the linear regression with a slope of 0.945 means, that this particular module on the DC-bus performs roughly 5.5% less well than the module on the PV monitoring setup. In the example in *Figure 21*, the converter is not working properly for unknown reasons, and cannot go beyond about 15% of the nominal power P_{stc} of the modules. Following this quantitative information, useful for debugging of the concerned DC/DC converters, Imperix has been informed, to develop a remedy to this issue.

Such regression has been performed for all modules that have a clone on the reference monitoring installation. The slope a, with its confidence interval [a_{min}, a_{max}] and R^2 coefficient are reported in *Table 6*. In general, the coefficient are greater than 0.9 with a few exceptions with the Imperix converter, which have shown some mal-functions.

id	Converter Type	a	amin	amax	fit_R2
String02	HES	0.941	0.940	0.942	0.962
String20	HES	1.008	1.007	1.009	0.992
String21	HES	0.945	0.944	0.946	0.993
String22	HES	0.935	0.934	0.935	0.993
String23	HES	0.938	0.937	0.939	0.991
String25	HES	1.001	1.000	1.002	0.991
String26	HES	0.993	0.992	0.994	0.993
String27	HES	0.917	0.915	0.918	0.986
String28	HES	0.956	0.954	0.957	0.984
String11	Imperix	0.569	0.546	0.592	-0.229
String12	Imperix	0.989	0.986	0.992	0.951
String13	Imperix	0.991	0.988	0.993	0.953
String15	Imperix	0.768	0.751	0.785	0.863

Table 6: Coefficients characterizing the analysis: Slope a, of the linear regression, its interval of confidence [amin, amax] and R^2 coefficient for each modules on the DC-bus. The id (string_xx) represents the name, which is given to the module throughout the entire evaluation.

In a finer way, the distribution of the relative power difference between the relative power of a particular module on the DC-bus $\frac{P_t^{dc}}{P_{stc}^{dc}}$ to the relative power $\frac{P_t^{PVm}}{P_{stc}^{PVm}}$ of the same module type on the monitoring installation is defined as:

$$relative\ power\ difference = \frac{\frac{P_t^{dc}}{P_{stc}^{dc}} - \frac{P_t^{PVm}}{P_{stc}^{PVm}}}{\frac{P_t^{PVm}}{P_{stc}^{PVm}}}$$

This relative difference is pictured in Figure 22 and Figure 23 for, respectively, HES converter and Imperix converter. Data above zero means that the module on the DC bus performs better than the module on the monitoring station while data below zero means the opposite. In both figures, the data

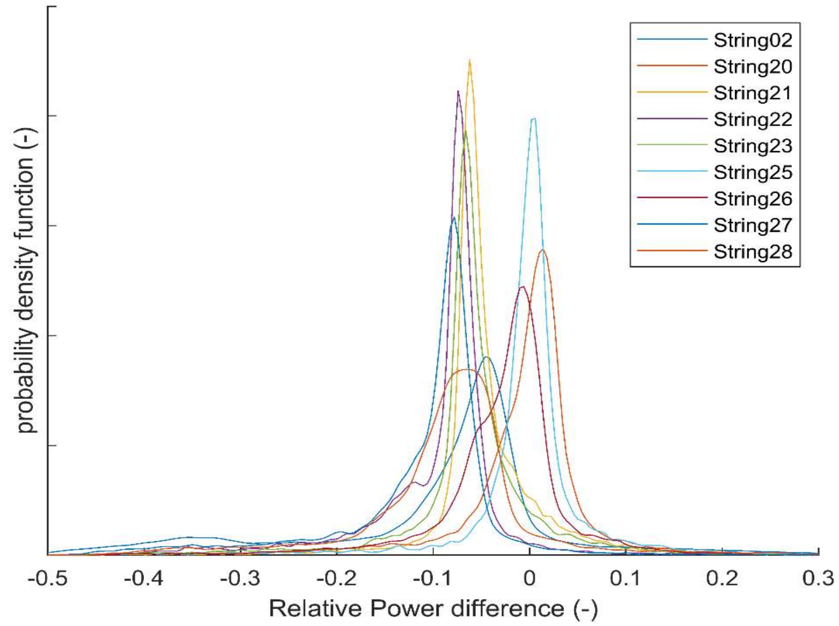

Figure 22 Relative power difference distribution for the HES converters.

are filtered to eliminate shadowing effects in the analysis. To filter-out shadowing, the condition is to keep the instantaneous performance ratio greater than 0.5 for every measurement at time t:

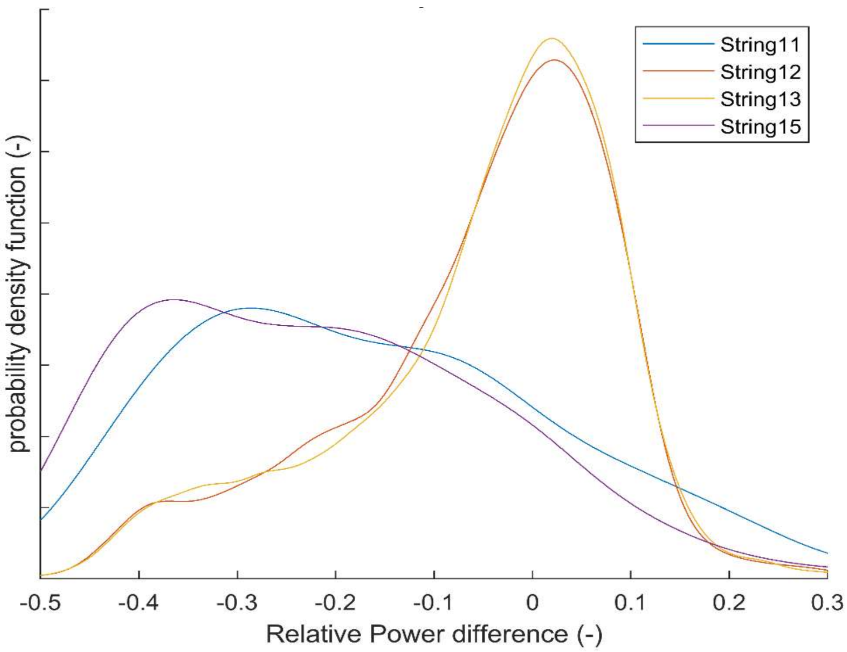

Figure 23 Relative power difference distribution for Imperix converter

$$t|0.5 < \frac{\frac{P_t^{dc}}{P_{stc}^{dc}}}{\frac{G_t}{1000\frac{W}{m^2}}} < 1 \;\&\; 0.5 < \frac{\frac{P_t^{PVm}}{P_{stc}^{PVm}}}{\frac{G_t}{1000\frac{W}{m^2}}} < 1$$

Where the global irradiance G_t in the module plane is precisely measured by a pyranometer, tilted and oriented exactly as the PV-modules. This filter also ensures that all systems are operating correctly, thus, the periods when the DC bus is down are also excluded. This condition is applied for both modules, the one on the DC-bus as well as for the module on the monitoring installation. Only for those times where this instantaneous PR is larger than 0.5 for both modules we consider no shadowing conditions. Note that this filter does not filter out measurements at lower irradiance G_t due to low sun position in the morning or evening, neither does it exclude a slightly overcast sky. These conditions with lower global irradiance G_t are still kept in the diagrams due to the division by Gt in the filter defined above.

The relative power difference distribution for all HES converters seems approximately centred between -10% and 0 as seen in *Figure 22*. This agrees well with the results of the regression of

. However, the distribution for the Imperix converter is wider (see Figure 23). Thus, more investigation

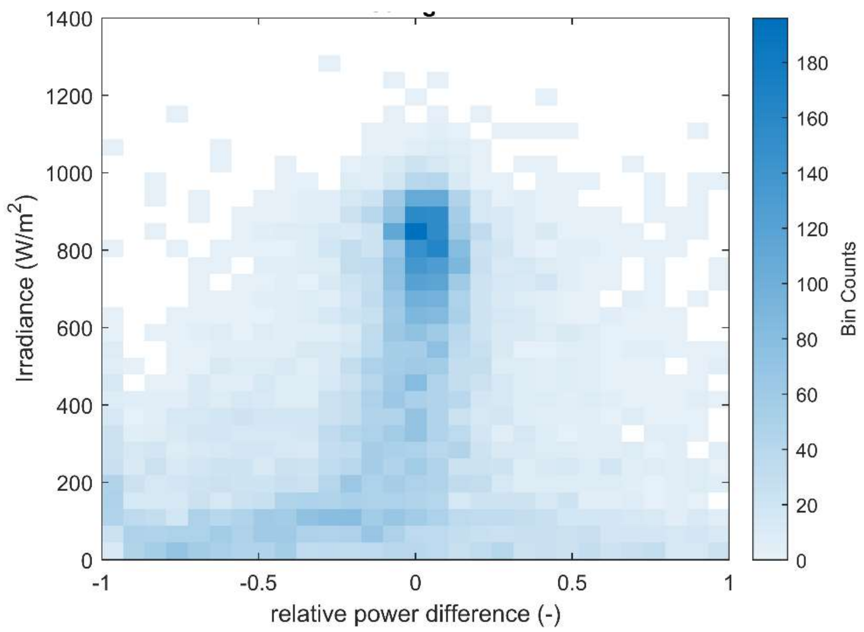

Figure 24 Distribution of the relative power difference and irradiance for String 12, with an Imperix converter behaving normally.

were conducted to understand these abnormally behaving Imperix converters.

There is a clear shape difference in *Figure 23* between String 12 and 13, both having a maximum around 0 relative power difference and String 11 and 15, where the peak is abnormally shifted towards large negative values. By plotting the very same distribution as a function of the irradiance, for converter String 12 or 13 (see Figure 24 for String 12), we notice that the relative power difference is close to 0 at high irradiance and the spread increases at low irradiance (moving also on the left). However, the same figure for converter String 11 and 15 (see Figure 25 for String 11) indicates that the same difference at all irradiance levels. This lets us think that the converter is unable to transfer the power to the bus although it is well connected to the lines.

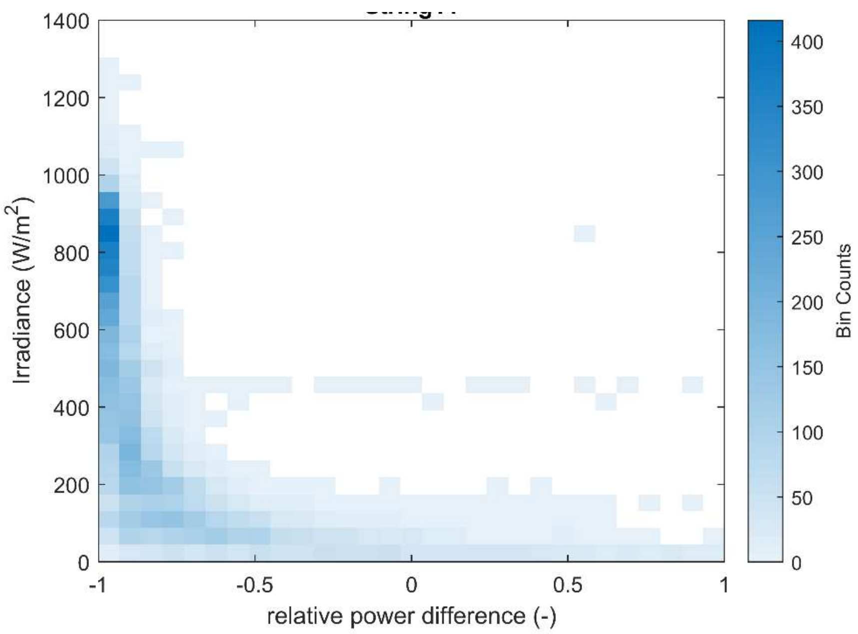

Figure 25: Distribution of relative power difference and Irradiance String 11, showing an abnormal behaviour.

Finally, the performance ratio *PR*, defined in the following equation are pictured for the whole analysis period in *Figure 26*.

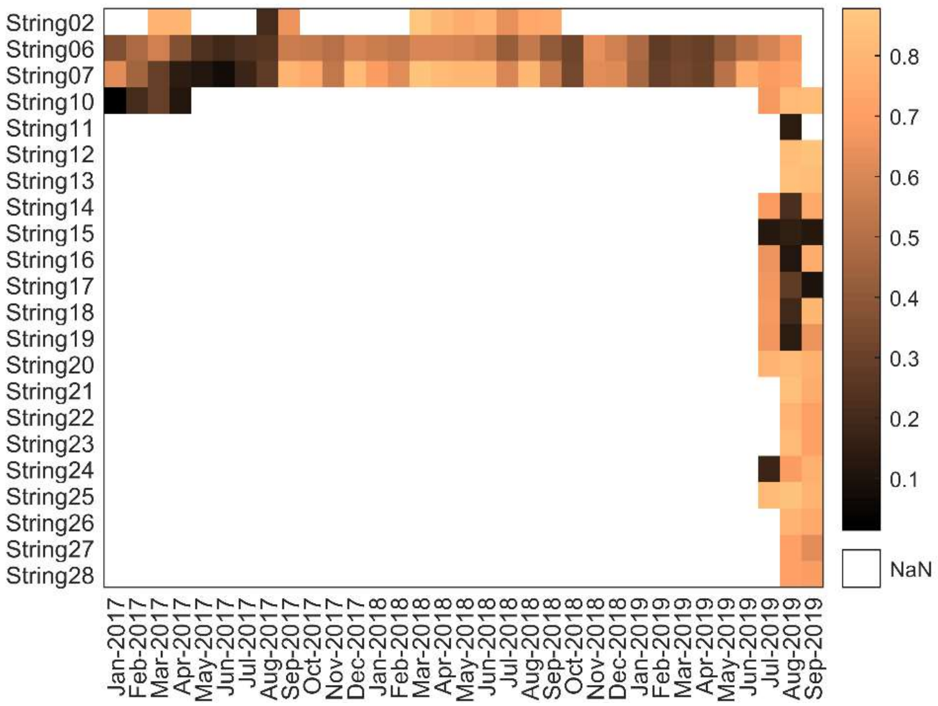

Figure 26: Performance ratio PR per module on a monthly basis for the entire evaluation period from January 2017 until September 2019. Only four converters were operational from the very beginning, since the new converters were only installed in summer 2019.

$$performance\ ratio = PR = \frac{\int P_t dt}{\int P_t^{stc} \cdot {G_t}/{1000}\, dt}$$

A comparison of the mean performance ratio of each DC module with those obtain on their clones on the PV monitoring installation highlights the fact the DC bus is performing well in average except for a few Imperix converters (see Figure 27 and Figure 28).

It must be noted that low-performance ratio may be due to the module itself. This is why the comparison

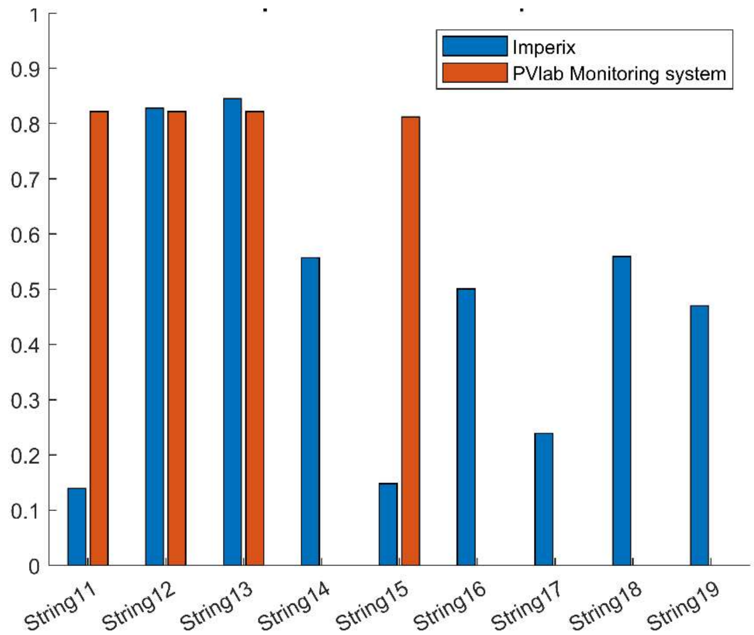

Figure 27: Mean performance ratio of all Imperix converters at PV-lab/EPFL.

with a reference lab-grade installation is useful as it highlights if any lack of performance on the DC converter may be present. This allows us to note that the HES converter seems to perform on average almost as good as the PV monitoring facility, while the Imperix converters may have a lack of reliability.

The comparison of the power output of each individual pair of modules allows us conclude that the DC-bus is performing to an acceptable level given that the difference with the monitoring set-up are small. In addition, we are able to identify potential paths for improvement for the developed Imperix converter. First, it seems that some converter suffer from reliability issues which might be easily corrected in future versions of the product. Second, the performance at low irradiance might be improved. Since the major part of the energy is not generated at low irradiance, this problem has a low impact on the total performance of the installation.

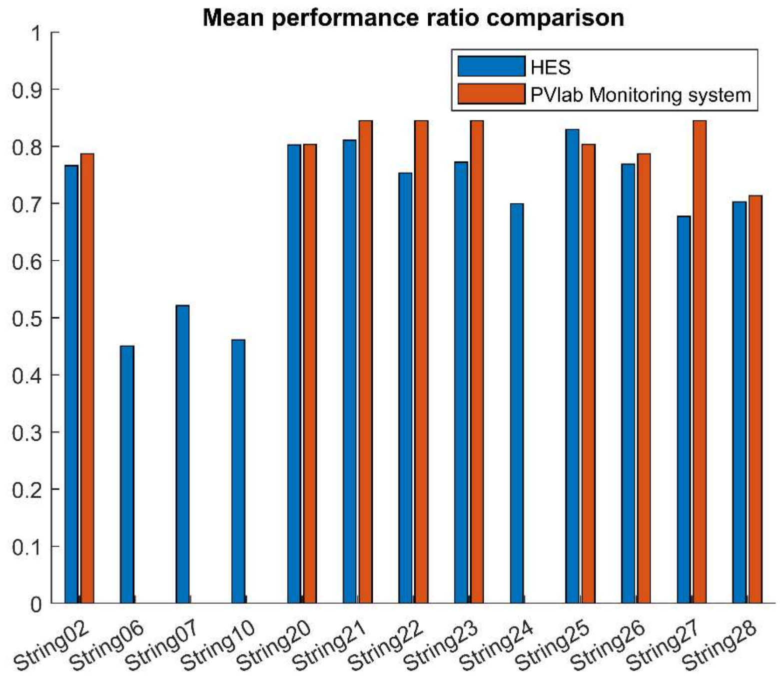

Figure 28: Mean performance ratio of all HES converters at PV-lab/EPFL.

4.4 Evaluation of reliability

The reliability of the DC-microgrid at HESSO-Valais is of high importance for any potential end user. This is due to two main reasons: firstly, electric power is in central Europe generally considered a commodity of high availability and secondly, power cuts usually cause major costs in every operation of any manufacturing company.

Data collection for the DC Bus began on 25.06.2015. Thus, an evaluation and demonstration of the operational reliability of the DC-microgrid uses data starting from the 1.07.2015. The corresponding graphs represent the results of the reliability analysis over the last five years.

For this analysis, all DC bus interruptions were taken into account:

- Defects ("failures")
- Maintenances
- Tests
- Voluntary shutdowns of the facility

This analysis shows a lower limit of the MTBF, caused by real defects. For example, the number of stops of the DC Bus in 2019 was 221 times but only 70 were due to faults. An annual evaluation of the number of failures per year, the resulting uptime and the MTBF is shown in *Figure 29*. Since the absolute values depend in some cases on the evaluation period, and in particular, the evaluation was accompanying the development, the evaluation period has been varied in order to show evolution with time.

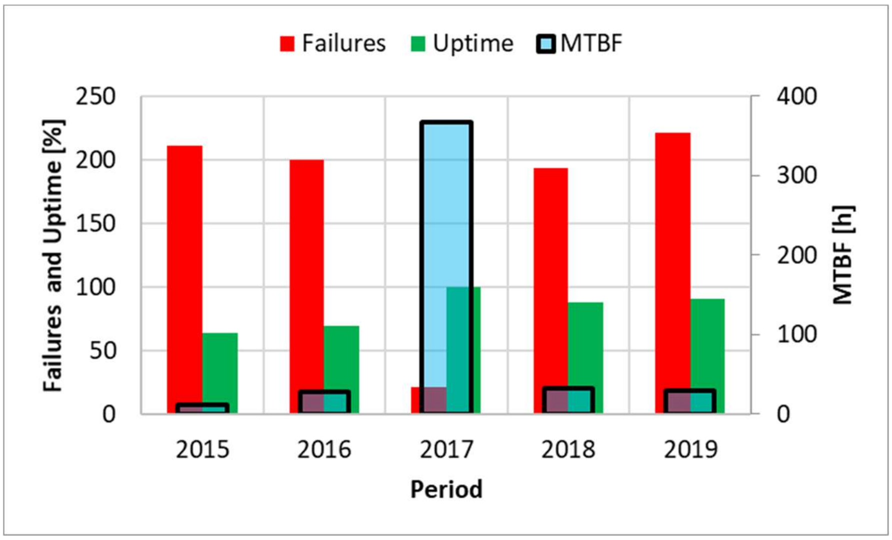

Figure 29: The number of failures, the corresponding uptime in percent and the mean time between failures MTBF, evaluated for the calendar years since 2015, the first installation of the original DC-microgrid, starting from 01.07.2015 until 31.10.2019.

At present, the DC bus is started manually. The shutdown of the system during faults could be shortened by setting up the automatic restart of the installation. This would increase the uptime significantly since every shutdown occurring during a weekend leads to an additional unnecessary downtime of about two days, whereas generally the elimination of a potential fault and restart only cause one or several hours.

From 2017 until spring 2019, when the AFE of first generation was in operation, the majority of failures was coming from ground faults and too high PV-production beyond the maximum of the AFE. The installation of battery storage and a first energy-balancing algorithm, which could store power excess into the batteries, allowed eliminating this cause.

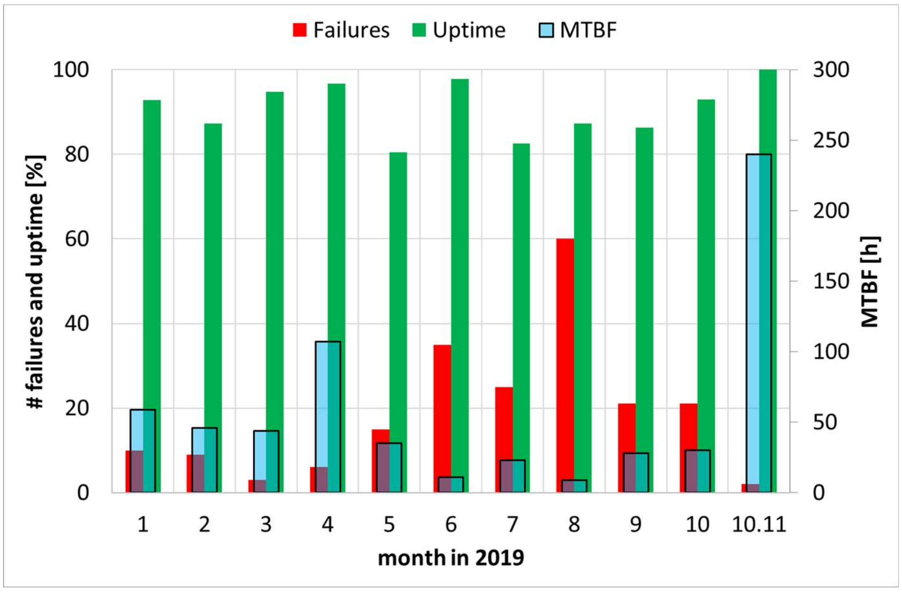

Figure 30: Evaluation of the total number of failures (including voluntary stops for maintenance and testing), uptime and MTBF on a monthly basis for the year 2019, from 01.01.2019 until 31.10.2019. The start-up issues of the AFE leading to frequent shut downs in the summer months are clearly visible.

After the installation of the AFE of second generation, the main stops of the DC Bus are due to the detection of errors caused by the newly developed AFE. As an error example, the internally programmed voltage limits were defined too tight compared to voltage excursion during operation. These “teething problems” have substantially been reduced throughout the operational month during summer 2019. The evaluation of the same quality parameters as in *Figure 29*, but on a monthly basis throughout 2019, is given in *Figure 30*. In general, the year 2019 is marked by multiple tests of the different modes of the regulation algorithm as well as equipment commissioning periods (battery storage, various DC-DC converters, AFE). The Month 10-11 in *Figure 30* corresponds to the period from 15.10.2019 to 14.11.2019 during which the DC Bus operated without any voluntary shutdown. Consequently, only two real errors occurred, one of which due a breakdown of the ICT network, which underlines the importance of separating regulation of bus-stability via the power electronics from ICT based regulation of the energy management system. During this period from 15.10.2019 to 14.11.2019, the uptime reaches almost 99.96% (down time = 8min for 31 days) and the MTBF correspondingly 240 hours. The values demonstrate the reliability, which is possible already now and sets the bar for further optimization reaching realistic reliability of the DC-microgrid in the coming years.

4.5 Regulation performance

The regulation algorithm for the energy management has been developed in order to fulfil various objectives. The smoothening of the PV-power at the DC/AC interface to the distribution grid has been one main objective. The regulation method changes according to the objectives pursued. For the mode 1, two different software packages were developed, using different optimization strategies. In the following two sub-sections the performance of both EMS is described: first, the version of HESSO Valais and second by HEIA-Fribourg. For more details on the latter refer to annex B1.

4.5.1 Regulation Mode 1 – version HESSO Valais

Mode 1 has been operated throughout the years 2015 until end of 2018 without considering a production forecast in order to test the entire DC-microgrid while improving the individual components.

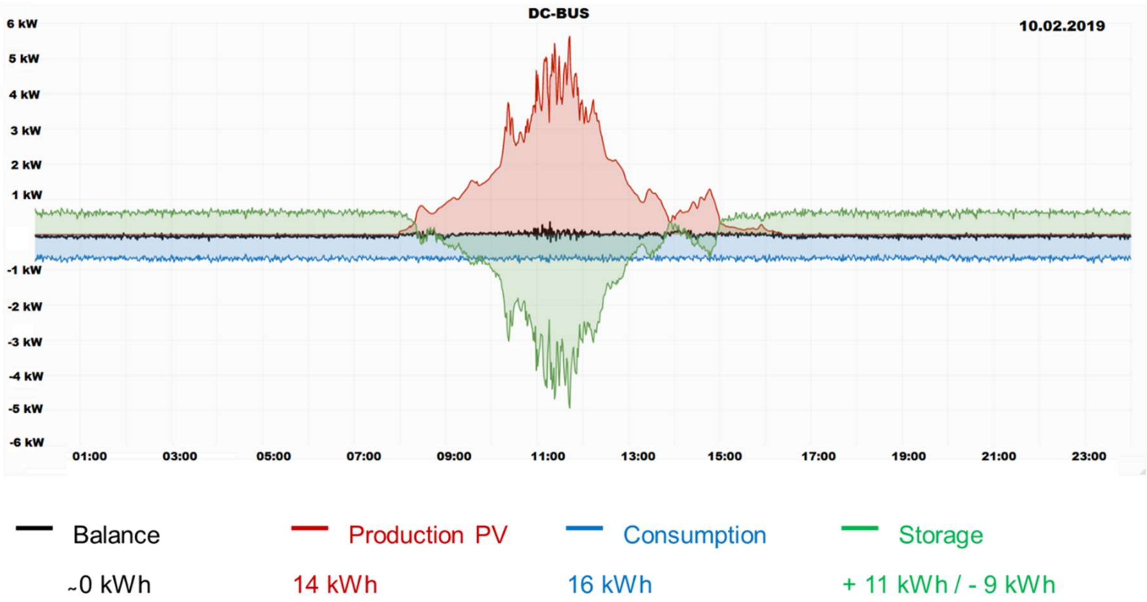

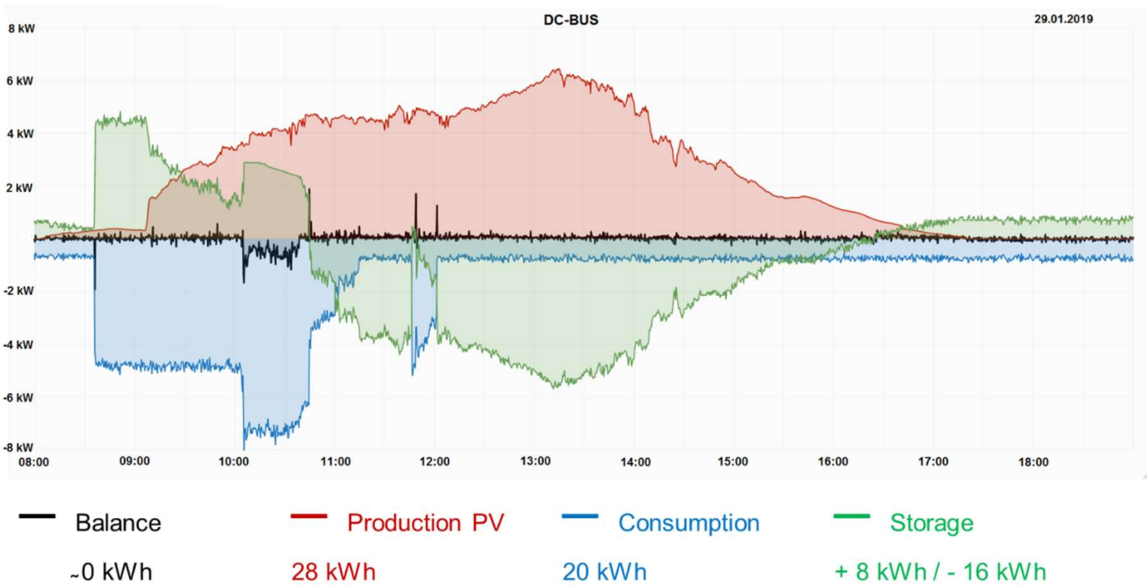

Figure 31: Example of the performance of the regulation algorithm, achieving a complete smoothening of the DC/AC balance in spite of strongly varying PV-power generation. The vertical axis displays the power in kW. The figures under graph show the integrated power over the day.

In this operating mode the regulation aim is to minimize the power balance between the DC-microgrid and the AC-distribution grid in spite of strong variations of either PV-generation or consumption. The economic benefit of the such a minimal DC-AC power balance is that an industrial user pays in addition to the amount of energy used a fixed amount per month for the maximum power received form the DGO, evaluated over an entire year. As can be seen from the examples in *Figure 31*, the algorithm smoothens the DC/AC balance at the interface to the AC-grid nearly perfectly, for slowly (above) or strongly varying (below) consumer power. In both cases, the energy balance (integrated power balance) is nearly zero.

At the beginning of 2019, the production forecast was available and could be integrated into a forecast algorithm. Using the predictive algorithm, described in section 3, the EMS calculates the optimal power trajectories of the BSS (Batteries Storage System) and AFE for two days in advance. These are calculated based on weather forecasts, installed photovoltaic production capacity and known load consumption. These calculations are updated every 6 hours (0h/6h/12h/12h/18h) to compensate for forecast errors, see an example of this outcome of such a recalculation at 12h in *Figure 32*.

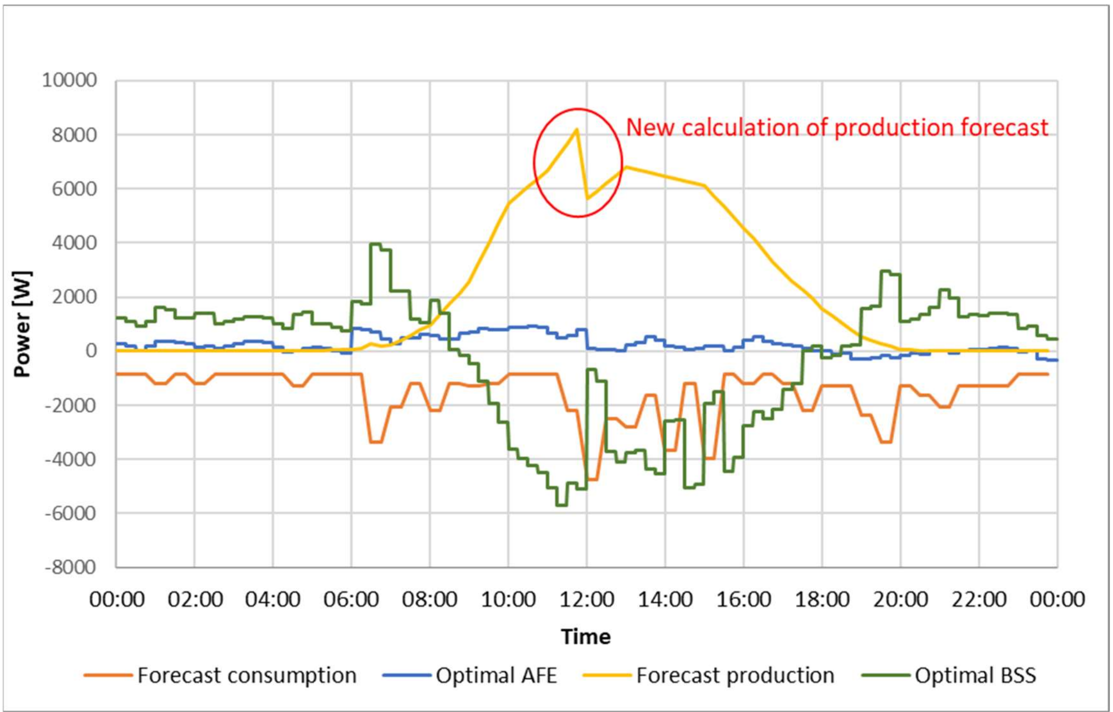

Figure 32: EMS Power Forecasts 24.09.2019 and adaption of the forecasts at 12h, after recalculation of the power trajectory by the genetic optimization algorithm.

The control of the power deposited into or extracted from the BSS allows indirectly the regulation of the energy flow through the AFE in mode 1. All converters connected to the DC Bus communicate their power and other parameters to the EMS in real time with approximately 5s latency. This latency is due to the transmission time of signal via gateways and cloud-IO to and from the EMS and thus clearly disentangles fast voltage regulation from energy management. Thus, in the event of unforeseen consumption, such as the arrival of an electric vehicle for battery charging, the EMS adapts the BSS setpoint so that the AFE power remains constant (see *Figure 33* at 4:30 pm). Since the storage system supplies the energy to the electric vehicle, the decrease of the SOC of the BSS is evidently faster.

In mode 1, deviations of the real consumption compared to the forecast are compensated using the BSS by the EMS. The AFE transmits the deviation between real PV-generation (green curve) and PV-forecast (yellow) into (or withdraws from) the AC-grid (blue curve in *Figure 34* between 8am and 18pm). After adaptation of the EMS (algorithm), production gaps could also be absorbed or compensated by the BSS. Rapid variations in production or consumption always pass through the AFE due to the delay of the measurement loop. This issue is solved by operating Mode 2 (see below), since then the rapid voltage control on ms-time scale becomes active.

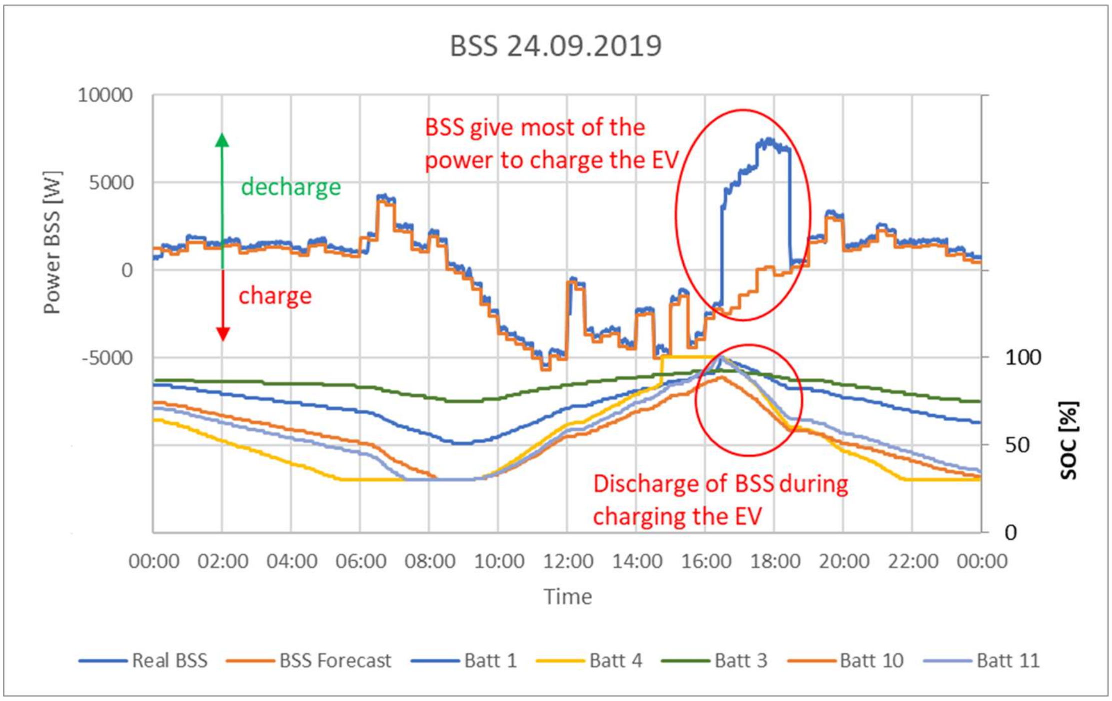

Figure 33: Battery charging event of an electric vehicle arriving unforeseen at the EV-charger on 24.09.2019. Below is shown the corresponding SOC of the batteries, which supply the required power such that the program of the AFE remains unchanged.

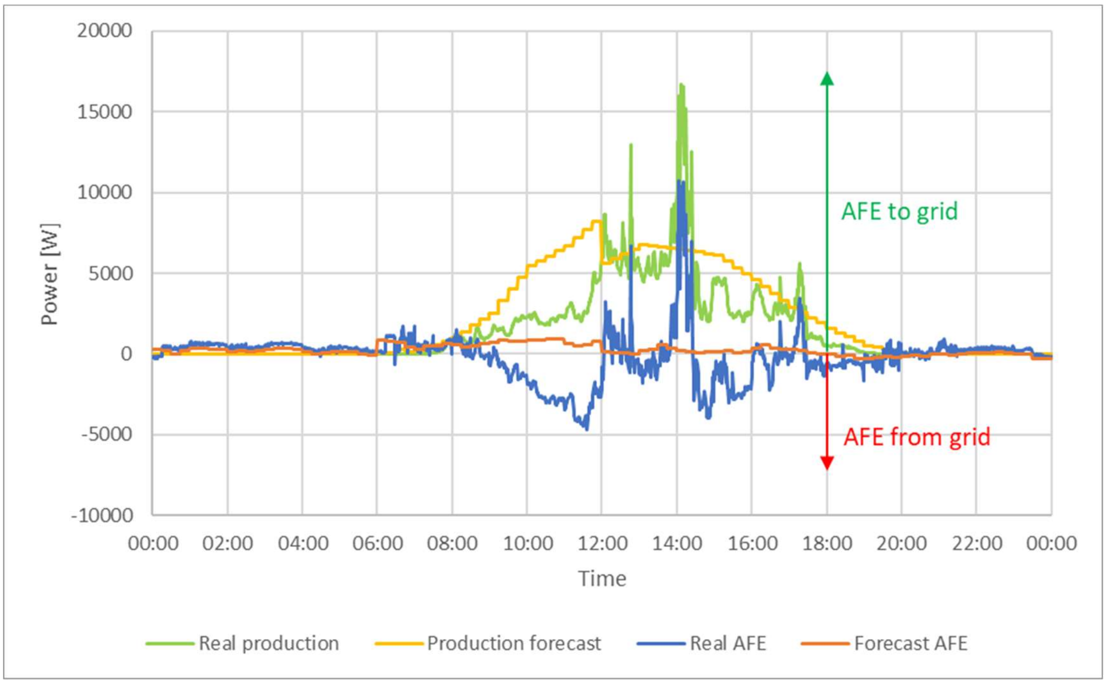

Figure 34: Sudden variations of PV-power generation on the 24.09.2019 and the resulting reaction of the AFE power.

4.5.2 Regulation Mode 1 – version HEIA-Fr

The EMS developed by HEIA-FR adopts the operating mode 1 to regulate the power flows in the DC-microgrid using the predictions computed with a forecast algorithm. Figure 35 illustrates one of the tests performed with the most recent version of the EMS.

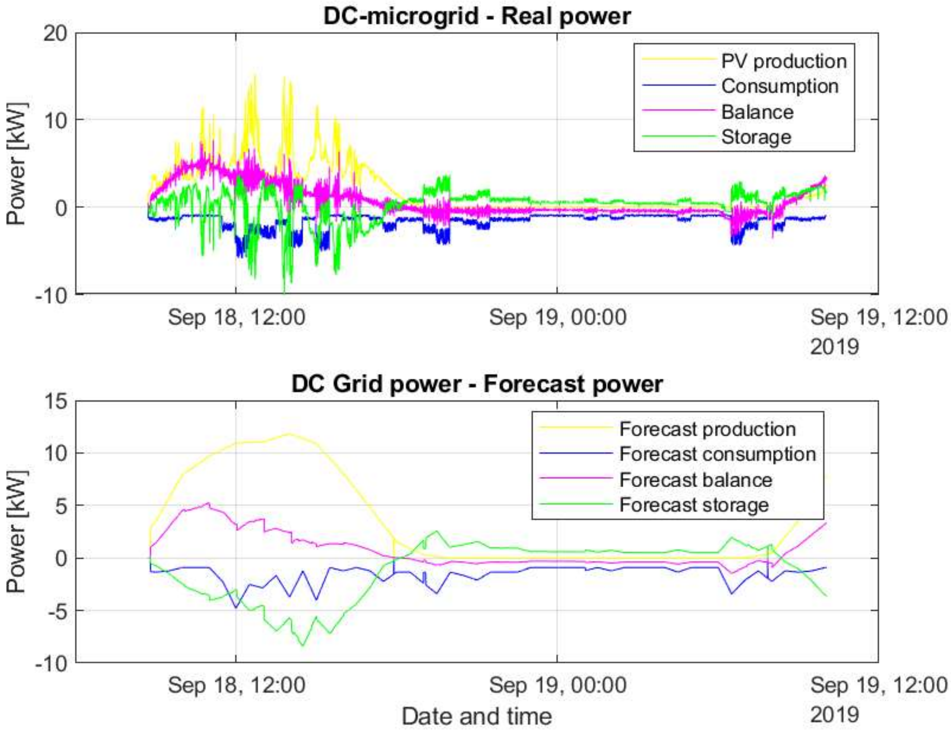

Figure 35: *Test results of the EMS in mode 1 on 18-19.09.2019. Above: real power values of PV-production, consumption, balance to the AC-grid and batter storage power. Below: the corresponding forecast values, as produced by the forecast algorithm of the EMS.*

To evaluate the performances of the regulation, the relative deviation of the energy from the forecast (defined as “Relative Delta” in section 3) is used as indicator and is computed every 15 min by comparing the forecast power exchanged between the DC-microgrid and the AC-grid (forecast balance) to the real power (balance), see Figure 36.

The smoothening of the DC/AC balance is successful if the absolute value of relative deviation from the forecast “Relative Delta” is lower than 1%. During this test, this goal was reached only 24.7% of the time. This result could be partially explained by the fact that the used indicator (Relative Delta) has some singularities, where it could not be calculated, despite having power profiles very close to each other. For example, for very small power values, only a few percent of the AFE nominal power, the relative Delta becomes already large for small deviations between forecast and real power profile, even though these situations are not significant for the power tax to be paid to the DGO. Furthermore, at this current state, the current state of the DC-microgrid has potential for improvement:

- Characterizing the health of the batteries,
- Testing and improving the robustness of the regulation,
- Increasing the accuracy of the algorithm computations.

By doing this, the percent of the success of the EMS could easily reach higher values. More details about the development of the EMS can be found in the appendix B.

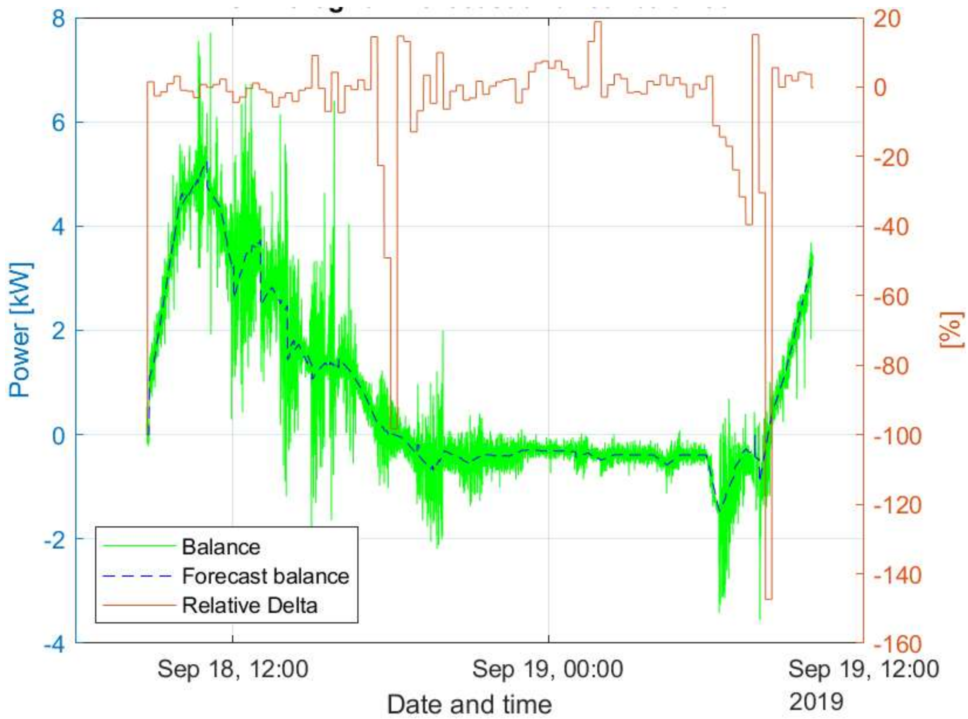

Figure 36: *Real balance, forecast balance and relative deviation from the forecast ("Relative Delta")*

4.5.3 Regulation Mode 2

An example for the performance of regulation mode 2 where the battery system regulates the DC-bus voltage is shown in *Figure 37* with high time resolution. Here the storage batteries have been used to simulate a sudden change in PV-power generation. While this (simulated) PV-power increases in two sudden steps at 18.65 s and 20.83 s, the regulation batteries are reacting instantaneously by extracting the required power from the DC-bus. Consequently, the DC-bus voltage is dropping correspondingly due to the droop control strategy and the power of the AFE (grey) stays perfectly constant at the set point of 2 kW as desired, not influenced by the sudden change in (simulated) PV-power. The same is observed at the (simulated) sudden reduction of PV-generation at 23.88s and 25.18 s, in the opposite direction.

In a future version of the EMS, the nominal working point for the SOC of the control batteries can be adapted according to the weather forecast of the following day. Thus, a high SOC will be the desired set point of the battery in the morning of a day, for which the weather forecast announces cloudy weather, and thus little expected PV-generation. On the opposite, a low SOC starting point will be the nominal working point at the beginning of day with favourable weather forecast, i.e. high expected PV-generation. Furthermore, in case the excursion of the real net production or consumption balance deviates strongly over a longer time interval from the forecast of production or consumption, the control

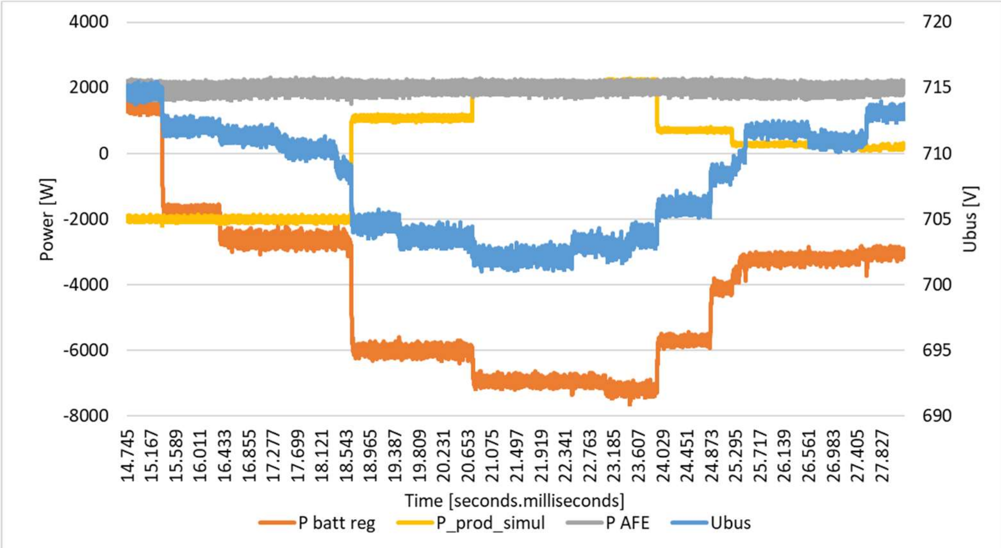

Figure 37: Regulation behaviour of the control batteries batt-Reg (orange) in response to a sudden power variation (yellow) on the DC-bus.

batteries will reach a SOC close to the edges of the allowed SOC range. Thus the storage batteries will give support to the control batteries by covering missing SOC range by releasing (or storing) the required energy, such that the control battery may permanently maintain the voltage of the DC Bus.

A critical criterion for the quality of the voltage stabilisation is the excursion time following a sudden power change on the DC-bus. The very fast return of the AFE-power to the set point value as measured with an oscilloscope is shown in *Figure 38*. Following a sudden (less than 8ms) power step of 3 kW

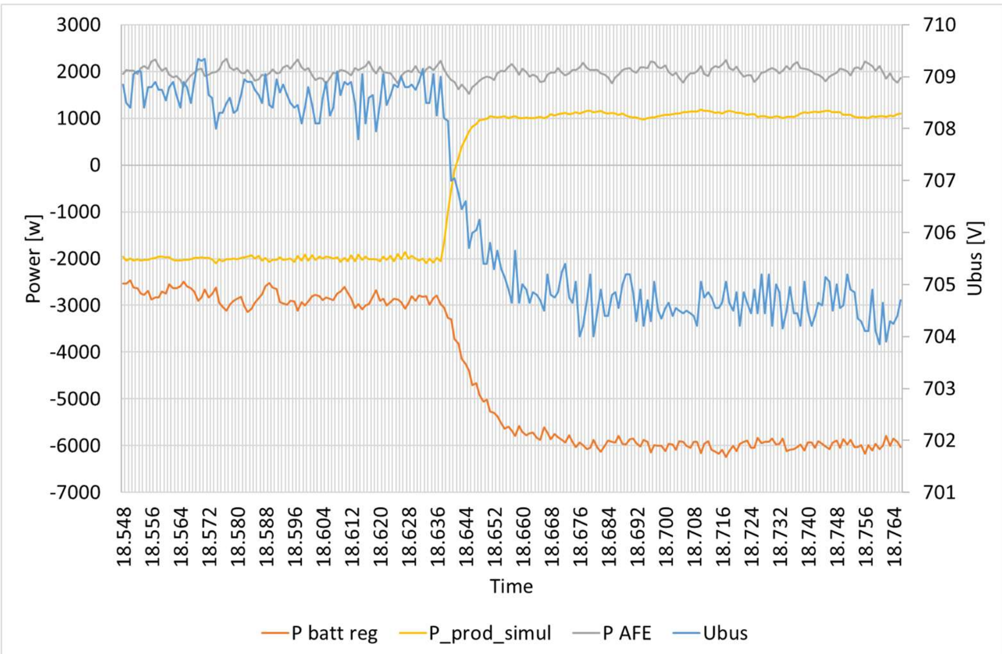

Figure 38: Zoom on the first event shown in Figure 37. It shows the power regulation of the regulation batteries and the AFE in response to a sudden positive power variation on the DC Link (P_prod_simul), The time scale is in seconds, i.e. the time resolution reaches milliseconds in this measured trace by an oscilloscope.

(yellow curve at 18.636 seconds), the AFE power (grey) drops only 250 W during 10 ms before it returns to its nominal behaviour. The DC-bus voltage reacts according to the droop control strategy of the regulation battery converter, shown as P_batt_reg (orange curve) in this regulation mode, the voltage is regulated automatically to the desired voltage by the regulation batteries.

Furthermore, a safety mode has been incorporated: in case a battery converter responsible for voltage regulation is dropping out, either due to loss of communication or due to reaching the limits of accessible SOC of the connected battery, the EMS will switch to another battery controller, such that sufficient regulation power and SOC range is always available.

The execution time of the genetic algorithm is about 20 minutes, thus it could be executed on a much shorter time interval than the presently used 6 hours. A future goal would be to implement a specific genetic algorithm, tuned for the domain of energetic optimization. This would further reduce calculation time and therefore allow an execution with high repetition time interval much shorter than the 6 hours, presently chosen. Currently, the EMS algorithm is not able to react on unforeseen events as for example high variations in consumption or production. Some experiences have been made by reacting on power consumption caused by an electrical vehicle connected to the DC-Microgrid. Some ideas how to react on such events may be carried out in a future research. One idea would be to implement an adaptive genetic algorithm with threshold trigger functionality. More frequent execution of the genetic algorithm at shorter time intervals would help to better respond to large variations in consumption and production, since the trajectory of the storage batteries could be adapted soon after the occurrence of such an event. This would help to reduce the deviation between forecast given to the DGO and the real AC-balance.

4.6 Influence of microgrid topology on distribution grid

The simulation of the impact on the distribution grid showed varying degree of impact on the required regulation needs for the three scenarios tested. Figure 39, Figure 40 and *Figure 41* illustrate the power to be supplied by the DGO for the three scenarios which are discussed in section 3.5 and, for clarity purpose, are repeated below.

Scenario 1: 5% of the clients of the distribution grid operator produce half of their electricity needs per year locally. This is approximately the situation in Switzerland in 2018.

Scenario 2: About 60% of the clients in a distribution grid produce 50% of their electricity needs per year locally. It means considering that about 30% of the electricity would be generated with strongly fluctuating renewable sources. For Switzerland, this scenario is far from the present situation. However, such situations are abroad already a reality today as seen for limited periods in Germany during 2019 where this situation was reached or even surpassed.

Scenario 3: 90% of all participants produce 50% of their electricity needs per year locally. It means considering that about 45% of the electricity would be generated with strongly fluctuating renewable sources, which in Switzerland is a big leap in the future, given the current slow installation rate of solar power generators.

The sign convention used in the figures is such that power values are negative if power is provided by the DGO and positive if it has to be absorbed. In this section the DGO, distribution grid operator, is as well referred to as DGM or DNM, i.e. distribution grid or network manager.

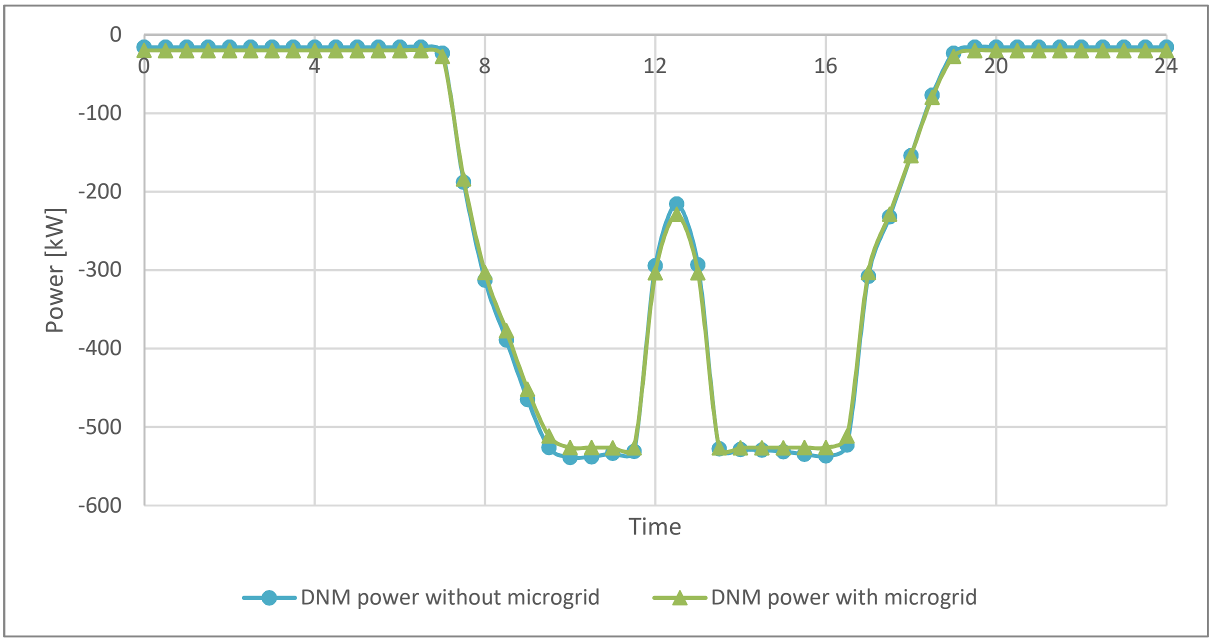

Figure 39 : Scenario 1: comparison of the influence of the DC-microgrid technology for the power provided by the DGO during the day.

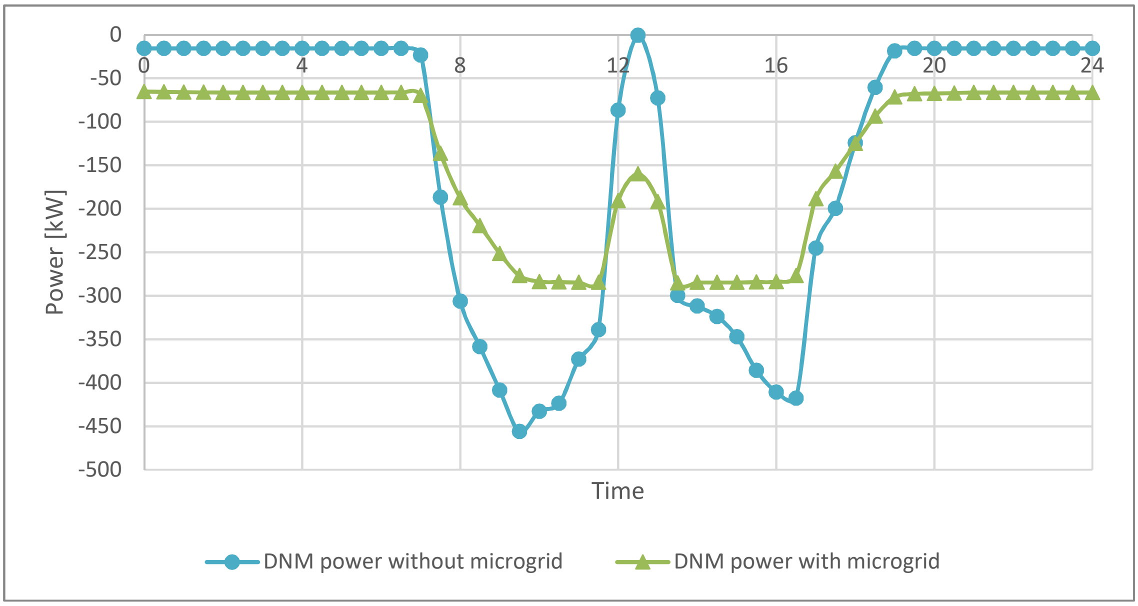

Figure 40 : Scenario 2: comparison of the influence of the DC-microgrid technology for the power provided by the DGO during the day (time in hours).

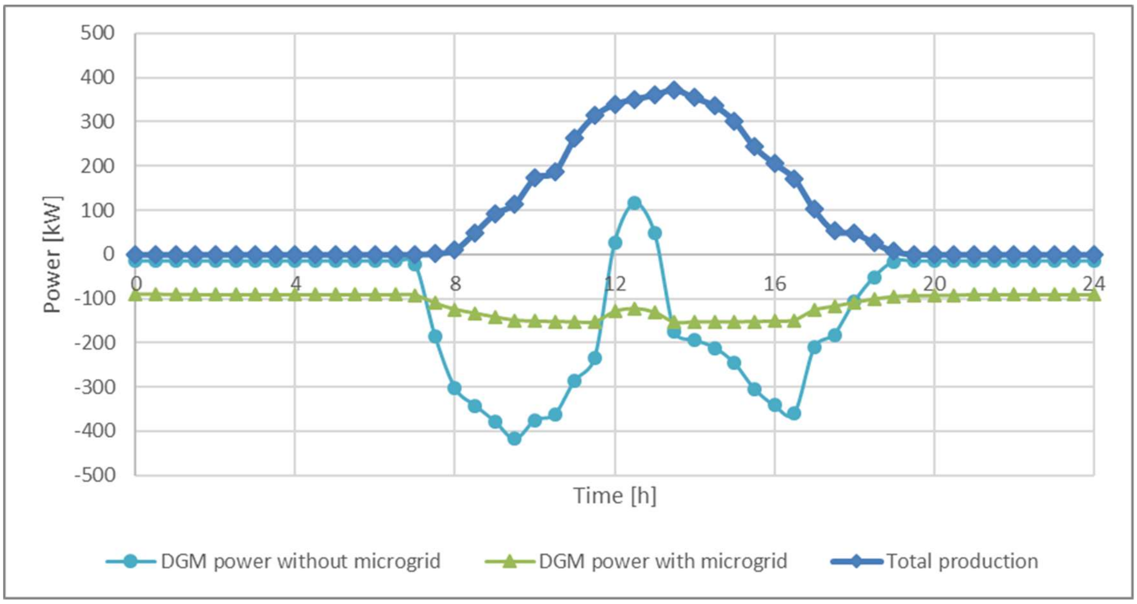

Figure 41: Scenario 3: comparison of the influence of the DC-microgrid technology for the power provided by the DGO during the day. For comparison, the total generated power by all PV-plants within the distribution grid is shown as well. It shows the positive influence of the multitude of microgrids for the incorporation of a large quantity of PV power.

The more clients are using microgrid, the lower is the power the DGO must provide and the lower are the power fluctuations. Scenario 3 represents the best situation for the DGO, as the maximum power is around 154 kW (instead of 418 kW) and its fluctuation is limited to 24kW/30min (instead of 260 kW/30min).

The DGO gains numerous advantages from this described widespread use of microgrids, like:

- The DGO does not have to cope with very dynamic power fluctuations, which makes the power management easier and cut down the corresponding costs.
- As less power is provided, smaller power reserves must be kept by the DGO, reducing the cost to buy or rent these reserves.
- The infrastructure components will be cheaper as they have to support lower power and lower power fluctuations.
- A good strategy may optimize the electricity transmission, leading to reduced power losses and increased global efficiency of the distribution grid, which presents a commercial benefit for the DGO.

The details of the simulation can be found in the annex B2.

4.7 Economy: Return on investment

Before we present the results of the economic analysis, we recall here the three tariff scenarios, as defined in section 3.6,

1. **Fixed price of 2018** : real electricity price of SIG for 2018, with 4 tariffs : full hours and low hours, both for winter and summer
2. **Fixed price, extrapolated to 2050** : as 2018 but increased by 30%
3. **Dynamic pricing, for 2050**: developed as described above, following essentially the common market rules of a scarce or abundant commodity.

For each scenario, three variants of the PV investment costs and three for the battery costs were examined (see section 3.6), which below we named “High”, “Medium” and “Low” price, as summarized in Table 7.

Investments variation	PV [CHF/kWp]	Battery [CHF/kWh]
High (2018 prices)	1100	500
Medium	900	200
Low (2050 expected prices)	740	50

Table 7 : Definition of the three cost variants for the investment costs for PV and battery.

A summary of the results can be found in Table 8 for which the following comments/definitions are useful.

- Maximum power: Maximum energy demand of the network over one hour, divided by one hour, so it is the maximum power of the year on an hourly average.
- Power utilization time (DUP): Ratio between maximum power (averaged per hour) and consumption. The higher this DUP is (i.e. closer to 8760 h), the smoother the consumption will be. DGOs use this indicator to establish pricing schedules.
- An interest rate of 1.5% per year was taken into account to calculate the total investment
- Payback time is the total investment cost divided by annual earnings (so interest rate is considered, but not panel aging). The latter simplification is unusual (since in most cases aging is considered), however, since many of our assumptions are very coarse, this detail does not change a lot on the conclusions drawn.

No optimization of the battery management is taken into account, i.e. the regulation of the battery does not take advantage of dynamic tariffs in order to have a better economic profitability. Instead, the battery is charged and discharged directly according to the difference between production and consumption to smoothen the strong PV variations as to maintain the technical promises of the microgrid.

General parameters	Actual conditions, no PV, no battery	Actual condition, only PV	Actual condition, PV and battery	Actual condition, PV and battery, no energy saving on DC motor	Dynamic prices 2050, low PV and battery prices	
Electricity prices	2018, Fixed prices	2018, Fixed prices	2018, Fixed prices	2018, Fixed prices	2050, Dynamic prices	
Installed PV power	-	2.5	2.5	2.5	2.5	MWp
Battery capacity	-	-	7	7	7	MWh
Energy saving on the DC motor	20%	20%	20%	0%	20%	
PV price	-	1 100	1 100	1 100	740	CHF/kWp
PV life expectancy	-	30	30	30	30	Years
Battery price	-	-	500	500	50	CHF/kWh
Battery life expectancy	-	-	15	15	15	Years
Energy balance sheet						
Total electricity demand	4.3	4.3	4.3	5.0	4.3	GWh
DC Request	4.1	4.1	4.1	4.8	4.1	GWh
AC Request	0.2	0.2	0.2	0.2	0.2	GWh
PV production	0.0	3.1	3.1	3.1	3.1	GWh
Network Request	4.5	2.9	1.5	2.2	1.5	GWh
PV						
Self-consumption rate	-	50%	94%	97%	94%	GWh
PV to DC	-	1.5	1.5	1.7	1.5	GWh
PV to AC	-	0.1	0.1	0.1	0.1	GWh
PV to Network	-	1.6	0.2	0.1	0.2	GWh
PV to battery	-	0.0	1.3	1.2	1.3	GWh
Battery pack						
Full battery proportion	-	-	6%	4%	6%	(90% or more)
Empty battery proportion	-	100%	39%	49%	39%	
Energy transfered to the battery	-	0.00	1.33	1.23	1.33	GWh
Power consumption						
Max. hourly power demand	1 019	1 019	943	1 097	943	kW
Max. power with battery smoothing	-	-	562	667	562	kW
Power usage time	4 250	4 250	7 713	7 551	7 713	Hours
Investments over the lifetime						
Battery pack	-	-	7 869	7 869	787	kCHF
PV installation	-	3 435	3 435	3 435	2 311	kCHF
Total investments	-	3 435	11 304	11 304	3 098	kCHF
Electricity savings over a year						
Resale of electricity	-	95	11	6	10	kCHF
Saving electricity	-	268	452	369	726	kCHF
Saving on power taxation	-	31	29	32	29	kCHF
Total earnings over the year	-	394	492	408	764	kCHF
Return time	**-**	**8.72**	**23.00**	**27.72**	**4.05**	**Years**

Table 8: Summary of results for selected main tariff scenarios with variants for investment cost (PV, battery), all assuming a DC-microgrid for electricity distribution on the reference industrial site.

The indicated power values in *Table 8* always represent an hourly average (i.e. the energy recorded for one hour divided by a time of one hour). For each hour, priorities of energy usage are defined as follows:

- The PV production is with first priority consumed by the DC part (engine, equipment and heating ventilation), then in second priority by the AC equipment, then to charge the battery and if anything remains injected into the AC-grid.
- In order to avoid losses at the DC/AC converter the energy of the battery is solely used to power DC equipment and never to power AC equipment.

Figure 42 shows the operation of the battery, hour by hour without optimization, i.e. the battery is directly charged by the power difference between PV-production and consumption or discharged when the consumers requires it. This serves as reference for comparison to the following, where optimization is applied.

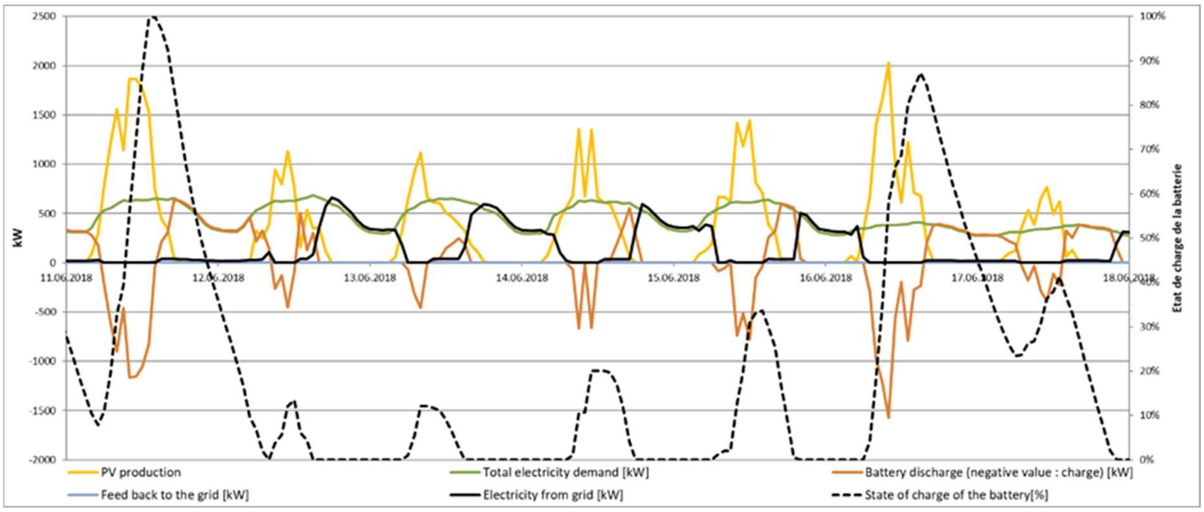

Figure 42: Example of charging and discharging of the battery, for a week in summer, without optimization.

To reduce the power tax, we make the hypothesis (as a consequence of the regulation algorithms developed and tested on the DC-microgrid demonstrator) that the battery is sufficiently large to smoothen the electricity demand from the AC-network by means of a 24-hour charge-discharge cycle. This hypothesis is justified by an hour-per-hour simulation of the power demand on the hypothetical site. The results for a typical week in winter and summer are, respectively, shown in *Figure 43* and *Figure 44*.

In these two figures, the "Total consumption - PV production" curve is the net electricity demand, which is the difference between the total electricity demand of the site and the PV production, i.e.$\Delta E = E_c(t) - E_{PV}(t)$, with time steps of 1 hour. When this curve is negative, PV production is higher than site consumption, and the battery is charged, and vice versa. The "Difference" δ curve is calculated, by integrating the difference between this net electricity demand ΔE and the daily average $\overline{\Delta E}$ of this net electricity demand ("Daily average"), i.e. $\overline{\Delta E} = \int_{0h}^{24h} \Delta E(t) dt$. Note that this daily average $\overline{\Delta E}$ can be positive or negative during summer (red curve in *Figure 43*), but is nearly always positive in winter, see *Figure 44*, since PV is almost never sufficient to supply sufficient energy for the consumption of the site. This is the underlying reason for the requirement that the site is semi-autonomous.

$$Difference\ \delta(t) = \int_0^t \overline{\Delta E} - \Delta E(\tau)\, d\tau$$

The integral δ named “Difference” quantifies the required storage capacity to smooth consumption over 24 hours.

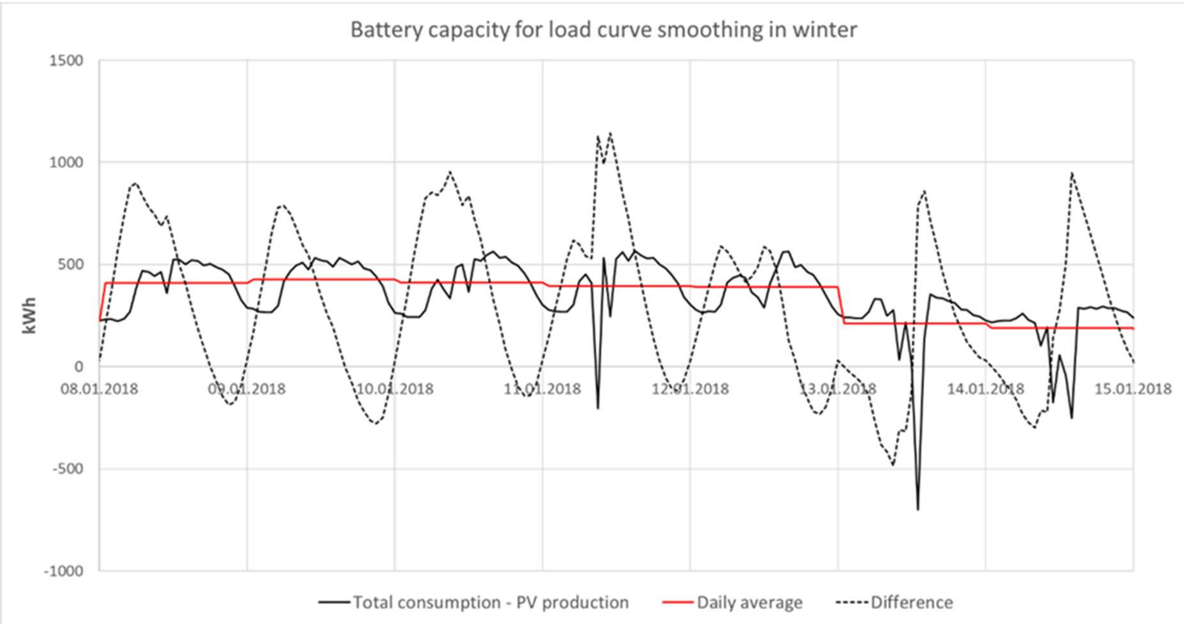

Figure 43: Representation of the storage capacity required to smooth the power of the site during a week in winter.

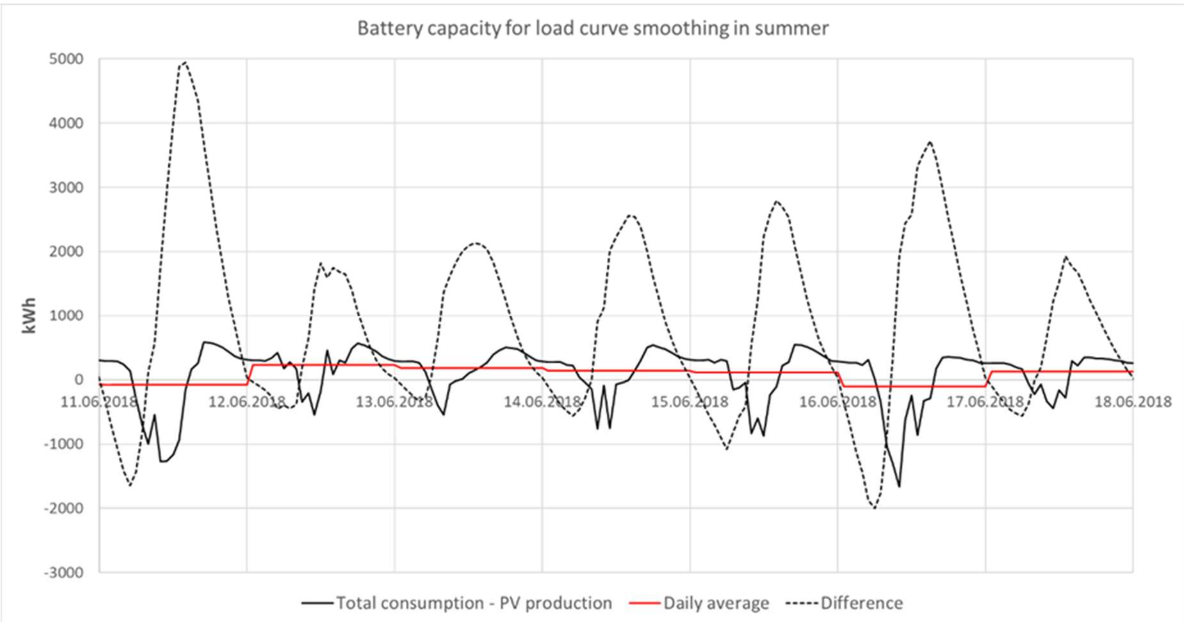

Figure 44: Representation of the storage capacity required to smooth the power of the site during a week in summer.

For the week of January 8th – 15th, a capacity of 1142 kWh is sufficient, while for the week of June 11th – 18th, 4938 kWh of capacity is required. Over the entire year, the maximum of required battery capacity turns out to be 6281 kWh. Since the economic evaluation assumes a capacity of 7000 kWh, it can be assumed that the batteries can indeed smoothen the daily consumption of the PV-installation such that the assumptions of the DC-microgrid are fulfilled.

This smoothing of the power profile at the AC-grid connection point reduces power taxes. In 2018, SIG was billing CHF 7.93 per kW per month, i.e. the maximum power (averaged over a quarter of an hour) for each month of the year. For example, if we look again at the week of June 11, the peak power of 721.5 kW is reduced to 549.7 kW, which would result in a financial saving of

$$Savings = (721.5 - 549.7)kW \cdot 7.93 \frac{CHF}{kW} = 1362\ CHF$$

We now present the results of the economic evaluation based on the calculated time for the return on investment (ROI) for the different tariff scenarios under various assumptions for the investment cost. From the simulation results for varying PV costs in Figure 45, we observe that the decrease the PV cost does not significantly change the ROI. This can be understood, since already today, with electricity prices such as those of SIG, for large installed PV power and large consumption (which allows high auto-consumption of 94%) make PV installations profitable with payback times of about 10 years.

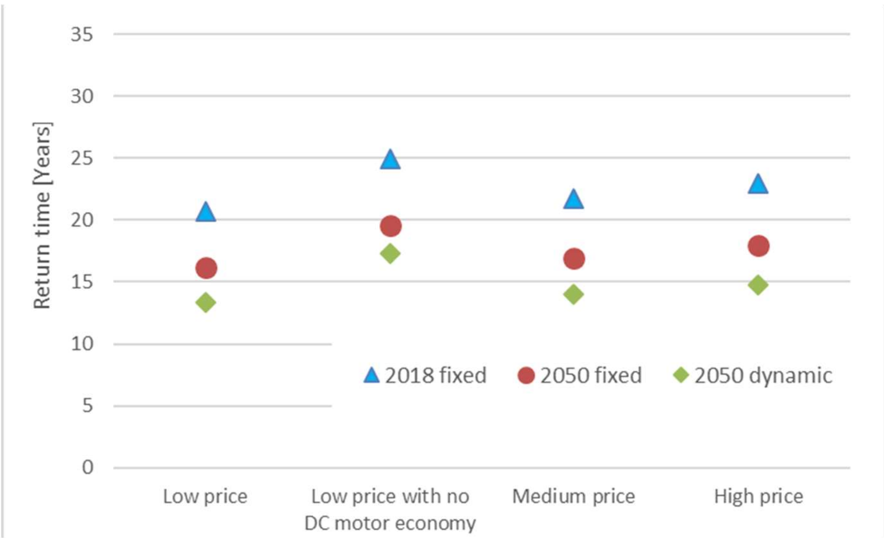

Figure 45: *The influence of PV-investment costs for DC-microgrid for all three tariff-scenarios is nearly negligible. Battery cost were kept constant at the high value, i.e. 500 CHF/kWh.*

The decrease of battery costs, see Figure 46, has a greater influence than that of the PV. Under current conditions, the battery capacity to store solar overproduction during the day is twice the price of the solar installation, i.e. 3.4 million francs for 2.5 MW_p of PV and 7.9 million for 7 MWh of battery for our hypothetical site.

Figure 46: *Influence of battery costs on the return on investment for the three tariff scenarios, at constant "high" PV investment costs.*

Assuming lower investment costs for both batteries and PV combined (as summarized in Table 7) leads to very short payback times for all three electricity tariff scenarios. Thus, the lowest ROI is reached for the dynamic tariff scenario with less than 5 years, see *Figure 47*.

Figure 47: Influence of investment costs of PV and batteries simultaneously. The terms "low", medium" and "high" price are defined in Table 7*.*

General parameters	A	B	C	D	
Installed PV power	2.5	2.5	2.5	2.5	MWp
Battery capacity	7	7	7	7	MWh
Energy saving on the DC motor	20%	0%	20%	20%	
Battery price	50	50	200	500	CHF/kWh
PV price	740	740	900	1 100	CHF/kWp
Investments over the lifetime					
Battery pack	787	787	3 148	7 869	kCHF
PV installation	2 311	2 311	2 811	3 435	kCHF
Total investments	3 098	3 098	5 958	11 304	kCHF
Return time					
2018, Fixed prices	**6.30**	**7.60**	**12.12**	**23.00**	Years
2050, Fixed prices	**4.91**	**5.95**	**9.45**	**17.93**	Years
2050, Dynamic prices	**4.05**	**5.27**	**7.79**	**14.79**	Years

Table 9: Overview of simulation output for simultaneous reduction of investment cost on PV and batteries for the three tariff structures. These data are shown graphically in Figure 47.

The 30% increase in electricity prices reduces return times by about 1.5 years, whereas dynamic pricing reduction is less significant for these already low ROI values. *Table 9* summarizes the assumptions for all investment costs and the calculated ROIs. Since we assumed cost reductions of battery of up to 90%, while the average electricity price increased by only 30% over the next 30 years, the decrease in investment has a greater impact on profitability than variations in electricity tariffs. However, in particular the influence of dynamic electricity tariffs should be investigated more in detail, since as described in section 3.6 we put heavy constraints on the minimum price, since in a market situation with by far dominating classical ribbon power production, dynamic prices are rare. We expect this situation to change with strongly reduced ribbon power production after elimination of nuclear and coal thermoelectric plants.

5 Conclusions

The technical functionalities and grid services that a semi-autonomous DC-microgrid with high PV-power production can offer for industrial sites were demonstrated, the technical impact on the distribution grid was analyzed and served as the basis for the hypothesis entering into the economic analysis that was performed.

5.1 Operational experience of a DC-microgrid

The presently operating demonstrator in a protected laboratory environment is a required stepping-stone for transferring the technology into real applications in the field. Indeed the entire system is sufficiently complex such that a straight implementation at a customer site is today too risky and no Swiss company is presently proposing the installation of such a system in Switzerland. However, the individual components are to a certain extent available and should in the near future be implemented and tested in the demonstrator system. The complexity of the system is due to two main elements: (i) the power electronics with its interplay for the regulation of voltage and power on the DC-bus link, and (ii) the communication system, which is required to regulate energy and power according to the requirements of the customer or end user.

A main issue is to be able to guaranty the safety of equipment and operating personal. Even though it has been addressed during this project, this topic is far from settled. Thus, the development of a safety concept will form a main objective of future projects.

The reliability of the DC-microgrid has been shown to reach close to 100% once the development were finished. However, this requires both fully tested hardware components, regulation system and software for the EMS. Therefore, for future projects where installation on end user sites will be the clear aim, the preliminary tests of all three elements must be assured. The possibility to test these hardware in real operating condition within the DC-microgrid demonstrator presented herein will allow reducing the risk of breakdown of the electric power system under real world conditions and thus will allow reducing installation, testing and operation costs for any future project.

The question of the suitable operation voltage for future DC-microgrids has been settled as well, since either +/-350 V or +/-380 were under discussion in recent years. In order to allow different power electronics topologies for the AFE, which connects the DC-microgrid to the AC world, the choice of 380 Volt seems to be more appropriate. However, this applies only for AC-connected grids, whereas islanded grids may operate in principle at lower voltages, since no AFE is required. Here the question arises whether it makes sense to establish two voltage standards for the DC-technology.

The quantification of the reliability of the DC-microgrid demonstrator has been established and applied. For comparison to competing technologies on a quantitative basis, this evaluation tool is indispensable. It could be shown that uptime and the mean time between failures reach already at the present status values interesting for industrial application. This was one of the major concerns at the beginning of the project, and the reason why the installation of the DC-microgrid demonstrator in a protected laboratory environment was necessary before the step into the Real World could be envisaged.

The demonstrator at the HESSO Valais fulfills thus all requirements to serve as a testing tool for future developments, equipment incorporation or evaluation of microgrid scenarios before installation of DC-microgrids under real operating conditions. It will thus serve as the ideal step for increasing the TRL of this technology to levels of TRL7 or above. The remaining challenges to reach these high TRL's are given in section 6. Outlook.

5.2 Simultaneous regulation of voltage and energy with various constraints

The feasibility of smoothening of the DC/AC balance between the DC-microgrid and the AC-distribution grid while following a program announced 48 in advance has been demonstrated. The regulation algorithm for controlling the DC-voltage on the DC-bus by several battery chargers in parallel via droop control has been successfully tested. Different EMS have been implemented with a choice of optimization aims, like power smoothing for either PV-generation or consumption, or both, with or without incorporation of PV-forecast. There remain however, numerous tasks to fulfil for developing further the EMS. This DC-microgrid can serve as a platform for testing the commercial solutions of EMS designed for microgrid that are currently offered by numerous companies. The data handling and storage via the cloud-IO is clearly an advantage to make the microgrid accessible for any EMS solution on the market. A survey of EMS, organised by the PV-magazine will appear in March 2020. This will be a great opportunity to invite the suppliers of EMS for microgrids.

5.3 Technical impact on the distribution grid

With respect to the results presented above in section *4.6 Influence of microgrid topology on distribution grid*, it is worth considering the importance of integrating microgrids in electric networks, especially from the point of view of a DGO. In fact, there are numerous advantages to gain from exploiting microgrids.

Management advantages

First, if customers announce in advance, what they will consume from the grid, the DGO has a constant and known cash-flow from it. Based on the forecast consumption, he can build a strategy to supply power to the users depending on the situation.

This will help him managing in advance the elements of production and the reserve according to the amount of power to be supplied to the consumers: which production mean to use; how much power is produced and how much is kept in reserve in case of unexpected consumption. If the consumers respect what they announced within the tolerance ($|\Delta E_r| \leq 1\%$), the DGO can even avoid situations where he must compensate for dynamic power fluctuations. Compared to today, the management budget can be drastically cut down.

With some experiences, the DGO can optimize the use of the whole system. Let us illustrate this with some examples.

- To use the means of electricity production in their optimal operating regime. A better use will lead to reduced maintenance costs.
- There will be less sudden starts/stops of these production means to compensate the unexpected power fluctuation (reduced dead time). The operating time will increase, and the income will be higher.
- To forecast and organize the reparation/maintenance phases, which will improve the flexibility of the grid for possible future improvements.

Secondary producers

Managing an electric grid means providing enough power to the consumers to keep the grid frequency around 50Hz, which is called frequency control. Nowadays, the DGO faces situations where the electricity demand is high, and the power fluctuation could reach unexpected values in very short time (234kW/30min in the simulation), creating difficulties to maintain the grid frequency at an acceptable range.

To achieve this goal, the production means must have the capacity to generate high power values in a short time. Sometimes, the DGO cannot produce all what the customers need. Based on a defined list of requirements, the DGO recruit secondary producers, which have enough power reserves to face such situations.

The results of the simulation show that, thanks to microgrids, the management of the electric grid will be simpler and easier as the DGO must provide low power with low power fluctuation (maximum at 24kW/30min in the simulation) already known in advance. We expect that the grid frequency can be easier to maintain around 50Hz and more secondary producers can be recruited. For the DGO, there will be more competition and more possibilities to choose between the secondary producers, which is translated into reduction of tariffs when buying or renting the power reserves.

Small reserves are needed in case:

- The DGO has to compensate the part of power he can't supply with his own production means
- If a user's consumption deviates from what was announced, the DGO can benefit from this situation as he can apply a penalty on the consumer (higher tariffs, fine, …).

Even if the DGO will gain less as the power to be supplied will be lower, he will save money related to the infrastructure (less regulation reserves) of the distribution grid.

Cost of the infrastructure

An electric grid is composed of different elements, like transmission cables, converters and rectifiers. The higher the power to be transmitted is, the more expensive these elements are, especially if they are made from copper (like cables).

As microgrids will help reduce electricity demand from the grid and the power fluctuations, the requirements to be fulfilled by the infrastructure of the electric network will also be lower. By choosing components with lower requirements and optimizing the electricity transmission, it is possible to:

- reduce the costs when buying these components,
- reduce the dissipated power. This is one way to increase the global efficiency of the grid.

For the DGO, a higher global efficiency is an additional advantage.

5.4 Economic impact

On the profitability side, we have shown that for the type of deployment to be profitable, several conditions must be present, in particular the costs per kWh of storage and the cost of PV per kW_p. The expected strong cost reduction of storage elements will dominate in the first place the return on investment for any combined solar-storage system for the owner of the investor. The discussed technical advantages of a smoothly regulated microgrid for the owner as well as for the DGO could be converted into economic benefits lower than those of reduced investment costs, however, are not negligible.

We underline the importance of dynamic pricing. Imposed by the metering system, the pricing is in almost all DGOs based on three elements, night hours, day hours and maximum power (monthly or annual). Some distributors such as SIG offer tariffs for 3/5 periods, i.e. to be able to bill power according to 3/5 periods, whereas in general, the maximum power is calculated over 1 period (from 6am to 10pm). If we can only encourage this type of tariff, it is more in line with the requirements imposed by the increase in renewable energy, which is necessarily stochastic. The determination of the price per kWh must follow the constraints of the grid, and therefore follow the balance between consumption and production. The proposed dynamic tariff should be able to be tested at customers' premises to verify whether price signals encourage the implementation of intelligent regulations based on the principles of predictability, making it possible to reward "good consumers" and penalize consumers who incur adjustment costs.

6 Outlook and next steps

The next steps for the deployment of DC-microgrids comprise the technical and economic requirements, the implementation on a test site in a non-protected real user environment (as opposed to the system presented here which is operating in a laboratory environment) and the pending issues which require further R&D in the laboratory.

6.1 Technical requirements

The technical requirements can be simply stated as raising the technical readiness level (TRL) by 3 positions. According to the TRL definition of the SFOE [SFOE-TRL] we position our present DC-microgrid closer to level 4 than TRL5. The components of the DC-microgrid are mostly build in-house and the entire system is still operating in a protected laboratory environment, where an undesired shutoff of the bus does not harm any relevant equipment, leading to major costs for repair or even productivity level. However, the system operates already technically on a power level, which comes close to relevant dimensions for industrial applications, i.e. between 10 and 20 kW for consumers and beyond 20 kW for the PV-production. In addition, the geometrical dimensions of the microgrid are already realistic since several buildings on the entire campus are interconnected by the DC-bus cable, leading to geographically distributed prosumers (production, storage and consumers of more than 100 meters. For the next steps, we aim therefore to raise the TRL to about 7 or 8, meaning to improve reliability such that the system can be operated 24 hours for several month with MTBF of at least 3 months or more. A proper automatic recovery mechanism needs to be developed such that even infrequent drop out events can be solved without major harm to the end user.

As can be seen in the description of the DC-microgrid itself in section 3, the implementation of realistic dimensions requires profound know how in power electronics and the regulation behaviour of a series of interconnected converters on the same power line. While in this project, most components were designed in house to make sure a smooth compatibility in future projects on real consumer sites the components must be purchased from companies active in the field. Since the combination of voltage levels between power link and device together with the options in communication protocols open up a nearly infinite dimensional parameter space, the identification of suitable equipment suppliers with nicely fitting elements will be certainly a challenging task. Before the first system can be delivered to a customer it will be required to join them together for suitable testing. For such a final testing before installation the herein developed DC-microgrid demonstrator may play an important role. In fact, it is planned to develop the required minimal hardware configuration in an upcoming Innosuisse project, with an industrial partner who has already been identified. This partner company will eventually be able to commercialize the entire technology as a whole to interested customers with greatly reduced risk at installation and start-up on site.

Another task will be to make the ICT system industry compatible. It is a debate whether the gateways can be accepted as hardware as a certain reluctance of industry towards raspberryPi as gateways was identified. Thus, other options must be evaluated, with as little as possible losses of the knowhow which was already built-up, due to the migration of the already available communication software from one platform to the other.

Furthermore, a compliance to existing or upcoming standards should be addressed. For example, the European/global SUNSPEC regulations are already accepted by significant number of companies in the solar market. Even though the DC-technology goes beyond solar equipment, the latter forms an inherently important part of the DC-equipment. One should keep in mind that it is to a large extend the advent of solar power as DC-source, which is one major argument for the renewal of DC-activities in recent years.

6.2 Implementation on pilot sites

Three follow-ups of the present project can be listed. As one of the aims was to find industrial partners interested to implement the DC-technology for end users, eventually in summer 2019 serious interest has been expressed by a Swiss engineering office. Subsequently, a follow-up project is presently pursued with funding applications to the European Eranet program. To achieve this implementation prior testing on a fully equipped testing site as we have it at our disposition now at the HESSO Valais is required.

Two potential candidates as end users of the DC-microgrid technology had to drop out since the DC-technology has not been mature enough for the required dimension and installation schedule. Note that the power levels for a scale up should not be increased in too large steps, in order to avoid unforeseen events, which could drown the DC-technology due to immature promises. This situation will steadily improve as further experience of larger dimensions in subsequent projects will be made together with the operational experience on the test site in Sion.

The HESSO Valais in Sion will move to new buildings in 2020. In preparation of this encouraging outlook for the engineering department, the DC-microgrid has become a key element in the development topics such that it will be installed in the new buildings as well.

Based on these prospects and in particular due to the intended system upgrade for the new campus building “Energypolis”, various component suppliers (power converters, electrolyser and fuel cell) were contacted and signalled interest in providing material for direct DC-bus connections instead of classical AC-power links in order to reduce conversion losses.

6.3 Economic analysis

Detailing the economic analysis integrating different scenarios including import/export, providing active storage service to the grid operator, etc. different dynamic energy pricing in line with literature should be reanalysed with higher accuracy and improved assumptions. In particular, the dynamic pricing scenario with a conservative artificially imposed lower bound seems unrealistic.

In a world where the NERs must be the basis of our electricity, it is important to prepare consumers to implement site management demand strategies and it is the author’s opinion that nothing can motivate consumers more to adopt these approaches than the implementation of dynamic pricing.

6.4 Pending issues

Various technical issues still need to be addressed in the future, some of which were already discussed in the corresponding preceding section, where the respective component was described or its performance evaluated. Here we state the most relevant ones, required to raise the technical readiness level from a presently estimated value of TRL-4 or 5 to a level of TRL-8. For this increase by 3 or 4 levels the experience and the demonstrator available at the HESSO Valais will be able to play a significant role. The topics to be addressed are the following:

a. A central feature of the DC-microgrid technology is the definition of an appropriate voltage level. As described above the present 700 V will in the near future be increased to 720 V or even to 760 V, being equivalent to +/-360V or +/-380V. This is linked to the question of standardization of the voltage in the mentioned range and already addressed by an international comity, see section 6 of reference [IEC2017].

b. Analyze the connection and underlying reason for the remaining error in PV-production forecast, since this error has a major impact on the uncertainty in battery management. This uncertainty requires larger battery capacity to be installed, which raises investment costs significantly as long as the battery costs remain high and thus one of the main obstacles (besides market and tariff regulations) for economic operation of a DC-microgrid.

c. Increase MTBF: evidently the MTBF, which has been shown to be already at this stage on the order of a week needs to be improved by at least one order of magnitude. This will be reached by two technical measures. Firstly, testing and implementation of DC-microgrids based on commercially available components, and secondly, running the regulation system on a permanent basis with real size components under real operating conditions in a protected environment as made possible at our DC-microgrid demonstrator. Every drop-out will be tracked down and the reason eliminated as commonly performed in quality insurance in machine and equipment supplier industry.

d. Combine forecast, voltage regulation and storage services in EMS (mode 2 upgraded)

e. Establish compliance with available or upcoming standards or pre-standards, which are likely to evolve into real international standards, as more and more companies are voluntarily joining these pre-norms. This applies not only to the power electronics but at least as important to the communication system, as many agreements have already been included for example in the Sunspec alliance, see reference [Sunspec].

f. Implement a visual interface for potential end users on different level of detail. As common for human machine interfaces, at least two distinct levels would be required. The first being for the ordinary end user, giving an overview of strongly simplifying overview values of the operating state of the DC-microgrid (e.g. like instant voltage, present remaining energy in the batteries or SOC, forecast power trajectories, etc.). The more detailed view should allow a potential service engineer to analyze quickly the status and any potential origin of occurring failure states.

6.5 Seasonal storage of energy

While the storage of renewable energy for short periods can be considered as being solved by the availability of various battery technologies alongside with intelligent regulation like presented in this project, the issue of seasonal storage is still pending. The smooth integration of power to gas is possible; however, the cost efficient storage remains unclear. The most promising option seems to be a significant overproduction of solar power generation in summer, of about 3 times the energy consumed during summer months. This strong overproduction would clearly drop costs of electricity during summer day times below any nowadays prices. To what extend electric energy prices would become even negative goes beyond the scope of our project and requires more detailed analysis. This in turn could render the investment in hydrogen conversion and in particular storage devices economically viable. The cost reduction of electrolysis systems and fuel cell will likely receive support from automobile industry. However, since cars do not need long-term storage this issue will remain on the shoulder of the owner of the energy infrastructure (either distribution grid operators or microgrid owners) to be solved. It is the author opinion that the mentioned solution for seasonal storage will only become viable under the condition that dynamic pricing of the kWh does not remain limited to the electricity stock markets or limited fractions of the market but become the main pricing principle for all customers.

7 National and international cooperation

Since the beginning of the project in 2017, the advantages provided by DC-microgrids have been the topic of a large development program in Germany, under the name DC-Industrie, see the conference proceedings of IDCM 2017 [ICDCM2017]. The German ministry of economy has funded this project with a significant number of industrial highly reputable partners [DC-Industrie]. Contacts to the Fraunhofer Institute for Integrated Systems and Device Technology IISB, could be established, as well as to Daimler, Stuttgart, both of them agreed to participate in the DC-microgrid workshop to be organized at HESSO Valais. Furthermore a contact to University in Delft, Belgium, led to the integration for a consortium for a major project, submitting twice (2018 and 2019) a funding application for a DC-microgrid development initiative, distributed over several countries in Europe (not accepted by Horizon 2020). For the Smart Energy Systems RA-Net Micall19, the HESSO Valais submitted a proposal together with partners from Germany, Finland and Scotland to apply the DC-microgrid technology.

8 Communication

The HEI in Sion intents to organize a workshop on DC-microgrids, in order to make this promising solution for integration or renewable energies and direct consumption better known in Switzerland, with the participation of international key actors in Germany and the US. The Fraunhofer Institute IISB in Erlangen and Daimler AG, Stuttgart, declared already their participation as keynote speakers.

9 Publications

1. [ICDCM2017] Christoph Ellert, Rodolfo Horta, Thomas Sterren, Dominique Gabioud, Dominique Roggo, Pierre-Olivier Moix, *Modular ICT based Energy Management System for a LVDC-microgrid with local PV production and integrated electrochemical storage*, 2017 IEEE Second International Conference on DC Microgrids (ICDCM), **DOI:** 10.1109/ICDCM.2017.8001056
2. [PV-Bern2018] Ch.Ellert, J. Holweger, H.-P. Biner, N.Wyrsch, L.Bloch, L.Barras, D.Blatter, F.Steiner, R.Horta, D.Roggo, T.Sterren, *First evaluation of two PV-generators exploited via individual DC/DC converters on a common 700 V DC-bus*, Poster presentation, 16th National PV-Tagung Bern, April 2018
3. [Capponi2018] Lino Capponi, Line Barras, Didier Blatter, René Rebord, Thomas Sterren, Christoph Ellert, *Integration of storage into PV-powered DC-microgrid*, Poster presentation, 17th National PV-Tagung Bern, March 2019
4. [Morey2019] Philippe Morey, Jean-François Affolter, Line Barras, Aurélien Carrupt, Didier Blatter, René Rebord, Thomas Sterren, Philippe Barrade, Christoph Ellert, *Power electronics for a LVDC-microgrid with local PV production and electrolytic converter*, Oral presentation, 3rd IEEE International Conference on DC microgrids, May 2019, Matsue, Japan – received the “Best presentation award” of the conference.

10 References

[BFE2019] *Gesamte Erzeugung und Abgabe elektrischer Energie in der Schweiz*, Tabelle, Mitteilung vom Bundesamt für Energie BFE, 2019

[BMWi2019] Bundesministerium für Wirtschaft und Energie, *Rahmen und nächste Schritte für die Kohleausstiegsgesetzgebung*, Pressemitteilung, 03.07.2019; https://www.bmwi.de/Redaktion/DE/Downloads/P-R/rahmen-und-naechste-schritte-kohleausstiegsgesetzgebung.html

[BNEF2019] Logan Goldie-Scot, *A Behind the Scenes Take on Lithium-ion Battery Prices*, Bloomberg New Energy Finance, March 05, 2019, https://about.bnef.com/blog/behind-scenes-take-lithium-ion-battery-prices/

[Breiman2001] Breiman, Leo. *Random forests,* Machine learning 45, no. 1 (2001): 5-32.

[cloud-IO] HESSO Valais, Institute for Industrial Systems, Documentation of the cloud-IO system 2017; available at https://cloudio.readthedocs.io/en/latest/

[DC-Industrie] Karl-Peter Simon, Forschungsprojekt DC-Industrie, Gleichspannungsnetze in der industriellen Produktion, ZVEI, September 2017, https://dc-industrie.zvei.org/

[EE-Markt2018] SFOE, Markterhebung Sonnenenergie 2018, Teilstatistik der Schweizerischen Statistik der erneuerbaren Energien, Swissolar, p.14, Sect. 4.3

[entsoe2019] European Network of Transmission System Operators for Electricity; https://transparency.entsoe.eu; accessed September 2019

[grafana] Description of the open source monitoring software for databases; 2019 https://grafana.com/

[IEA2011] Paul Waide, Conrad U. Brunner, Energy-Efficiency Policy Opportunities for Electric Motor-Driven Systems, International Energy Agency, Working Paper (2011), pages 14, 47 and 48

[IEC2017] LVDC: electricity for the 21st century, Technology report, IEC 2017, Geneva, Switzerland, ISBN 978-2-8322-4610-8

[IEEEIMIS] Mariam Barque, Luc Dufour, Dominique Genoud, Arnaud Zufferey, Bruno Ladevie, Jean-Jacques Bezian, Solar production prediction based on non linear meteo source adaptation, IEEE conference IMIS, (2015), DOI 10.1109/IMIS.2015.54

[Jung2012] J.-H. Jung, H.-S. Kim, J.-H. Kim, M.-H. Ryu et J.-W. Baek, «High Efficiency Bidirectional LLC Resonant Converter for 380V DC Power Distribution System Using Digital Control Scheme» IEEE Conference Publications, 2012.

[kWhCost] Review of Swiss Electricity Scenarios 2050, Report prepared for the Group Energy Perspectives and the Swiss Competence, Center for Energy Research "Supply of Electricity"(SCCER SoE), Martin Densing, Stefan Hirschberg, Hal Turton, 2014

[Lin2010] Lin, R.-L. Lin et a. Chiao-Wen, «Design criteria for resonant tank of LLC DC-DC resonant converter,» IECON 2010 - 36th Annual Conference on IEEE Industrial Electronics Society, 2010.

[NatureEn2017] O. Schmidt, A. Hawkes, A. Gambhir and I. Staffell, *The future cost of electrical energy storage based on experience rates*, Nature Energy 2, 17110 (2017), DOI: 10.1038/nenergy.2017.110

[SFOE-TRL] Swiss Federal Office of Energy SFOE, Directive on the submission and applications for financial support of energy research, pilot and demonstration projects, Appendix 1: Technology readiness levels, version 17.12.2019

[SFOE2018] Swiss Federal Office of Energy, Statistique suisse de l'électricité 2018, Tab 8 pp 14, Confédération Suisse, Bern

[SIG2018] Pricing data of SIG (Service industriel de Genève) https://media.sig-ge.ch/documents/tarifs_reglements/electricite/tarifs/tarifs_electricite_2020_tous_clients.pdf

[Steiner2013] Florian Steiner, Hans-Peter Biner (Dir.), Maximum power point tracker MPPT mit galvanischer Trennung, Bachelor Thesis 2013, HESSO Valais-Wallis

[Sunspec] Sunspec Alliance, Information Standards for Distributed Energy, San Jose, CA-95117 https://sunspec.org/ visited 15.11.2019

11 Annex A : Power electronics & data communication

This annex describes the development of the power electronics components and the data communication system, required for smooth functioning of the entire microgrid.

The specifications for the interface between the DC-bus and the DC/DC converters injecting the power of individual PV-modules are shown in Table 10. The specifications for the DC/DC converter injecting the power of a serial string of PV-modules into the DC-bus are equivalent, with modified specifications for the input power and MPP-voltage, according to typical string values.

Feature	Parameter	value
DC bus	Nominal voltage	**700V**
	Min/max voltage in operation	**650-750V**
	Absolute maximum	**800V**
PV side	Min/max voltage in operation	20-60V
	Maximum power	300-600W (TBD)
	Mpp Maximum power range	40-60V
"plug a chaud"	serial/individual PV-converter to an operating bus	without disturbing DC-bus, precharge must be integrated
Isolation	DC bus to PV terminals	1.5kV 1 min
	DC bus to earth	1.5kV 1 min
	PV terminals to earth	0.5kV 1 min
Protection	DC bus	indiv PV-converter: ICL + fuse les autres: fuse
	PV side	None
	("Pseudo") Islanding mode = loss of AC grid	Valid in case of loss of AC grid, all energy suppliers to the bus must be shut down
Working modes	Start/stop conditions	Undefined
	Remote controlability/logging	Undefined

Table 10: *Specifications for the DC/DC converters for individual PV-modules.*

For integrating the bidirectional converters of the batteries as well as the commercially purchased converters for the consumers, a pre-charge box has been developed at HESSO Valais. This was the easier to implement, since components available on the market did not match the required specifications.

11.1 AFE - active front end

The link between the DC-microgrid and the AC-grid is established by means of a bidirectional AC/DC converter. The task of this converter is not only the conversion of power in both directions, but is should as well maintain the power level of the DC-bus. In addition, this converter should be able to switch is working mode from maintaining the DC-voltage level as “master” to a mode where it is operating in a slave mode. In the latter case the AFE receivers a power order from the central EMS to inject/extract power from the AC-grid, while the voltage level of the DC-bus is maintained by the bidirectional converters of the batteries.

Throughout the first half of the project the DC-microgrid was operated using the previous AFE, available already from preceeding projects, which however can only operate in voltage regulation mode (as Master) and thus the project aim of maintaining a very tight tolerance could not be achieved with this AFE. After accomplishing the development of the particular AFE, capable of operation in both modes this AFE has been operated permanently.

11.2 DC/DC converters for individual PV-modules

As depicted in *Figure 1*, the DC feeder (or DC-bus link) realizes the interconnection of the different elements composing the microgrid, such as energy storage systems, energy consumers and producers. From the DC/DC individual converters point of view, such a structure raises the challenge of an important voltage difference between the photovoltaic module output (around 30 to 50 Vdc) and the 700V of the DC feeder, typically separated by a factor comprised between 15 and 20. The market currently lacks such products. In this context, designing and commissioning DC/DC individual converters able to operate with an important voltage difference while providing a high efficiency while optimizing each PV panel is an important improvement to the field of Renewable Energy Sources (RES). Indeed, such a solution would significantly increase the system modularity and versatility.

The DC/DC converters for individual PV-modules were developed by Imperix SA, with the aim to push the previous design (done by HESSO Valais [Steiner2013]) towards a more industry-realistic design. Those focus points have been as key topics for the re-design phase:

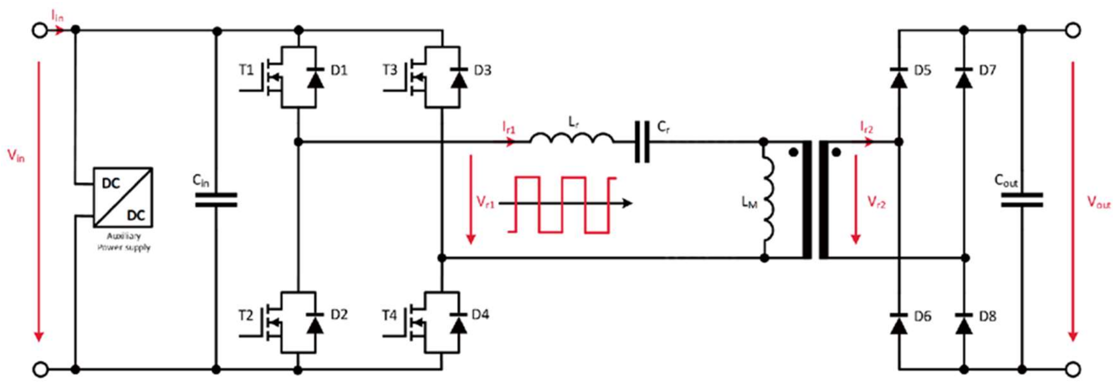

Figure 48: Illustration of the selected power conversion topology: LLC resonant for the DC/DC converters of the individual PV-modules as developed by imperix SA.

- **Operation area (i.e. maximize PV panel compatibility)**. One of the key requirements is to expand the input voltage range and rated power, hence allowing the connection to recent PV panels (that have higher V_{MPP} and V_{OC}). Since jumping from [18;42]V to [15;60]V is more than doubling the range, a complete redesign of the resonant converter was required, even though the conversion topology used (LLC resonant inverter [Lin2010]) has been untouched, see *Figure 48*. Indeed, given that the *resonant* behavior of the low-voltage side of the converter mainly defines the admissible input range, the latter had to be entirely redesigned. As a side effect of the wider input range, the losses were expected to be higher (due to a higher resonance, leading to higher currents and voltages flowing in the input stage). Consequently, the redesign had to be carefully executed, while paying attention to the overall losses of the conversion stage.

- **Reverse flow operation.** Taking advantage of redesigning the power stage, Imperix has studied the reverse power flow [Jung2012] of such a converter topology. Even if such a feature is useless in PV applications, it could have turned the converter in a much more polyvalent device (for powering loads from DC-bus e.g. electrolyzer) at a very low additional cost. The preliminary study and measurements have shown a poor efficiency (around 82%) as well as a very reduced output voltage range. For these reasons, this mode has not been implemented in further prototypes.
- **Size reduction.** As of today, most of commercial DC/AC individual converters are available in a form factor that allows the integration to the PV-panel. Consequently, the volume constraint has driven most of the design choices (PCB design and construction, thermal design, enclosure choice, …) while making them more complex. As an example, a small enclosure is much more difficult to cool down than a large one. Finally, the produced design is 63% smaller than its predecessor.

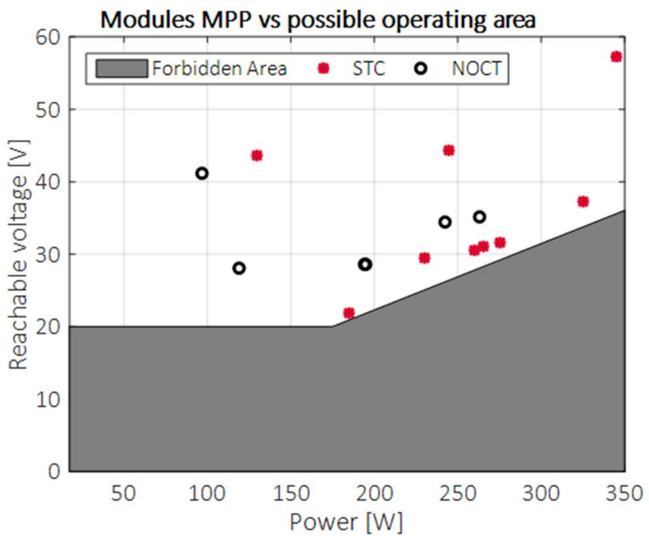

Figure 49: Definition of the converter safe operating area (SOA) based on the available PV panels specifications.

The design process has been executed in three steps. By September 2017, an early lab prototype has been assembled for validating the early choices as well as allowing the evaluation of the reverse power flow mode. Confirming the theoretical approach, these early measurements have demonstrated the low efficiency of the reverse power flow. By May 2018, a pre-series of two individual modules has been assembled and integrated in their final enclosure. These units have then benefited from a real-life test at HESSO Valais facilities. By January 2019, after applying minor changes to the design, the production of 30 modules has been started. Impacted by various delays, the units have been delivered to HESSO Valais by June 2019.

The path from the prototype to the industrial is not over, though. Indeed, focusing on the key topics described above did raise a few points to investigate in a further revision:

- **Converter efficiency.** Due to the broader voltage input and output ranges as well as suboptimal performance of the magnetics, the targeted efficiency has not been achieved. Also, at this stage, power saving modes are to be implemented in a later development phase, hence contributing to an overall better efficiency. In addition, the overall power consumption of all the auxiliaries (integrated sensors, processors, communication, …) should be reduced in order to dramatically enhance the converter efficiency under light loads (smaller than 50W). As an example, at 50W power output, approx. 7% of the power losses are due to the auxiliaries.

- **Mechanical design.** Given the quantity of 30 modules only, a standard enclosure has been selected, leading to an expensive choice (due to the low quantity), as well as many mechanical constraints that made the assembly procedure expensive.
- **Control execution.** The use of a well-known, high performance yet expensive control platform has been selected in order to spare engineering and development costs rather than bill-of-materials cost. The porting of the control code in a low-cost microcontroller is an upcoming task that is expected to be achieved in the next step of the industrialization process.
- **Certification.** As of today, the inverter modules are lacking all certification steps that are required to commercialize such products.

Aside from the technical development, an economical study has been carried out by imperix SA. Its main outcomes are as follows:

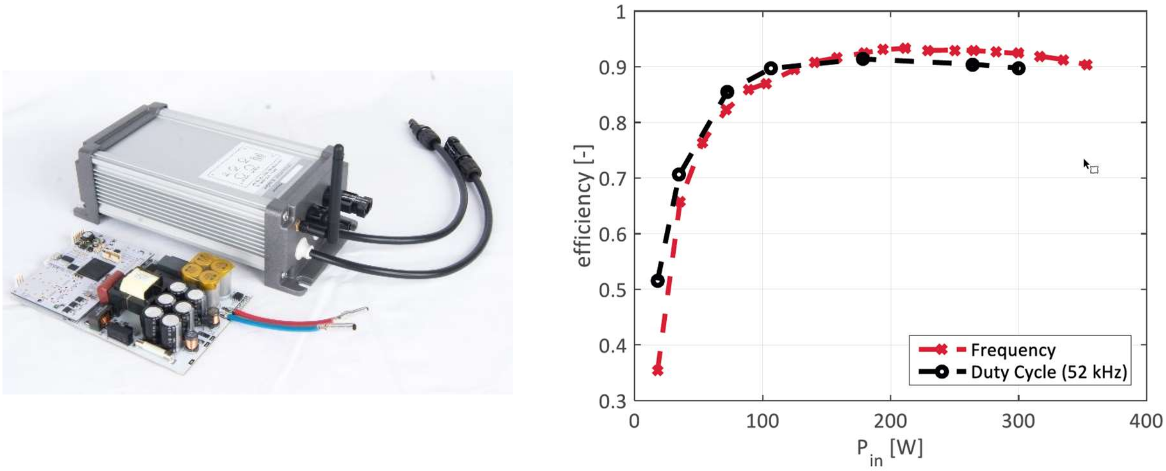

Figure 50: (left) Individual converter - enclosed version and internal board (right) typical power stage efficiency (under different control strategies)

- **Component costs.** BOM (bill-of-materials) costs are strongly dependent on the quantity of units to be manufactured. Taking an example with the individual converters, a comparison with a single-unit production batch, ordering 30 would lead in 21% component discount (compared to the BOM of a single unit), 100 in 28%, 1000 in 44%. Consequently, the BOM-related volume savings provided by a production of 30 units have a rather low impact on the overall costs.
- **Cost share.** The cost share of a 30 units production (unit cost of 746 CHF/piece) is depicted below. If component share is at 64%, the remaining 36% are mostly HR-intensive tasks as partial manual soldering, mechanical assembly and testing. Unless part in a larger production batch (e.g. 200+ pieces) the HR-intensive cost will remain high. Lowering this being only achieved by standardizing the process and avoiding high staff training costs.
- **Production fixed fees.** With a produced quantity as low as 30 parts, production management as well as setup fees impact the overall costs as high as 15%.
- **Defects.** All figures above are based on the fact the production process to be 100% reliable and generating zero devices with defects. This is generally true for small, locally-sourced production batches, but wrong for series production with larger quantities. As an example, it is generally accepted that an outsourced production batch in China generates 2-15% of defective parts.

In the table below, a list of actions and design changes has been established in order to estimate a realistic production cost for 1000+ units. These costs obviously exclude the prior engineering work required for achieving each of those tasks.

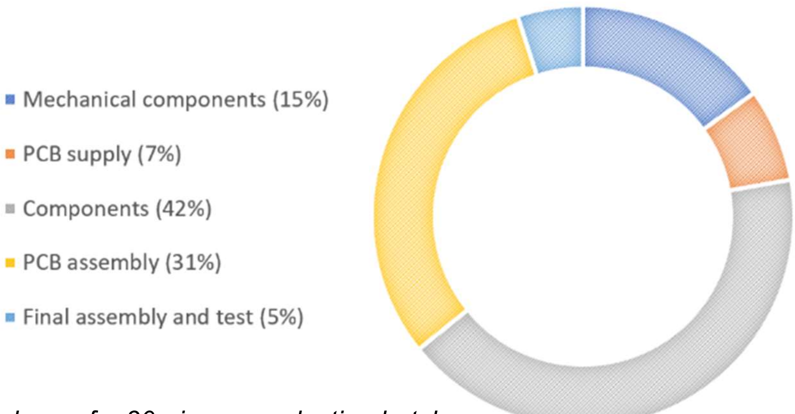

Figure 51: Cost share of a 30-pieces production batch

In the table below, a list of actions and design changes has been established in order to estimate a realistic production cost for 1000+ units compared to the mini-series of only 30 units. These costs exclude the prior engineering work required for achieving each of those tasks.

Action items in next industrialization phase	cost reduction per unit	Total
(current production cost, mini-series of 30 pieces)		746.00 CHF
Fully custom enclosure (molded, excluding set-up fees)	- 75.00 CHF	
Porting control to low-cost microntroller unit	- 170.00 CHF	
Volume discount on PCBs production and components	- 145.00 CHF	
Volume discount on assembly tasks	- 130.00 CHF	
Margin for defective units	+20%	
Forecasted production price with all abovementioned actions		**271.20 CHF**

Table 11 Projection of the converter cost with further industrialization steps for production batches of 1000+ units. The table does not take into account investment costs (i.e. engineering) for each of the actions listed.

11.3 DC/DC converter for a serial string of PV-converters

The DC/DC converter for a string of several PV-modules connected in series as is standard in PV-generators nowadays has been developed at HEIG-VD. A first prototype has been installed in April 2018, operated for several months and been replaced by a subsequent prototype in December 2018. Based on the latter a second and a third model are being assembled at HEIG-VD in 2019.

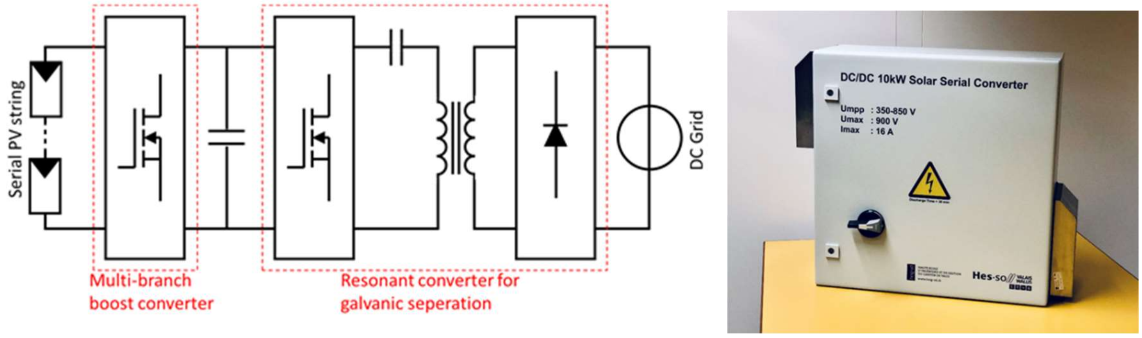

Figure 52: *Topology and photo of the serial DC/DC converter developed at the HEIG-Vd for injecting the power of a string of series connected PV-modules into DC-microgrid, including an MPPT.*

The converter was designed with a topology in two parts, see Figure 52 (left). The first part is a multi-branch boost converter and the second part is resonant converter. The multi-branch controls the converter and offers high efficiency possibilities, while the resonant part offers a galvanic separation and only mirrors the output on the input side.

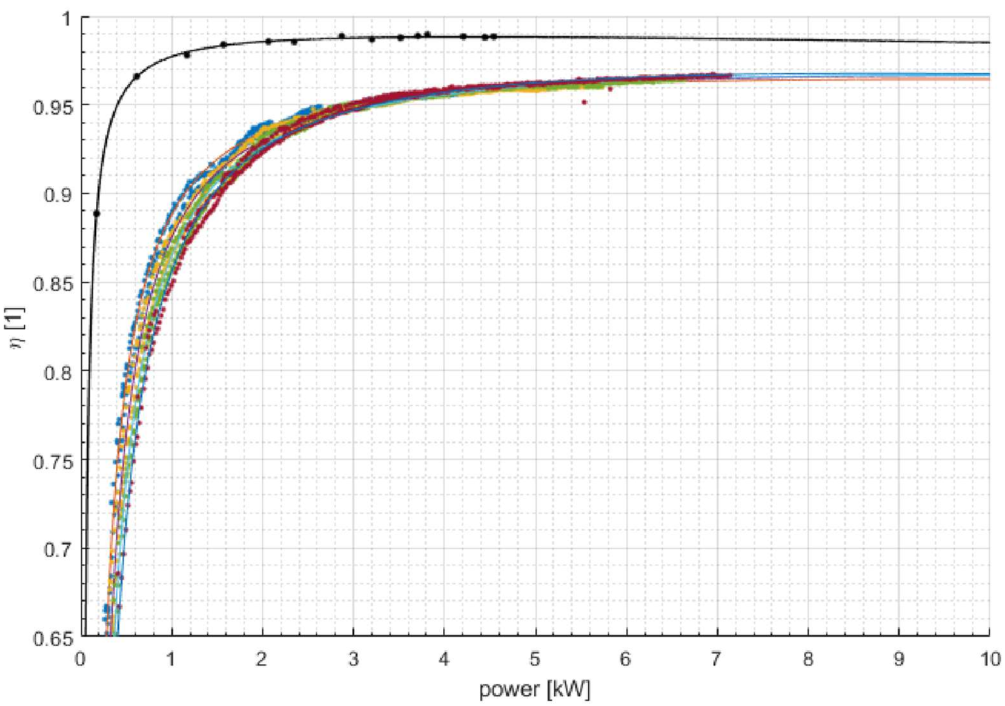

Figure 53: *Measured DC/DC conversion efficiencies of the serial DC/DC converter. In color: the efficiency of the converter with different input voltage levels. In black: the efficiency of the converter with the resonant converter bypassed, that is without galvanic separation.*

The high efficiency is possible with the multi-branch topology because of two reasons: Firstly, the current is kept at a low level due to it being distributed between several inductances. Conduction losses being proportional to the square of the current are strongly reduced. Secondly, because each branch is kept in a discontinuous conduction mode, half of the switching is done without losses.

The galvanic separation stage was designed as a resonant system to limit switching losses as well. The converter was designed in such a way that, in the case that galvanic separation is not necessary, the resonant part can be bypassed to reduce losses as much as possible.

Figure 53 shows the different efficiencies depending on the input voltage and whether or not the resonant converter is bypassed. As shown in, the Euro efficiency passes from 94.5%, with galvanic separation (that is when bypassing the resonant converter), to 98.6% without.

For security reasons the galvanic separation is used in the first phase of the testing and development of the microgrid. In a second phase, the converter will be ready to work without the galvanic separation with minimal transformations to achieve higher efficiencies. This is in line with the usual design for PV-converters on the market, for which most if not all galvanic separations have been abandoned in order to increase the total conversion efficiency.

11.4 DC/DC converter for a water electrolyser

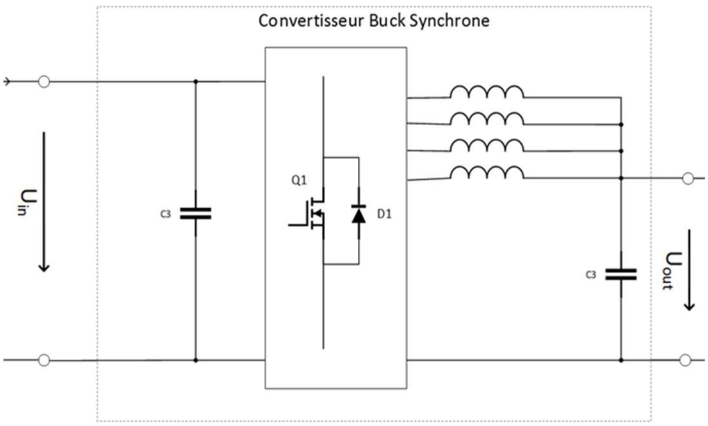

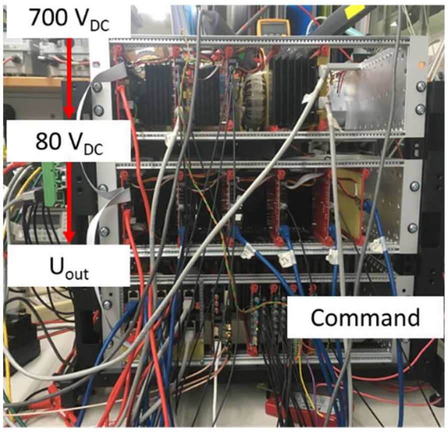

Figure 54: The DC/DC converter for the electrolyser developed at HESSO Valais for a commercial stack purchased a GINER Inc. USA. On the right are shown the three level: top: the 700 V to 80 V conversion, in the middle the 80 V to low voltage Uout, which is the input voltage to the electrolyser. In the final version the upper stage has been replaced by a commercial VS120 (Studer Innotec), the same system as for the batteries.

The DC/DC converter for connecting the electrolyser directly to the DC-bus voltage has been developed at HESSO Valais, by the group for power electronics. This development work has been co-sponsored by EOS-Holding between 2016 and 2018. Electolyser stacks (PEM and alkaline) generally operate at several hundred mA/cm to about 1 A/cm2 and have a typical active electrode on the order of hundred cm2. Thus, the current of a typical electrolyser in the 5 kW range that we are aiming for in this project is around 50 to 200 A. This leads to very low voltages around 30 to 50 V. As the voltage difference between the 700 V bus voltage and the required voltage for an electrolyser in the power range of several kW is very large a two level approach was implemented. In a first step reducing the voltage from 700 V to a constant 80 V level and in the second step from the 80 Volt down to the required and regulated electrolyser voltage, see Figure 54. The design has been held flexible such that it can be adapted to power upgrades in case in a future application project a different model (PEM or alkaline) will be integrated into the DC-microgrid, which is actually foreseen for the new system setup at the new Campus Building Energypolis of the HESSO Valais in Sion.

11.5 Bidirectional DC/DC converter for battery storage

The bidirectional DC/DC converter for charging and discharging the batteries took a key role in this project, since the storage elements are the central requirement for smoothening the strongly varying PV-power with time. In addition in this project, the battery charger needed to take the role of the voltage

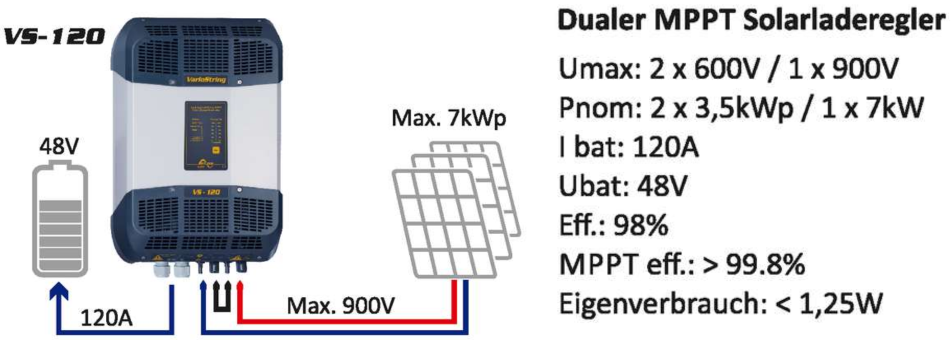

Figure 55: Bidirectional DC/DC converter from Studer-Innotec employed for all batteries and the upper voltage stage of the electrolyser.

regulator in the operating mode 2, where the AFE is only the slave to transmit the programmed excess or missing power to the AC-grid and cannot regulate the voltage anymore. This central element has been provided by Studer-Innotec SA with specific modifications compared to the commercial model of the VS120, see Figure 55.

11.6 Hydrogen electrolyser and hydrogen storage system

The electrolysis system has been setup, based on a purchased electrolysis stack. This allowed obtaining insight into the electrolysis system, opposed to purchasing an entire system, and subsequently dismantling and modifying the power electronics and data acquisition inside. Due to this procedure, all relevant parameters are directly accessible, like liquid and gas flows, pressure, etc. A schematic of the system with all components is shown in Figure 56. Initially a stack with only 300 W nominal power had been installed, which was after successful operation upgraded into a 5 kW from Giner Inc. USA.

After generation, the hydrogen needs to be stored for relevant storage cycles of electric power. As storage element, a pressure bottle filled with metal-hydride has been assembled and installed by the group of Prof. Andreas Zuettel, EPFL/LMER. The capacity of the metal hydride system amounts to

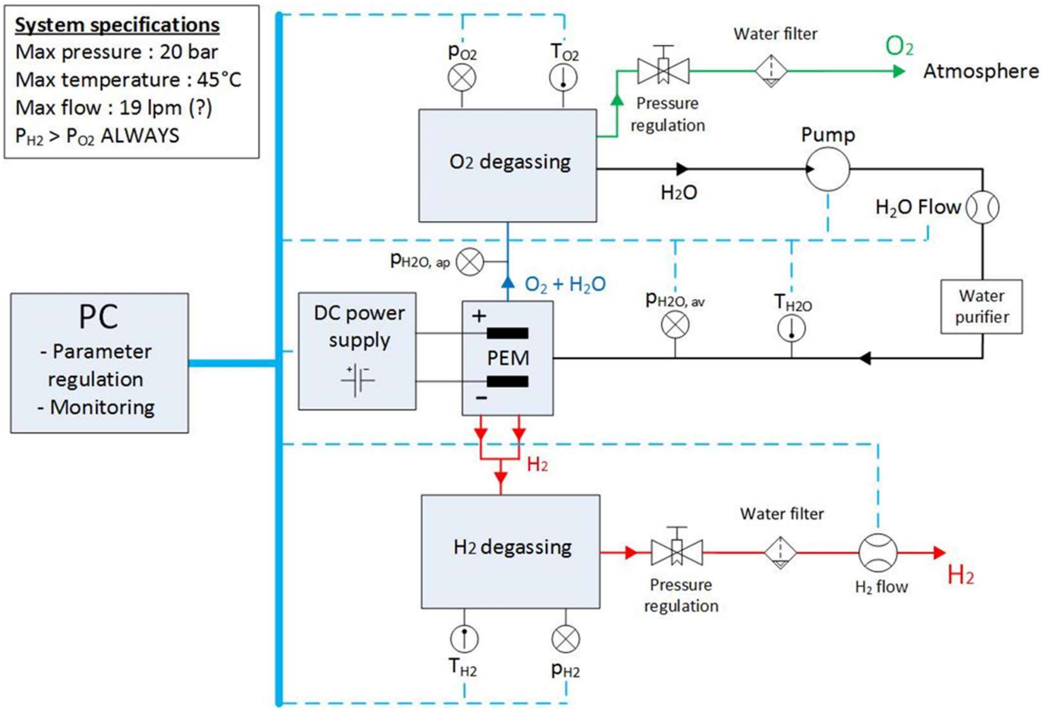

Figure 56: Schematic of the electrolyser system, which was setup around the purchased PEM stack, shown in the centre.

about 12 kWh, which is therefore sufficient for more than two hours of operation at nominal power of the electrolyser stack and can thus act as an additional storage element.

11.7 DC/AC converters for various consumers

The integration of consumers into the DC-microgrid required a compromise in terms of power conversion, since only few direct DC-appliances are available on the market. This is presently the main obstacle for the market introduction of the DC-technology. Therefore, we choose to create local AC-subloads, using commercially available variable frequency drives, supplemented with a filter and a transformer for reduction of higher harmonics and galvanic separation, see *Figure 57*.

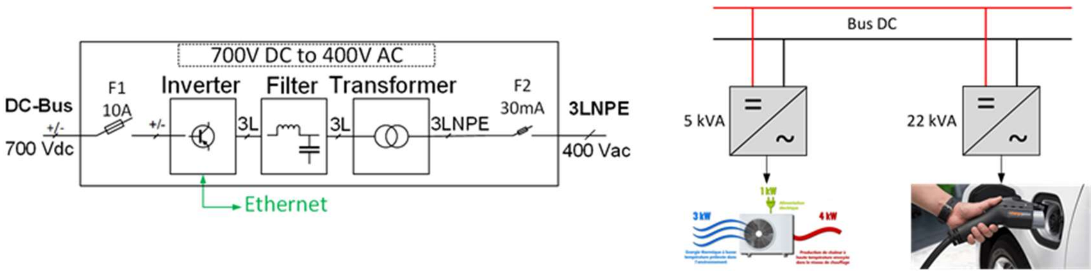

Figure 57: Schematics of the integration method chosen for the consumers. Two circuits of this type were implemented, one for the tow air conditioning systems and the heat pump, of about 5 kW maximum power, the other for the EV-charger of about 22 kW power.

11.8 Safety and supervision

The present microgrid is built as an extension of the previously operating DC-bus link connecting 30 DC/DC individual PV converters to an active front end AFE of 10 kW nominal power. This first AFE (DC/AC converter) caused current faults to ground and thus had the DC bus tripped regularly. In order to be able to analyse these problems, ground fault measurements have been installed. The standard topology of the "Bender" equipment used for earth fault current measurements is shown in *Figure 58*.

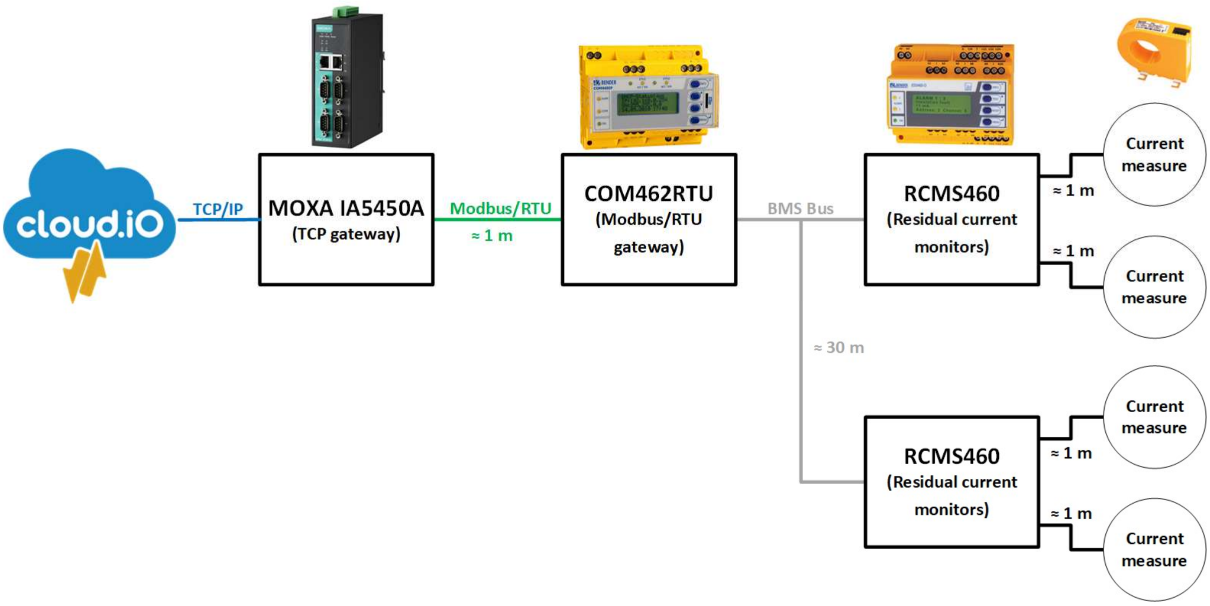

Figure 58: Topology of the default current detection system from Bender with its communication equipment.

For the installation in our DC-microgrid, we have chosen six key positions, which we estimated to be the most critical in our topology, see *Figure 59*.

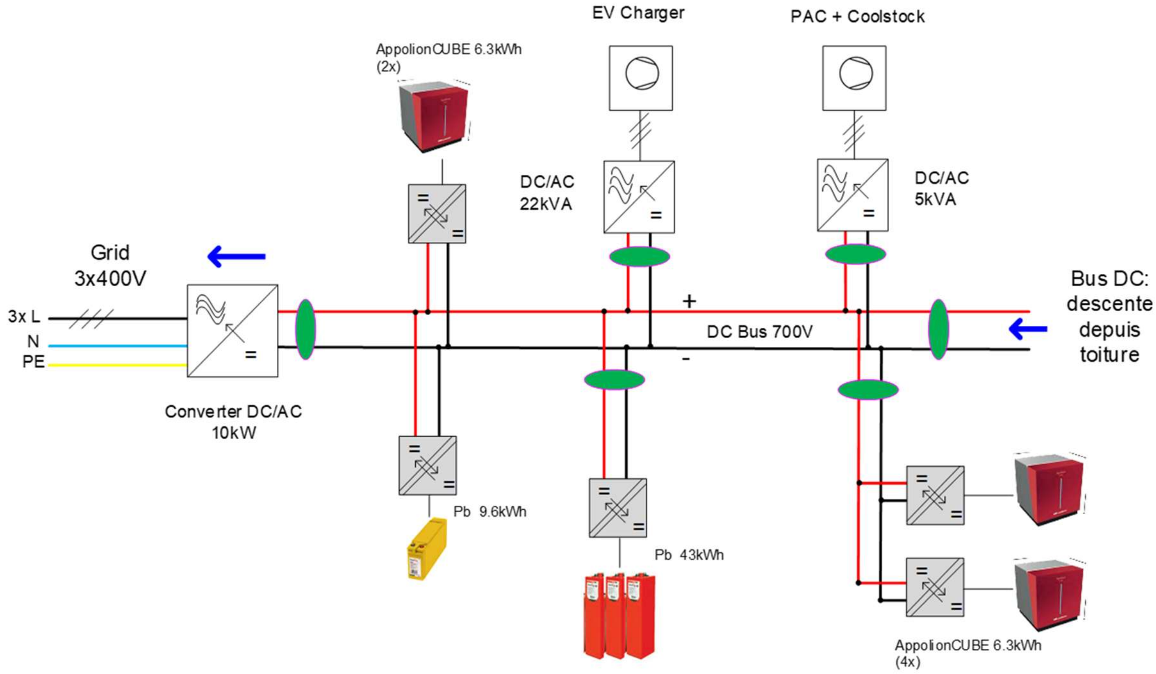

Figure 59: Installation points of the differentially measuring fault current detection sensors (6 sensors), marked as green ellipses around the bipolar DC-bus cable.

This leakage current detection system measures the leakage current of the six channels every 10 milliseconds. If no errors are detected, i.e. the leakage current is in the correct range below 30 mA, the measured current values are recorded via our cloud-IO system every 10 seconds, since recording every 10 ms would explode the size of the storage database. However, if the leakage current exceeds the limit of 30 mA (predefined in a configuration file) the recording time is set to 10 ms to allow the user to view all leakage current problems. Below a certain current level of 4mA, the measured values are not stored. The Grafana display is therefore visible for measurements above this level only.

Figure 60: Leakage current measurements on the AFE (red) and on a storage battery pack (yellow).

Figure 60 shows an example of an alarm given according to a predefined threshold (which is 15 mA in this case) in the fault current detection device. Based on this alert function, indicating a leakage current exceeding a predefined threshold, a rapid shutdown of either the entire DC-bus system or a sub branch can be triggered. We estimate such a rapid shutdown system to be a crucial element for any further development of the technology, required for to comply with modern safety standards.

11.9 Data communication system

Data handling and storage is shown in Figure 1 and Figure 61. The data transmitted via the cloud-IO broker are stored in databases for the use by all other clients, which can be the devices themselves, the EMS or a displaying program or a human operator who likes to retrieve data directly. The storage in terms of time series is done presently on a regular 10 sec basis for most of the devices. This interval leads to significant amounts of storage space in the range of GigaBytes over one year of operation.

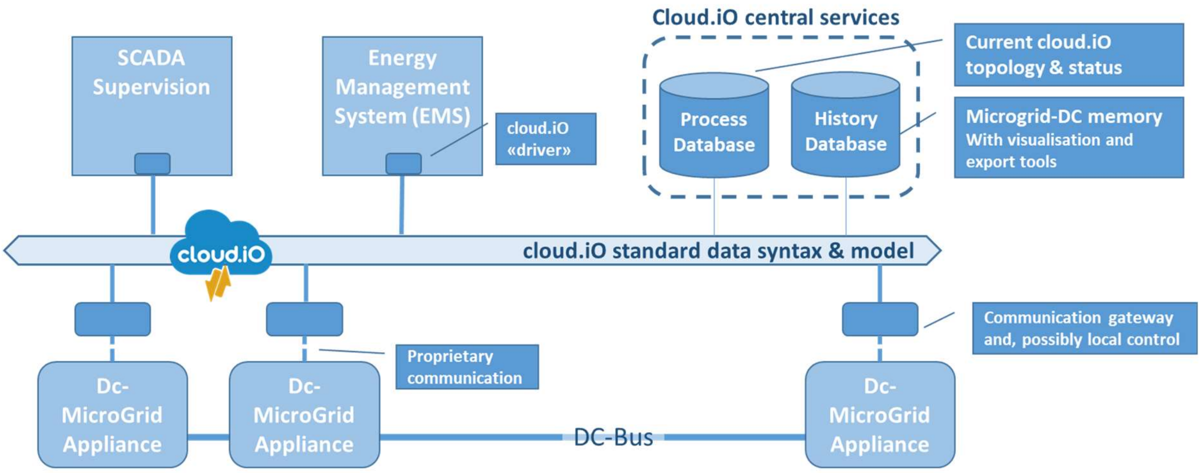

Figure 61: Schematic representation of the cloud-IO broker and it data exchange with the components of the DC-microgrid, see reference [cloud-IO].

12 Annex B1 - EMS of HEIA-FR

12.1 Objective

The HEIA-FR had the goal of building an energy management system (EMS) that will control and regulate the power flows within the DC-microgrid of HE-VS. While deployed, the regulation of the EMS must ensure that the difference between the power consumed from the AC-grid and the forecasted 48 hours power is lower than 1% ($|\Delta| \leq 1\%$) for every time step of 15min.

12.2 Forecast algorithm

To optimize regulation and reach the tolerance range of $|\Delta| \leq 1\%$, the forecast power flows must be taken into account. Therefore, an algorithm was developed, which predicts the power flows in the DC-microgrid for the next 48 hours.

12.2.1 Forecast production

Using the weather forecast, eEnergy Center computes the forecast production of the PV installation on the roof of HE-VS. As an example, Figure 62 illustrates the production forecast of the 27 of September 2019.

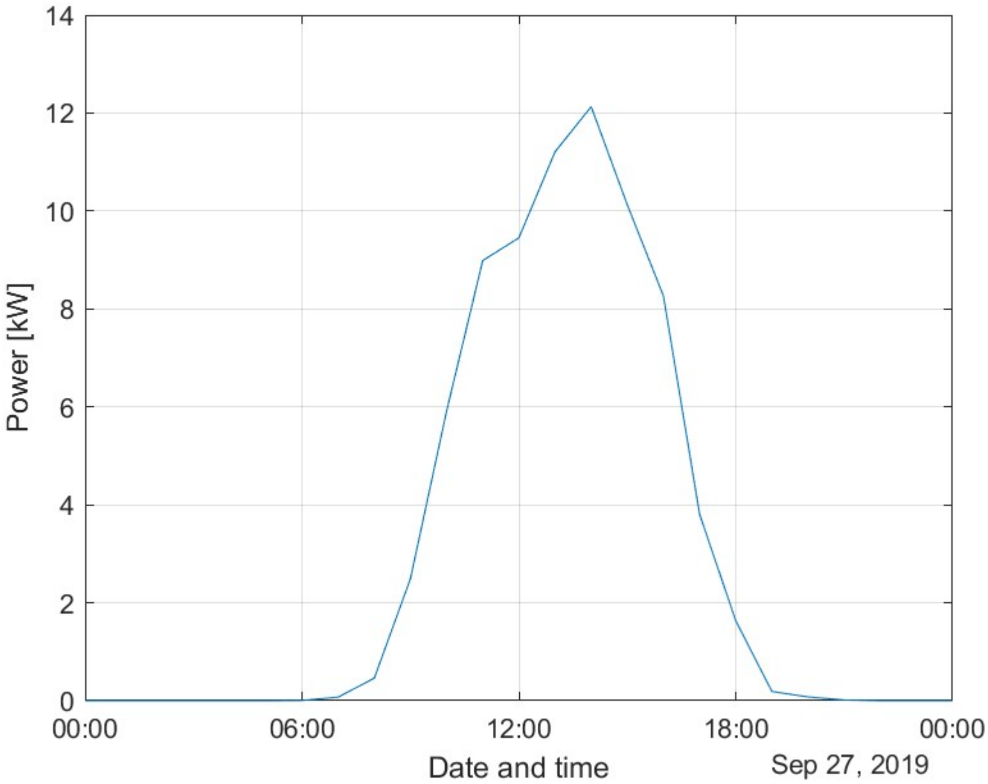

Figure 62 : PV production forecast of the 27.09.2019

12.2.2 Forecast consumption

The second input is the forecast consumption of the DC-microgrid. First, we consider a constant 750W consumed by the PAC (heat pump) and the air conditioning system. Although the EV charger is used, its consumption can’t be predicted yet. For more realistic situation, 2 households are emulated by 2 resistances, each having the consumption profile as shown in Figure 63.

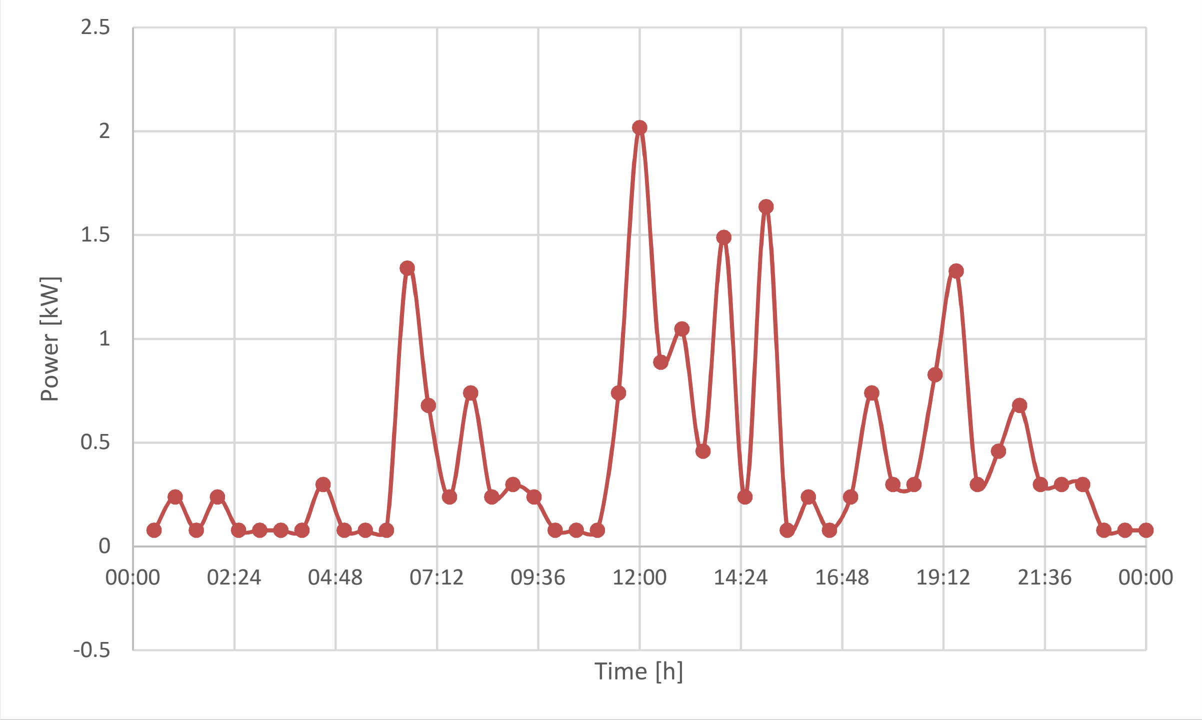

Figure 63 : Household daily consumption

Figure 64 illustrates the total daily consumption forecast of the DC-microgrid.

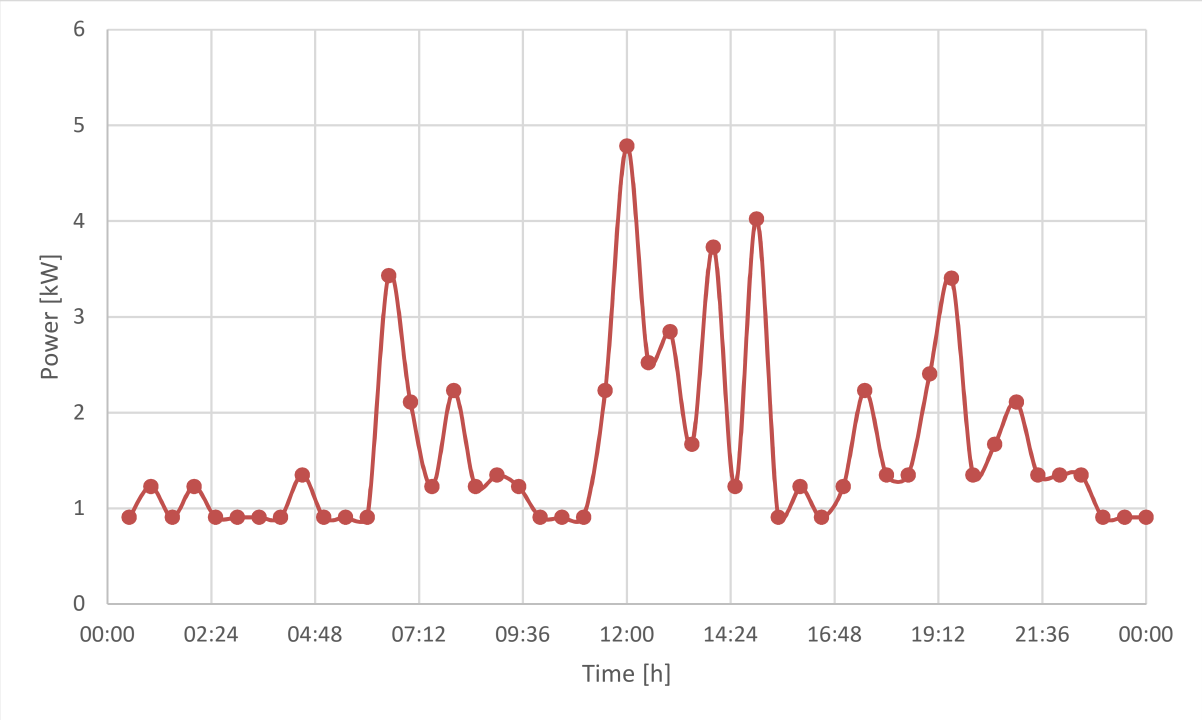

Figure 64 : Daily consumption forecast, consisting of two households plus constant consumer.

12.2.3 State of charge and specifications of the batteries

To accurately predict the behavior of the power flows in the DC-microgrid, the real time state of charge (SoC) of each battery is retrieved from the broker CloudIO. Furthermore, Table 12 illustrates the main batteries specifications needed to compute the amount of power to be sent/retrieved to/from the batteries, i.e. the maximum power to charge/discharge the batteries and the maximum energy which could be stored.

Table 12 : Batteries specifications

Battery number	Designation	Chemistry	Maximum power [kW]	Maximum energy [kWh]
01	Apollion cube	Li-ion	7.0	13.6
03	CE01c	Pb	4.5	45.0
04	Apollion cube	Li-ion	7.0	13.6
10	BMZ	Li-ion	7.0	10.0
11	BMZ	Li-ion	7.0	10.0

12.2.4 Algorithm criterion

Based on the daily production, the daily consumption and the real time SoC of the batteries, the algorithm of the EMS will compute the forecast power profiles to maximize the self-consumption, i.e. maximize the use of the batteries and minimize the power profile exchanged between the DC-microgrid and the AC-distribution grid.

The algorithm outputs are:

- The predicted profile for the next 48h of the exchange between the DC-microgrid and the AC-distribution grid ($B_{forecast}(t)$).
- The forecast storage: prediction of the power to be sent/retrieved to/from the batteries for the next 48h.
- The predicted state of charge (SoC) of the batteries for the next 48h.

12.3 Regulation of the DC-microgrid

12.3.1 Graphic interface

To monitor the DC-microgrid, a graphic interface was developed (Figure 65). It shows the real data (from CloudIO) and the forecasted ones, computed with the developed algorithm. The first scrolling chart illustrates the power flows in the DC-microgrid, which are:

- PV production: Amount of power produced by the PV installation of the HE-VS
- Consumption: Total consumption of the DC-microgrid
- Balance: Power exchanged between the DC-microgrid and the AC-distribution grid
- Storage: Power sent/retrieved to/from the batteries. It is positive if the power is retrieved from the batteries.

On the second scrolling chart are plotted the real and forecast SoC of the batteries. In the lower section of the user interface, there are indicators which designate the real and forecast power at the moment, the real time state of the batteries in more details and the power setpoint sent to each battery. When the screenshot of Figure 65 was taken (30.10.2019), the DC-microgrid was being tested by HE-VS. To avoid having an interference with the ongoing test, the regulation was deactivated, and the EMS was deployed on reading mode only.

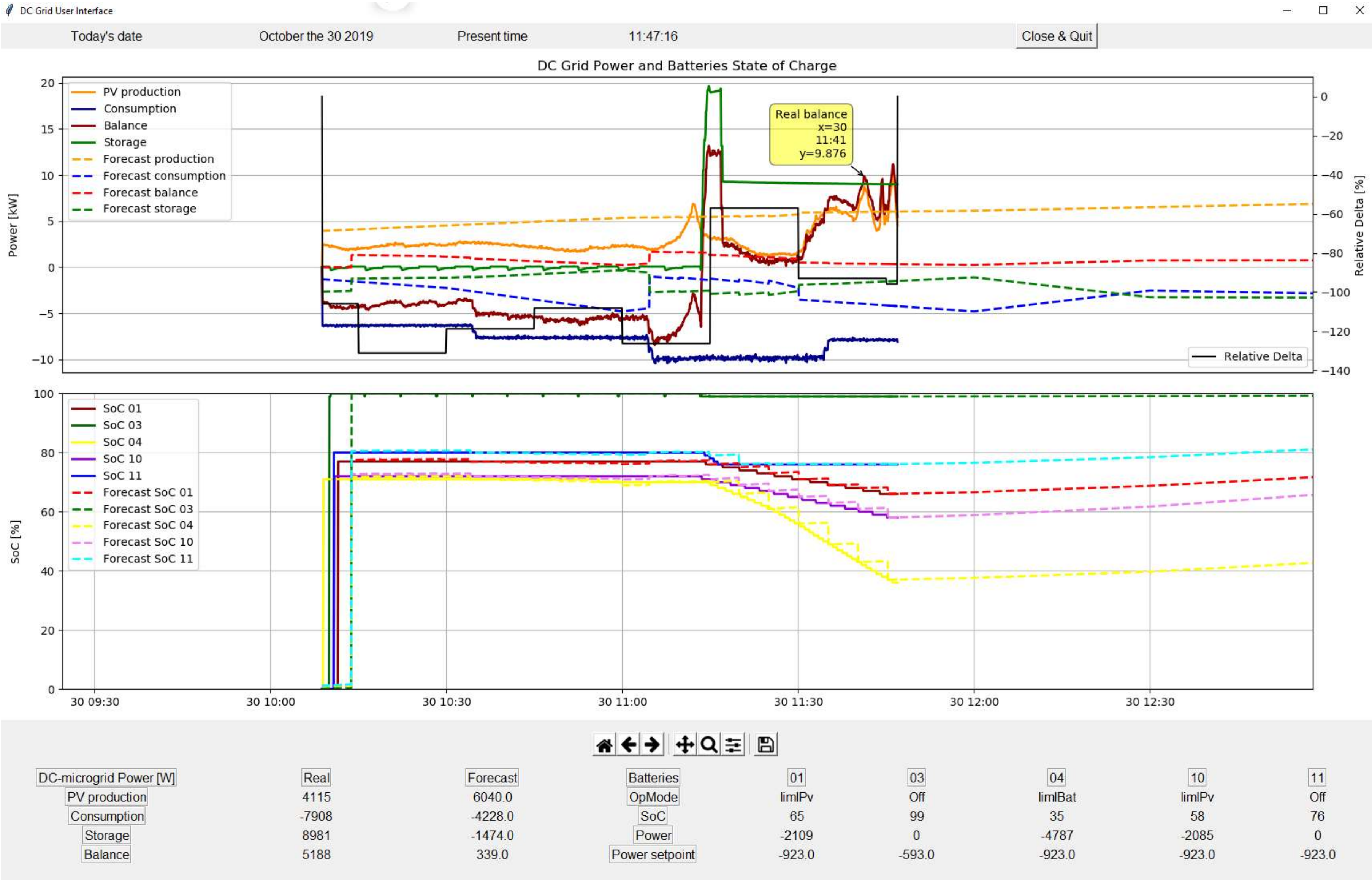

Figure 65 : Screenshot of the graphic interface

12.3.2 Regulation of the DC-microgrid

In this EMS, the operating mode 1 is adopted to control and regulate the power flows in the DC-microgrid. At each time step, orders to charge/discharge the batteries are sent so that the real power exchanged between the DC-microgrid and the AC-distribution grid (balance, $B_{real}(t)$) is as close as possible to the forecast power computed with the algorithm (forecast balance, $B_{forecast}(t)$):

$$B_{real}(t) \cong B_{forecast}(t)$$

The inputs of the regulation are:

- The forecast balance $B_{forecast}(t)$ in [kW]
- The real production $PV(t)$ in [kW]
- The real consumption $C(t)$ in [kW]
- The real time SoC of the batteries.
- The batteries specifications.

At each regulation time step (5s), the amount of power to stored/retrieved from the batteries ($S(t)$) is computed as follows:

$$S(t) = PV(t) + C(t) - B_{forecast}(t)$$

$S(t)$ is divided between the batteries, giving the power setpoints to be sent to each battery.

12.3.2.1. Performance indicator

To evaluate the performances of the regulation and to quantify if a microgrid user respects the forecast balance $P_{forecast}(t)$ for the next 48 hours, the relative Delta (Δ) is used as an indicator and computed as follows:

- The forecasted energy consumed from the grid is given by integrating the forecast balance over a time step of 15min:

$$E_{forecast} = \int_{t_1}^{t_2} B_{forecast}(t)\, dt$$

$$t_2 - t_1 = 900s = 15min$$

- The same computation can be done on the real balance:

$$E_{real} = \int_{t1}^{t2} B_{real}(t)\, dt$$

- Each time step of 15min gives one value for $E_{forecast}$ and E_{real}.

- The Relative Delta is the percent of the forecast energy related to the real consumed energy from the grid.

$$\Delta = \frac{E_{forecast} - E_{real}}{E_{real}} * 100\ [\%]$$

- For each microgrid user, the absolute value of Δ must be lower than 1%:

$$|\Delta| \leq 1\%$$

Around 13 tests were performed with the most recent version of the EMS. In the next section, the results of one of these are exposed.

12.4 Test results

From the 18.09.2019 08:43 until the 19.09.2019 10:03, the EMS was tested for 1 day, 1h and 20min. Figure 66 illustrates the power flows during the test. The first subplot shows the real power flows and the second illustrates the predicted power profiles computed with the algorithm.

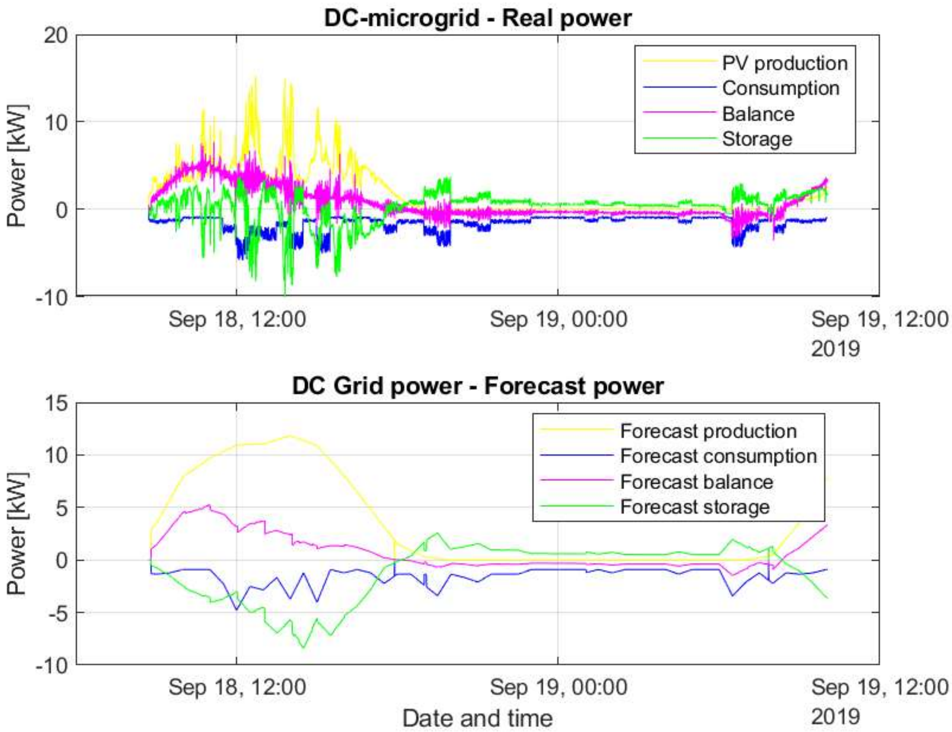

Figure 66 : Test result of the 18-19.09.2019

Figure 67 illustrates the forecast balance, the real balance and the Relative Delta (Δ). Despite the fluctuation, the real balance is centered around the target values (forecast balance).

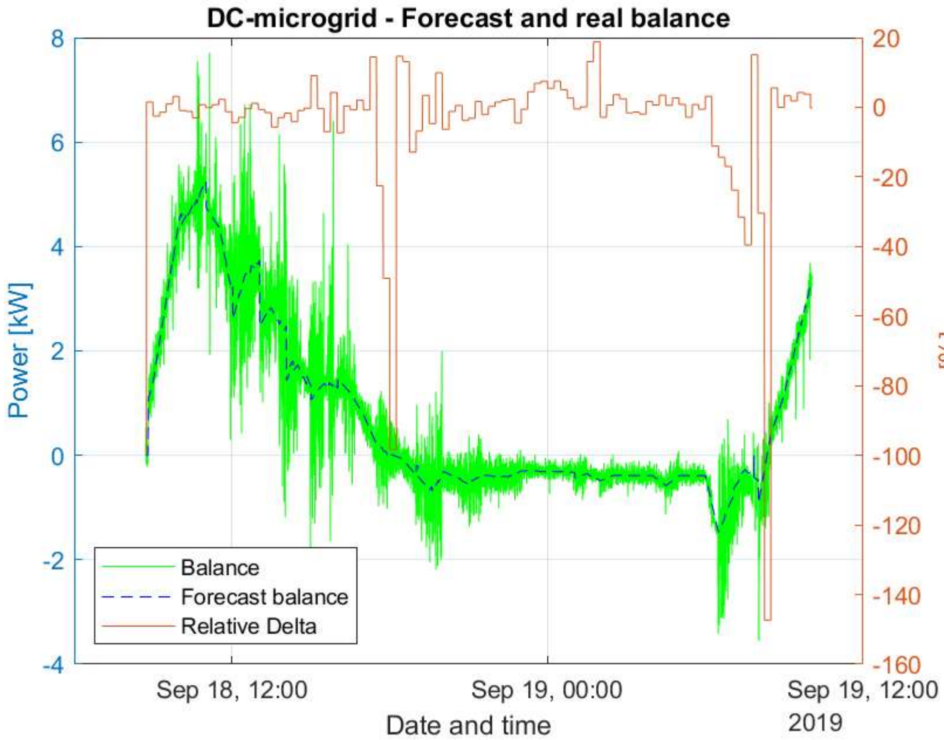

Figure 67 : Real balance, forecast balance and Relative Delta

Figure 68 illustrates the Relative Delta distribution, which represents the frequency of appearance of each value (N).

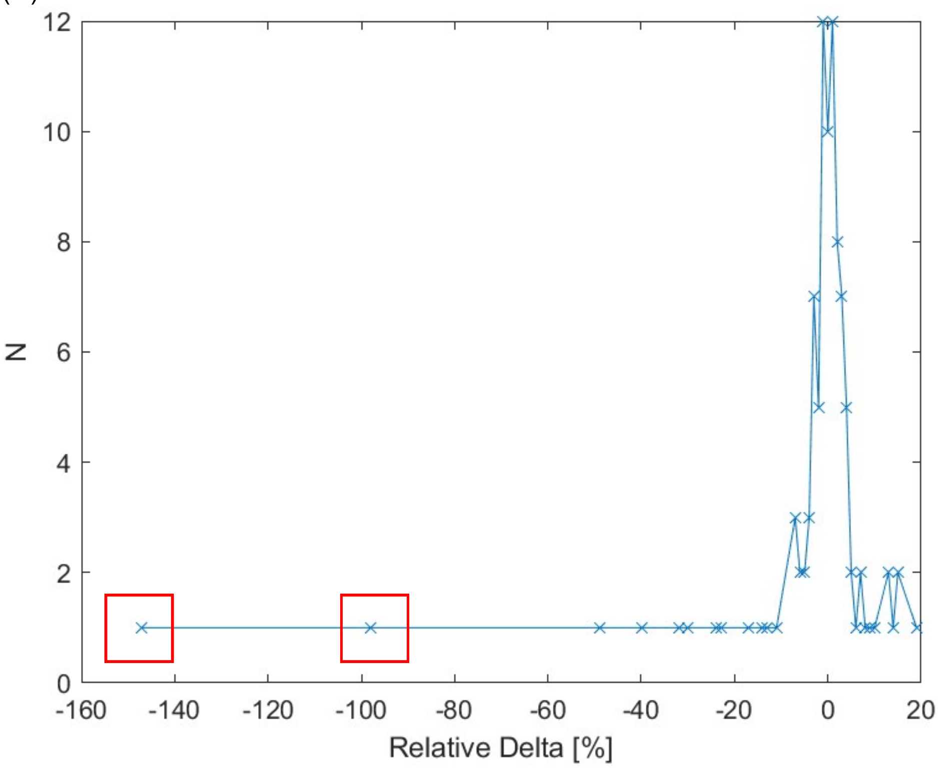

Figure 68 : Relative Delta distribution

Most values are centered around 0%, i.e. in range from -20 to +20%. Among 102 values of Relative Delta (N_{total}), 25 are satisfying the tolerance $|\Delta| \leq 1\%$, which represents:

$$\frac{N_{\pm 1\%}}{N_{total}} = \frac{25}{102} * 100 = 24.7\%$$

This means that, during this day of testing, the tolerance range of $|\Delta| \leq 1\%$ is only achieved in about 25% of the time.

12.4.1 Special cases

With respect to the results presented above, it worth observing the presence of special cases, where the Relative Delta has values far away from the tolerance range (red squares in Figure 68). In this test, we selected the most extreme values, i.e. $\Delta = -147\%$ and $\Delta = -98\%$ to be analyzed.

a) $\Delta = -147\%$

This value was obtained 19.09.2019 during the time step from 08:15 to 08:30.

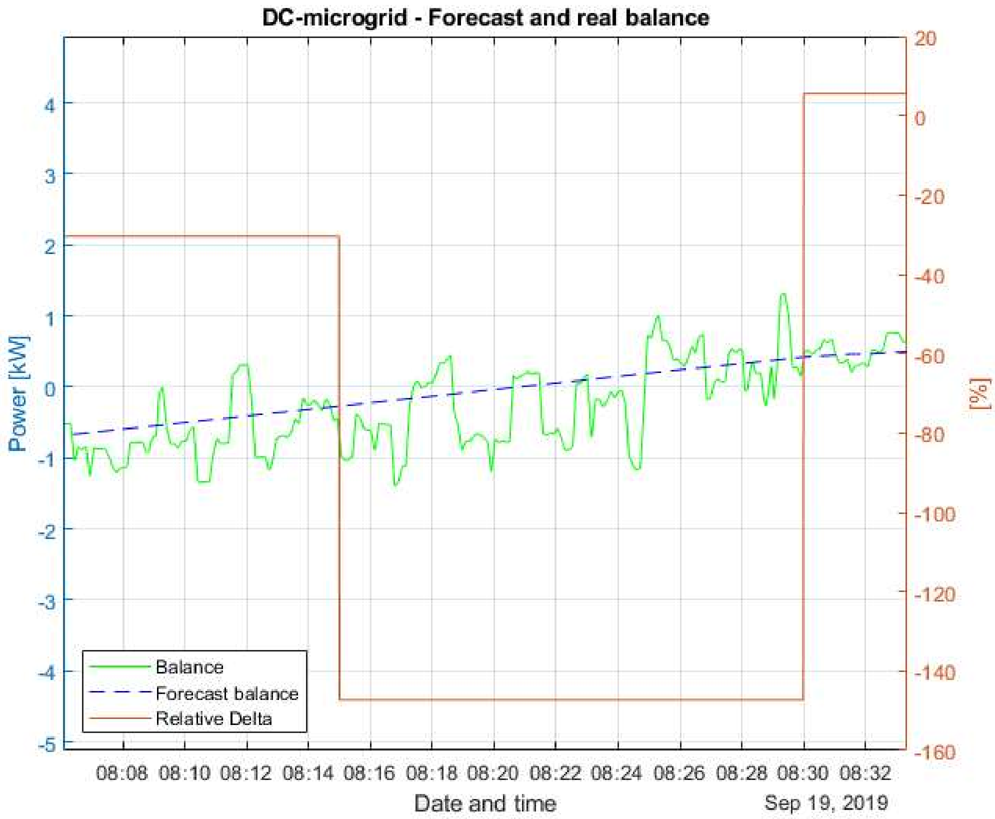

Figure 69 : Illustration of case a (Δ=-147%)

As we can see on Figure 69, $B_{real}(t)$ and $B_{forecast}(t)$, fluctuations are about 0kW. Integrating during this time step gives the following result:

$$E_{forecast} = 67.7kJ = 18.8Ah$$

$$E_{real} = -143kJ = -39.7Ah$$

$$\Delta = \frac{E_{forecast} - E_{real}}{E_{real}} * 100 = -147\%$$

b) $\Delta = -98\%$

This value was obtained the 18.09.2019 and corresponds to the time step from 18:00 to 18:15.

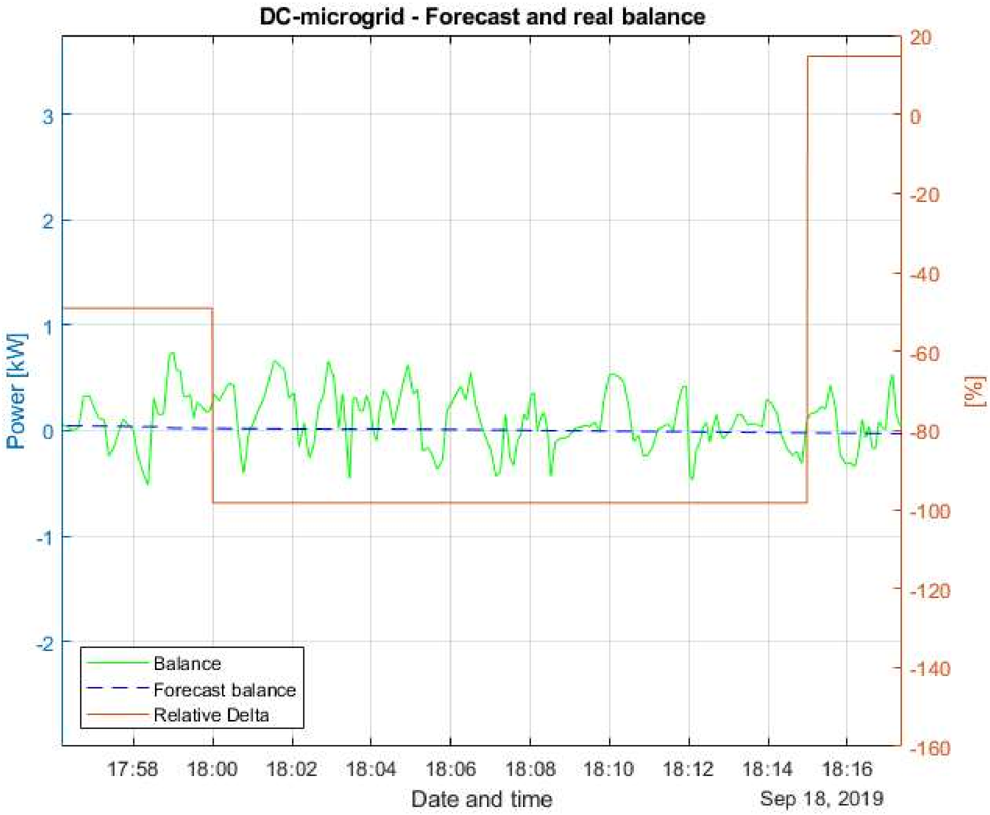

Figure 70 : Illustration of case b ((Δ=-98%))

Figure 70 illustrates the same situation than the previous case, where the power profile fluctuations are around 0kW. Integrating during this time step gives the following result:

$$E_{forecast} = 1.52kJ = 0.42Ah$$
$$E_{real} = 91.98kJ = 25.55Ah$$
$$\Delta = \frac{E_{forecast} - E_{real}}{E_{real}} * 100 = -98\%$$

From these situations, we can try to synthetize a generalization, in case the power profile fluctuation is around 0.

In such situation, while integrating, a positive energy value is compensated by a negative one computed in the next step and vice versa. At the end of the integration, the total energy is close to 0Ah. Consequently, it is possible to have a high difference between $E_{forecast}$ and E_{real}, even if the power profiles are close to each other, like in case b. This leads to a Δ value very far from the tolerance range of $|\Delta| \leq 1\%$.

Furthermore, there are also 2 other special cases, which could be described as singularities:

c) If $E_{real} = 0$, Δ is not defined because of the division by 0.
d) If $E_{forecast} = 0$, we have the situation where Δ is always equal to:

$$\Delta = \frac{E_{forecast} - E_{real}}{E_{real}} * 100 = \frac{-E_{real}}{E_{real}} * 100 = -100\%$$

whatever power profiles are obtained from the tests.

In these exposed cases, it is worth observing that the DC-microgrid user is momentarily “blind and can’t evaluate the performance of the regulation. Despite having $B_{real}(t)$ very close to $B_{forecast}(t)$, information on the behavior of the DC-microgrid is lost and the user will have the same result as a situation where there is a much wider gap between the power profiles.

12.5 Synthesis and possible improvements

Based on the development of the EMS and the performed tests results, the objective of the EMS is partially achieved. There are situations where the tolerance range of $|\Delta| \leq 1\%$ could be reached. Unfortunately, this could be maintained only in 25% of the time.
However, many improvements of the configuration of the DC-microgrid are identified to boost the performances of the EMS.

Here is a list of what could be accomplished in the next phases of this project.

a) Test the EMS during a longer time:

The EMS was tested several times, with a maximum duration of one day. Despite these short tests, it was possible to detect different faults and malfunctions and solve them.
To improve the regulation, it would be helpful to test the EMS for an entire week to check the robustness of the EMS for a long term deployment.

b) Investigate the real maximum power of the batteries:

During some tests, the real power sent to the batteries was lower and couldn’t reach the power setpoint. As an example, during the above-presented test, the maximum real power of battery 11 was 1.35kW, despite having power setpoints up to 2.4kW. This could explain why only 25 values of Relative Delta are in the tolerance range.
To solve this kind of situation, the power limit for each battery, in charge and in discharge, must be tested. Checking if the power depends on the SoC will help know exactly the maximum amount of power that could be set. Consequently, the gap between the power setpoint and the real power will be the smallest, getting the Relative Delta more often in the tolerance range.

c) Characterize the health of the batteries:

Some batteries (i.e. batteries 01,03 and 04) are already several years old and have lost an amount of their autonomy. The used specifications correspond to the batteries when they are new. Characterization tests are useful to know the remaining capacity, the real amount of energy which could be stored and to verify the accuracy of the SoC, in order to increase the accuracy of the algorithm forecast.

d) Improve the prediction of the consumption:

During the EMS tests, the consumption of some elements (PAC and air condition) was supposed to be constant. However, the consumption depends on the season of the year and the daily profile. Therefore, these factors must be taken into account to have a more accurate prediction.

Furthermore, the EV charger is usable, but its consumption couldn't be predicted yet. Knowing that the EV charger could consume up to 10kW for several hours, it is worth investigating this matter and include its forecast to improve the global performance of the EMS.

e) Detect at any time if a battery could be used:

In the current situation, a broken-down or disconnected battery can't be detected. The EMS will still take it into account during deployment. Therefore, the power flows from the batteries will different than expected, which will certainly reduce the performances of the regulation.
A parameter can be used to have information on the usability of the batteries. For example, if it is a Boolean, its value will be true if the battery is usable and false if not (the battery is broken-down or in reparation, etc.). In this case, the battery will be excluded from the algorithm computations.
By including this information, the inputs of the algorithm will be corrected, and the computations accuracy will increase.

f) Find suitable parameters to evaluate the performance of the regulation:

In the test analysis, we encountered some difficulties with the computation of the Relative Delta in some cases (singularities when energy is close to 0Wh). In these situations, the client loses information on the performance of the EMS.

Therefore, a new indicator is needed. Like the Relative Delta, it must quantify the performances of the EMS but without the presence of singularities (no division by 0). Here are two examples of indicators, which could fulfil the presented objective.

- Fixing the maximum value for the power difference.

At each regulation time step, this difference must be lower than a predefined value:

$$\Delta B = |B_{forecast}(t) - B_{real}(t)| \leq \Delta B_{max}$$

Then, D_B quantifies the performance of the EMS:

$$D_B = \frac{\Delta B - \Delta B_{max}}{\Delta B_{max}} * 100 + 100$$
$$D_B \in [0,100]$$

The goal is to have D_B between 0 and 100%. $D_B = 0\%$ if $\Delta B = 0$, and $D_B = 100\%$ if $\Delta B = \Delta B_{max}$.
The best situation is to have ΔB as small as possible, i.e. D_B the closest to 0%.

By doing this, we fix also a maximum value for the energy difference:

$$\Delta E_{max} = \int_{t_1}^{t_2} \Delta B_{max}\, dt = \Delta B_{max} \cdot (t_2 - t_1) = \Delta B_{max} \cdot \Delta t$$
$$\Delta E = |E_{forecast} - E_{real}| = \left| \int_{t_1}^{t_2} B_{forecast}(t)\, dt - \int_{t_1}^{t_2} B_{real}(t)\, dt \right| \leq \Delta E_{max}$$

At each time step of 15min, this difference could also be evaluated to reach the same goal: D_E must be between 0 and 100%.

$$D_E = \frac{\Delta E - \Delta E_{max}}{\Delta E_{max}} * 100 + 100$$

- An indicator based on the formula of method of least squares

The sum of the squared residual is computed as follows:

$$S = \sum \left(y_i - f(x_i)\right)^2 = \sum r_i^{\,2}$$

It is possible to compute the residual (r_i) between the real and the forecast power exchanged between the DC-microgrid and the AC-grid:

$$y_i = B_{forecast}(t)$$

$$f(x_i) = B_{real}(t)$$

$$S_B = \sum \left(B_{forecast}(t) - B_{real}(t)\right)^2 = \sum r_i^{\,2}$$

Each time step of 15min, S_B must be lower than a predefined value:

$$S_B \leq S_{max}$$

D_B evaluates the performances of the EMS:

$$D_B = \frac{S_B - S_{max}}{S_{max}} * 100 + 100$$

$$D_B \in [0{,}100]$$

The regulation fails if D_B or D_E are higher than 100%.

With such indicators, it will be possible to:

- avoid situations with singularities (as long as the reference values are different from 0),
- quantify the EMS performances at any time,
- test the limit of the regulation,
- find new ways to improve the global efficiency of the EMS.

13 Annex B2 - Simulation of the integration of microgrids for distribution grid managers

13.1 Objective

The purpose of the simulation is to study, from the point of view of distribution grid managers (DGM), the consequences of having several microgrids connected to the grid.
Technical and economic advantages of such integration for the DGM will be highlighted, for the case in which every microgrid user respects its consumption profile from the grid (announced 48 hours before) with a difference lower than 1% for each time step of 15min.

13.2 Relative Delta

If a consumer is exploiting a microgrid, he has to respect the following conditions:

1. To announce its consumption profile 48h in advance.
2. To have a difference on the consumed energy lower or equal to 1% ($|\Delta| \leq 1\%$) for each time step of 15min
3. Manage the consumption with the different elements of the microgrid to reduce the maximum power fluctuation. In this situation, the Customer consumptions will look like a continuous function and doesn't have high power fluctuations.

To quantify if a user respects his consumption forecast $P_{forecast}(t)$ for the next 48 hours, the relative Delta (Δ) is used as an indicator and computed as follows.

The forecasted energy is given by integrating the consumption forecast with a time step of 15min:

$$E_{forecast} = \int_{t_1}^{t_2} P_{forecast}(t)\, dt$$

$$t_2 - t_1 = 900s = 15min$$

The same computation can be done on the real consumption of the user:

$$E_{real} = \int_{t1}^{t2} P_{real}(t)\, dt$$

Each time step of 15min gives one value for $E_{forecast}$ and E_{real}.

The Relative Delta is the percent of the forecast energy to the real consumed energy.

$$\Delta = \frac{E_{forecast} - E_{real}}{E_{real}} * 100\ [\%]$$

13.3 Simulation

13.3.1 General situation

N consumers (factories in an industrial area) are connected to the electricity grid. Each one retrieves a power time evolution $P_i(t), i = 1, \dots, N$ from the grid. In consequence, the DGM must provide a power

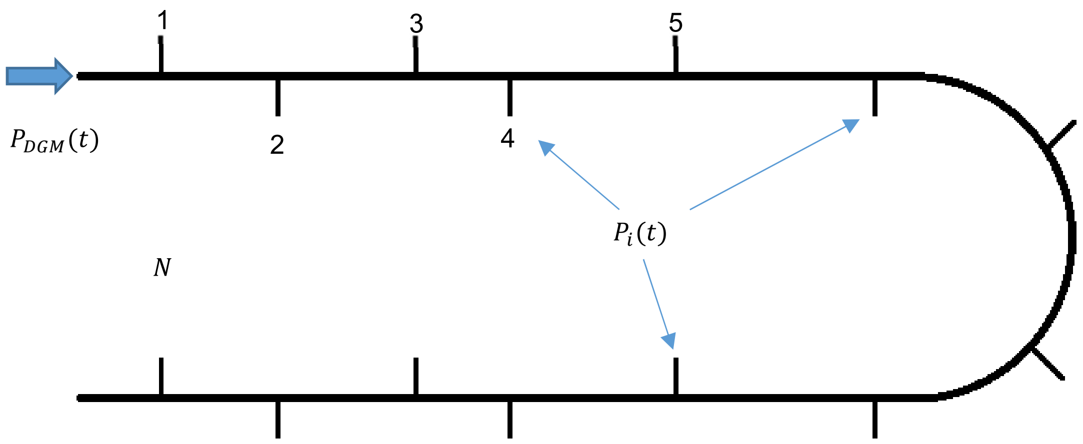

Figure 71 : General situation

$P_{DNM}(t)$ to satisfy the power balance:

$$P_{DGM}(t) + \sum_{i=1}^{N} P_i(t) = 0$$

13.3.2 Scenarios

We assume that 20 consumers are connected to the DGM grid. Among them, n factories consume power from the grid and produce a certain percentage of their consumption energy using PV panels. We call these n factories “prosumers”.
3 different situations will be studied, where the percent of prosumers ($\frac{n}{N}$) varies from 5 to 90%.

1) Only 5% ($n = 1 \rightarrow \frac{n}{N} = \frac{1}{20} = 5\%$) of the clients produce half of their needs. We suppose that this case represents the situation nowadays.
2) In 10 years, we expect that 60% of the factories ($n = 12 \rightarrow \frac{n}{N} = 60\%$) produce 50% of their consumption.
3) In 20 years, almost all factories ($n = 18 \rightarrow \frac{n}{N} = 90\%$) produce 50% of their needs in term of energy.

For each of these scenarios, two simulations will be performed:
- Simulation 1

The n prosumers produce power without a microgrid. The power balance for each prosumer is computed as follows:

$$balance = production + consumption$$
$$P_i(t) = PV_i(t) + C_i(t)$$

with,

$$PV_i(t) \geq 0$$
$$C_i(t) \leq 0$$

The prosumer will directly use what he produces. If $P_i(t)$ is negative, the prosumer doesn't produce enough and will have to retrieve what he needs from the DGM grid. If positive, the production is higher than the consumption. The prosumer will inject the power equal to $P_i(t)$ in the grid.

- Simulation 2

The n prosumers are using microgrid within the factories. In addition to the PV installation, battery modules allow storing energy during night and then to reuse this energy during the day. An EMS (energy management system) allows a smart regulation of the power and energy flow within the microgrid. This helps reducing the power retrieved from the DGM ($P_i(t)$).

13.3.3 Hypothesis

13.3.3.1. Forecast consumption from the grid

In this simulation, we suppose that all consumers respect the forecasted consumption from the grid. The consumers retrieve from the grid exactly the amount of power they announced 48h in advance. In this case, we have:

$$P_i^{forecast}(t) = P_i(t) \rightarrow E_{forecast} = E_{real} \leftrightarrow |\Delta| = 0\%$$

13.3.3.2. Daily consumption

The consumers are N factories, situated in an industrial area. Each one has 15 machining machines with a maximum combined consumption of 24.1kW. 5kW are supplied to 5 offices and other installations within the factory. The total consumption is 27.4kW. One value is given each 30min. Figure 72 illustrates the daily consumption of all consumers $C_i(t)$.

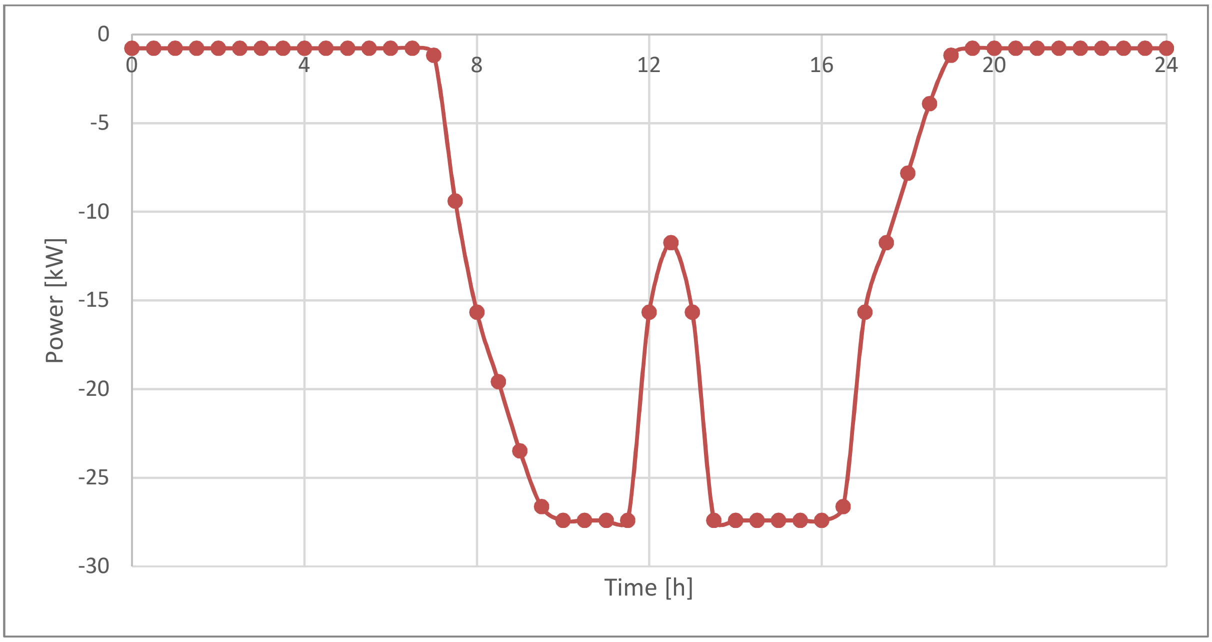

Figure 72 : Daily consumption

Out of office time, 780W are consumed to supply lights, servers and security systems.

Work time starts around 07:00, by turning on the machining machines and starting the production, until reaching the maximum consumption of 27.4kW. The same amount of power is used from 13:00 to 16:30. During the lunch, the consumption is lower as the machines are in standby mode. In the end of the afternoon, only 780W are used starting from 19:00.
In case the consumer doesn't use a microgrid (usual client), the consumption is equal to the power retrieved from the grid:

$$C_i(t) = P_i(t)$$

13.3.3.3. Prosumers without microgrid

A consumer becomes a prosumer when he produces an amount of the energy he needs. In this simulation, we use the real production of the PV panels deployed on the roof of HE-VS, in Sion, of the 21.09.2019 as reference. The peak power is 20.7kW.

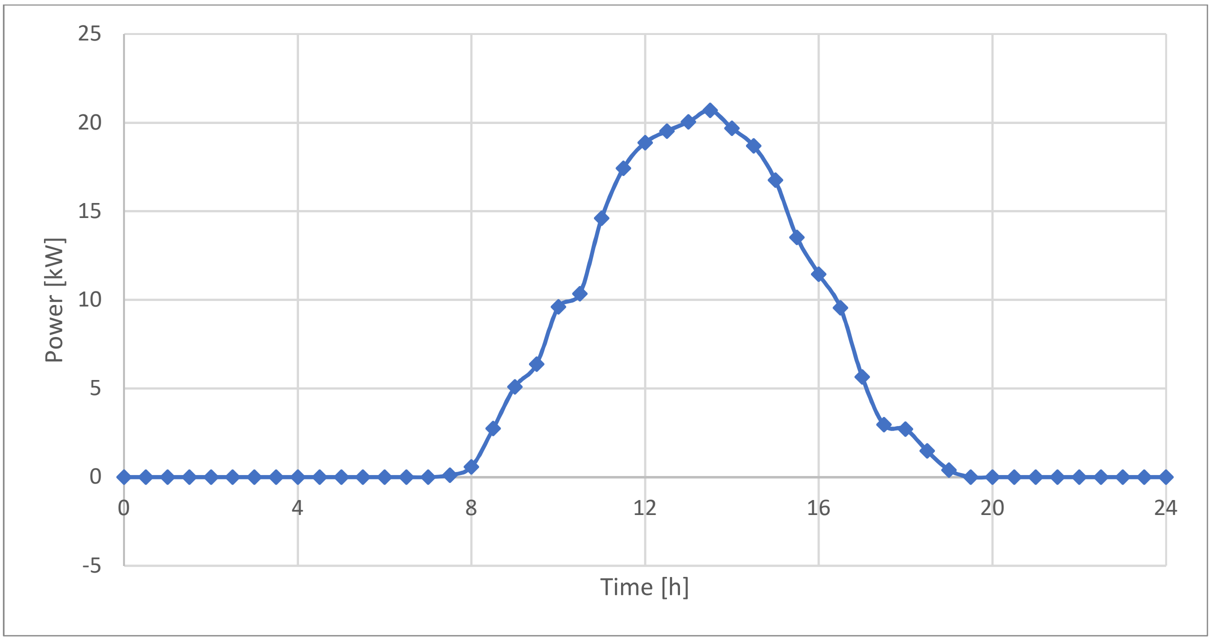

Figure 73 : Prosumer daily production reference

We suppose that all the prosumers produce the same amount of power $PV_i(t)$ with their PV panel (daily production). In this simulation, each prosumer produces half of his needs, which means that the daily produced energy must correspond to 50% on the daily consumption.

$$E_{PV} = \frac{1}{2} E_{consumption} \leftrightarrow \int_{00:00}^{24:00} PV_i(t)\,dt = \frac{1}{2} \int_{00:00}^{24:00} C_i(t)\,dt$$

In case prosumer without microgrid, the power balance is equal to:

$$P_i(t) = PV_i(t) + C_i(t)$$

Figure 74 illustrates the daily consumption, the daily production and the daily power retrieved from the grid for a prosumer without a microgrid.

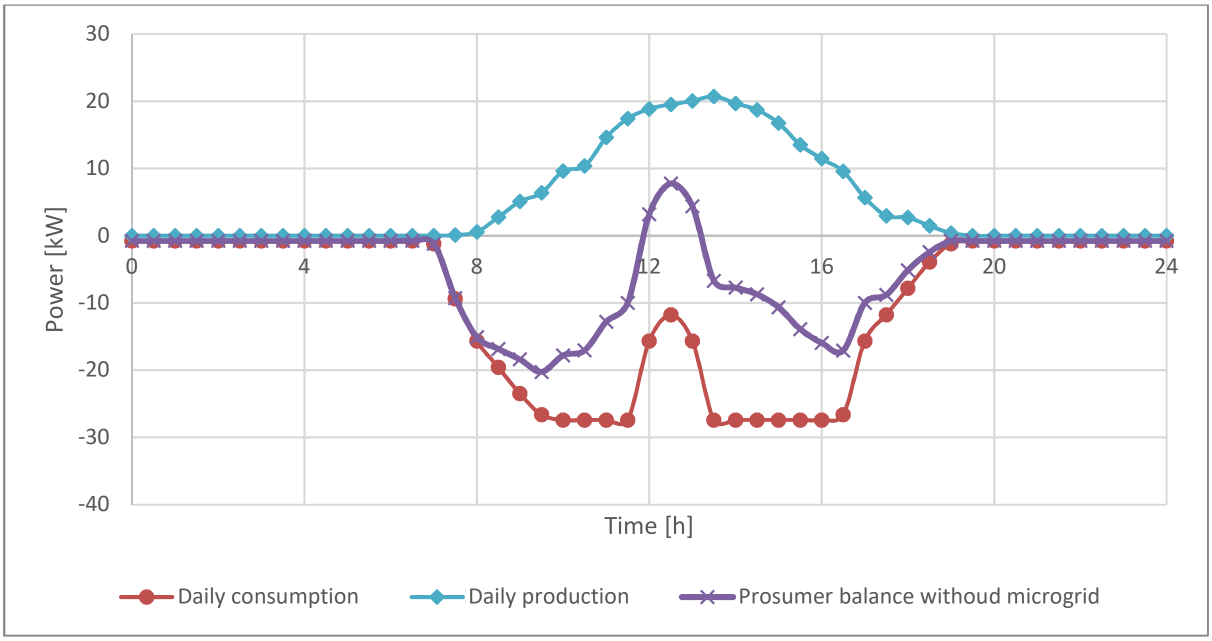

Figure 74 : Prosumer power profiles without a microgrid

The other 50% of the needed energy comes from the grid. In this case, we have the energy balance:

$$E_{consumption} = E_{PV} + E_{Grid}$$

with,

$$E_{Grid} = \frac{1}{2} E_{consumption} \leftrightarrow \int_{00:00}^{24:00} P_i(t)dt = \frac{1}{2}\int_{00:00}^{24:00} C_i(t)dt$$

13.3.3.4. Prosumer with microgrid

In a microgrid, several elements are used to manage the energy and power flow from the grid: PV panels, batteries and consumption elements.

Smart EMS and regulation algorithms help reducing and smoothing the power retrieved from the grid $P_i(t)$. In this situation, it will be easier for the DGM to provide a power corresponding to $P_i(t)$ to the consumers.

To achieve this, several strategies can be adopted. One of them is to use a part of the DGM power to charge the batteries during the night. Then, during working time, the EMS will use these batteries to regulate the power and energy flow to satisfy the power balance:

$$PV_i(t) + P_i(t) + Batteries_i(t) + C_i(t) = 0$$

In Sion, an EMS was deployed by HE-VS to regulate the energy and the power flows in the microgrid. The results show that the peak power exchanged by the DGM with microgrid is about 5 times lower than the maximum consumption in a situation without microgrid.

$$\max(P_i(t)) = \frac{1}{5}\max(C_i(t))$$

In the simulation, we adopt this result as condition to bound the maximum value of $P_i(t)$, which is around 6kW. Then the shape of $P_i(t)$ is adjusted in order to satisfy the energy balance:

$$E_{consumption} = E_{PV} + E_{Grid}$$

with,

$$E_{Grid} = \frac{1}{2} E_{consumption} \leftrightarrow \int_{00:00}^{24:00} P_i(t)dt = \frac{1}{2} \int_{00:00}^{24:00} C_i(t)dt$$

We also adopt the strategy mentioned before: the EMS will charge the batteries during the night and then use them during working time. Combining the previous conditions, the daily consumption, production and balance of one prosumer with a microgrid are illustrated in Figure 75.

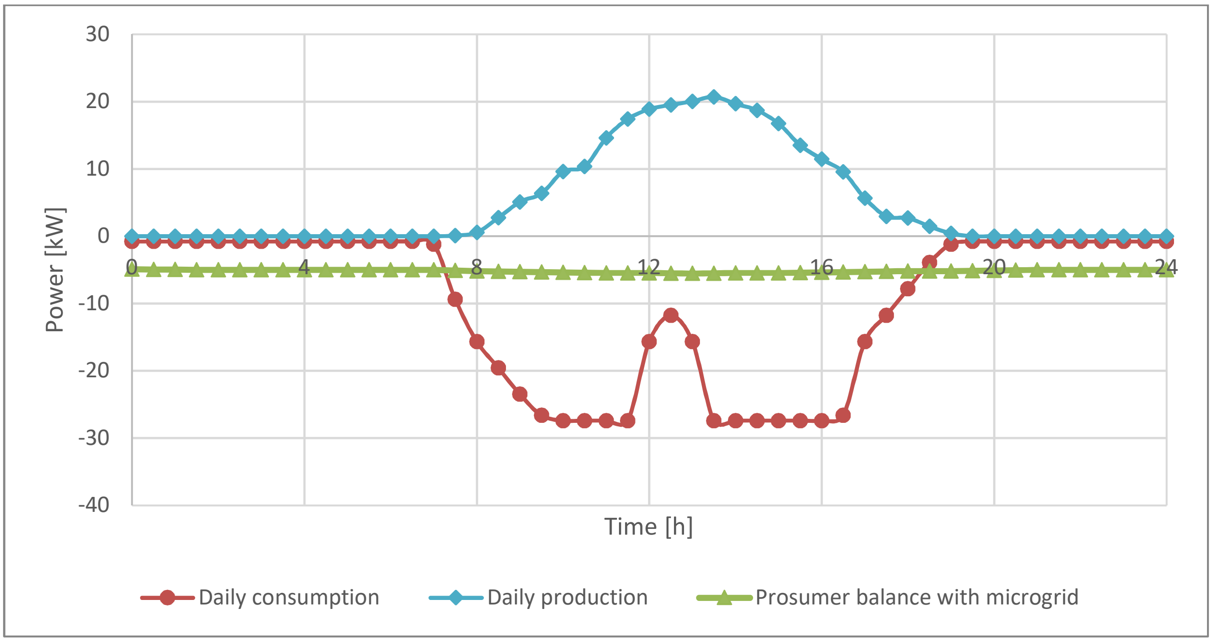

Figure 75 : Prosumer power profiles with a microgrid

13.3.4 Computations

We adopt the point of view of the DGM as a reference to set the sign of the power values. If a value is negative, the DGM must provide the power to the consumers. If positive, the DGM has to absorb it.
The total consumption of the usual clients is computed as follows:

$$C_i^{total}(t) = (N - n) \cdot C_i(t)$$

The total power produced by all prosumers is equal to:

$$PV_i^{total}(t) = n \cdot PV_i(t)$$

The power balance for the prosumers without microgrid is computed as follows:

$$P_i^{total}(t) = n \cdot (C_i(t) + PV_i(t))$$

If the prosumers are exploiting microgrids, the total power balance is the sum of the balance exposed on Figure 75. The power the DGM must supply to all consumers is given by adding the prosumers balance to the consumption of the usual clients:

$$P_{DGM}(t) = C_i^{total}(t) + P_i^{total}(t) = (N - n) \cdot C_i(t) + n \cdot PV_i(t)$$

Integrating this power for each day gives the daily energy to be provided by the DGM:

$$E_{DGM} = \int_{00:00}^{24:00} P_{DGM}(t)\, dt$$

13.4 Results

13.4.1 Scenario 1

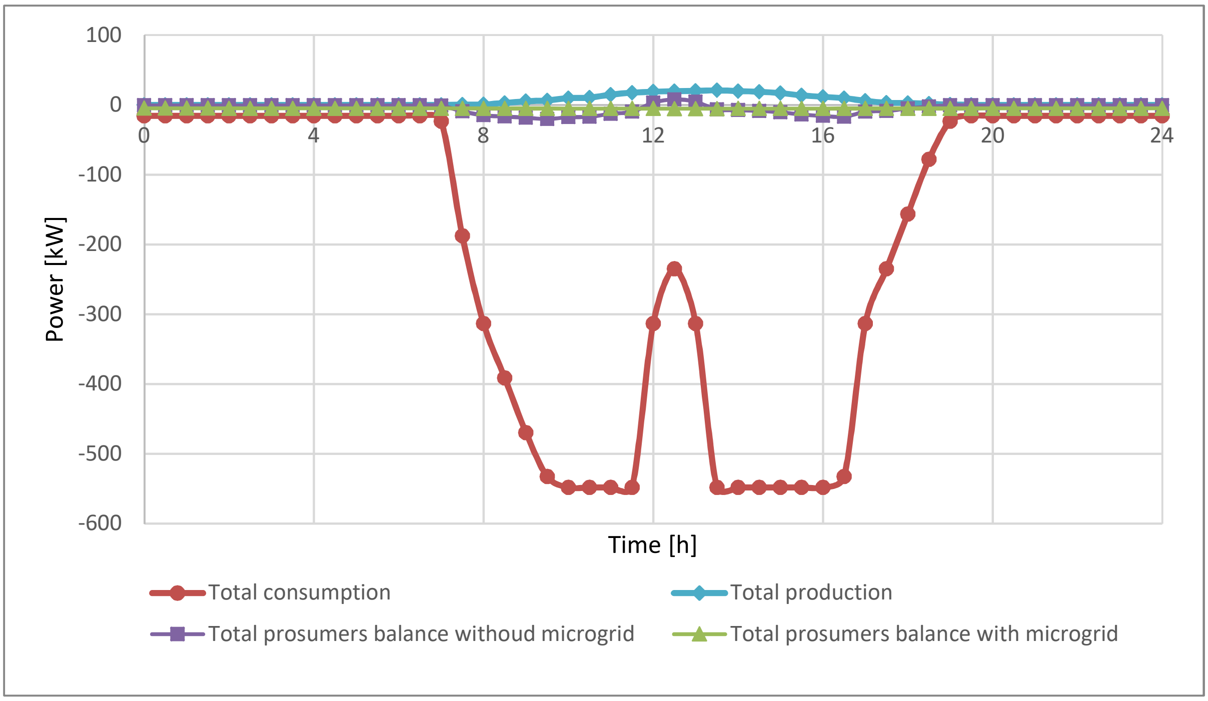

Figure 76 : Scenario 1: Prosumers total power profiles

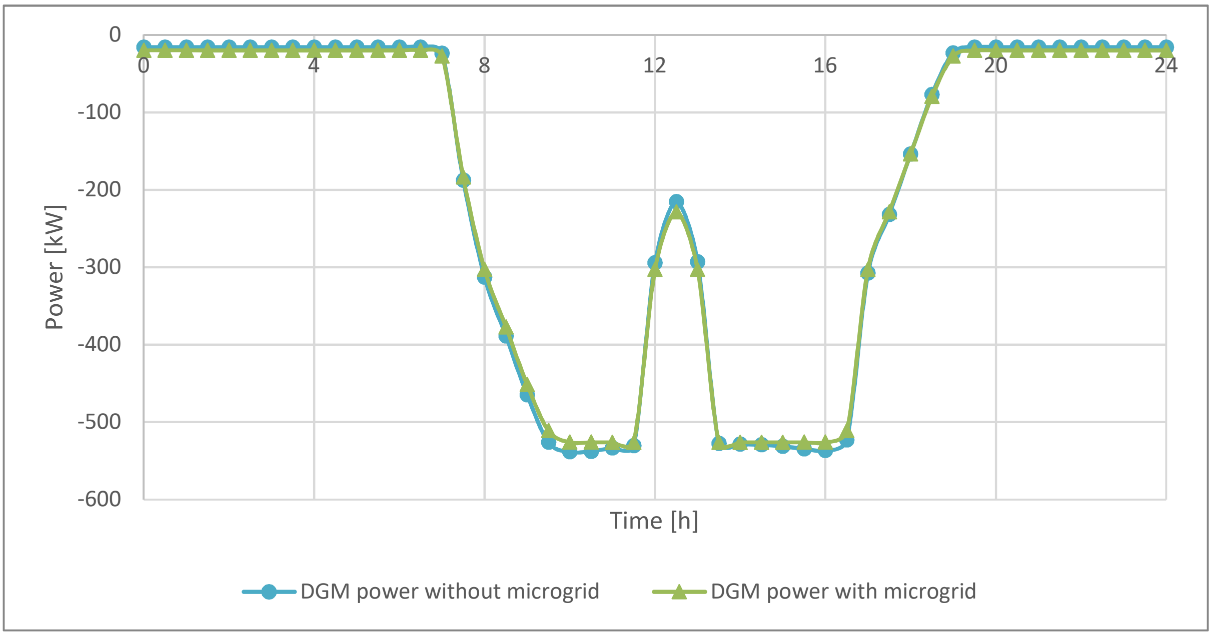

Figure 77 : Scenario 1: DGM power profiles

13.4.2 Scenario 2

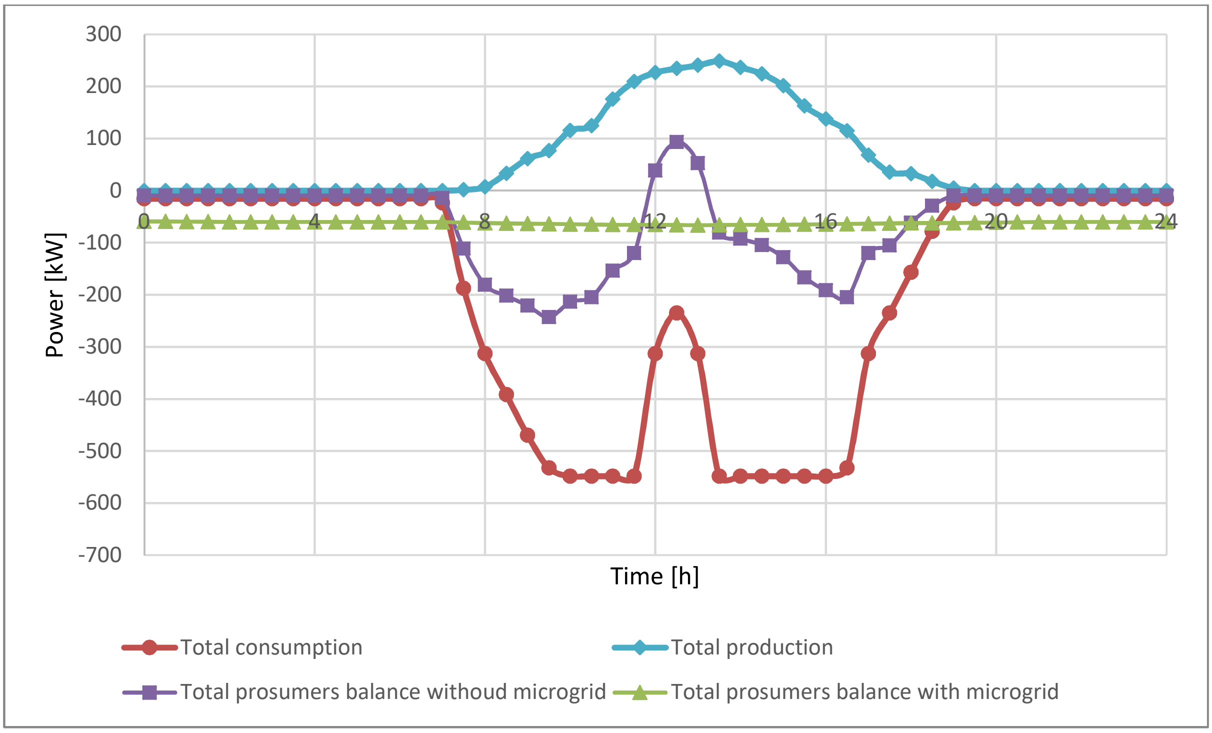

Figure 78 : Scenario 2: Total prosumers power profiles

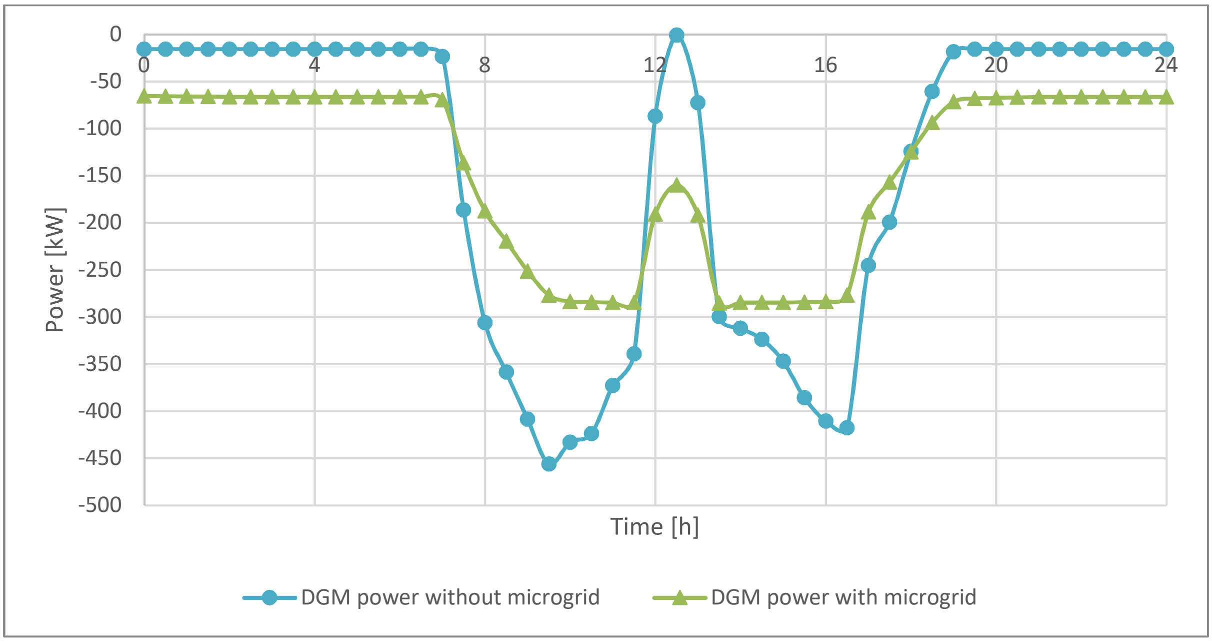

Figure 79 : Scenario 2: DGM power profiles

13.4.3 Scenario 3

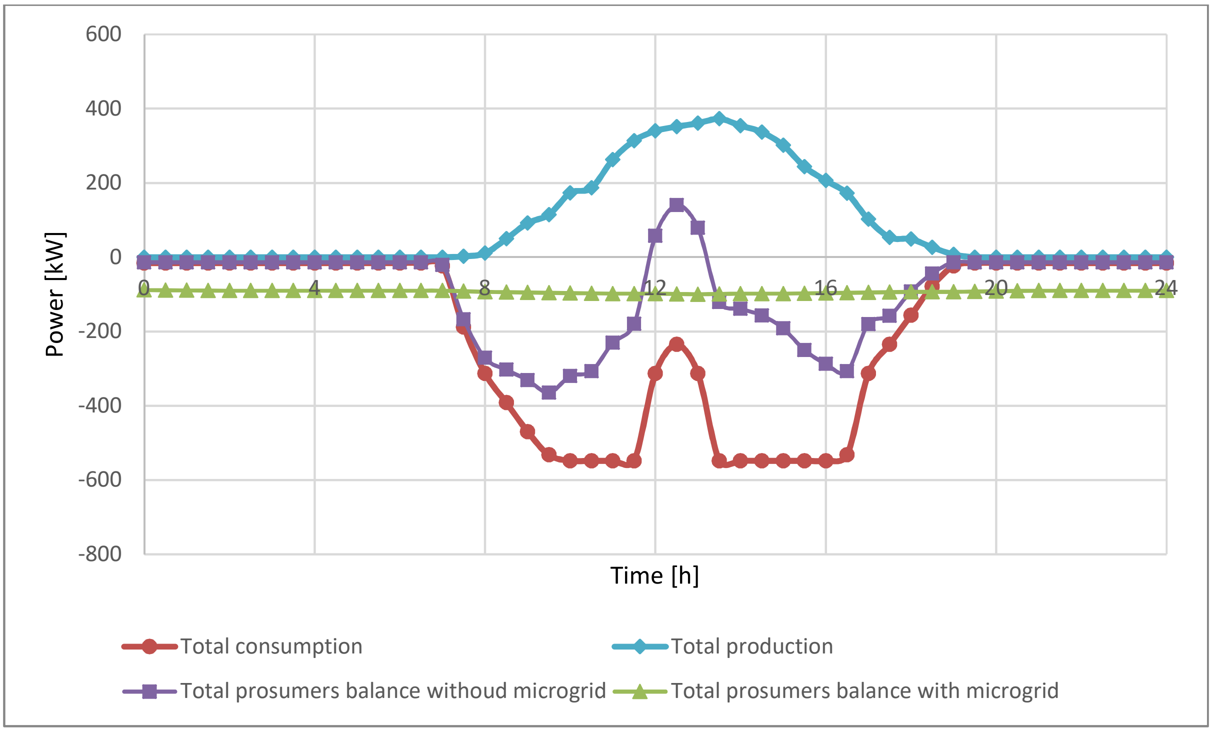

Figure 80 : Scenario 3: Prosumers total power profiles

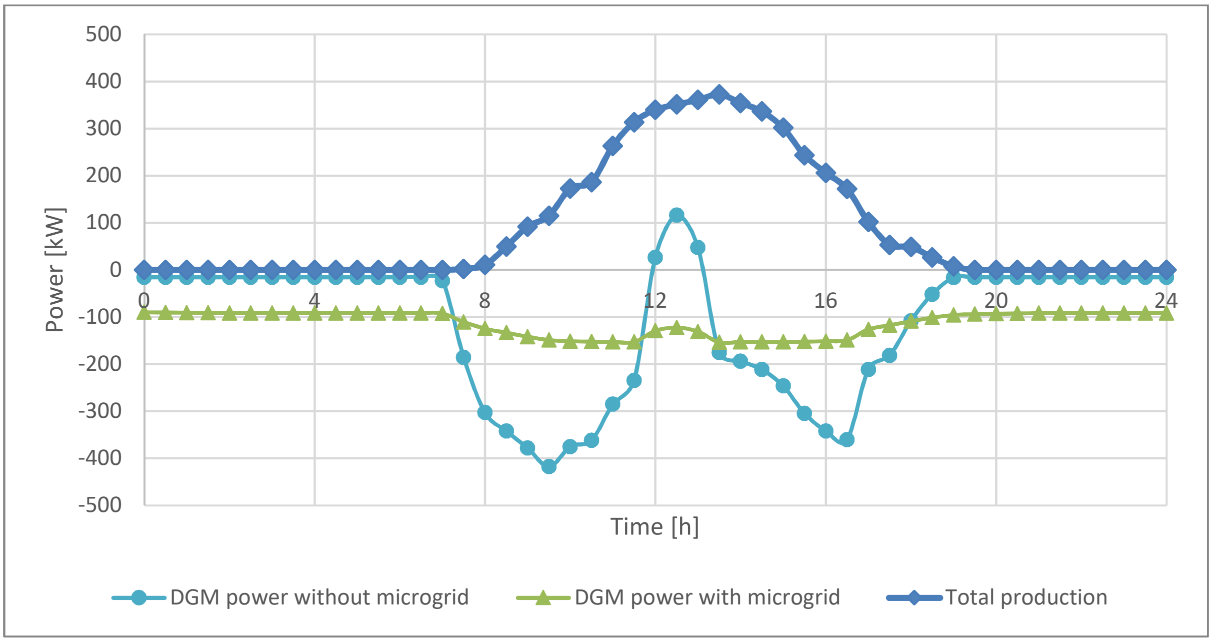

Figure 81 : Scenario 3: DGM power profiles

13.4.4 Results analysis

On Figure 77, it is worth observing that, with only 5% of prosumers (Scenario 1), the DGM will deliver the same power profiles, whether the prosumers have microgrids or not. The only difference is the amount of power: with microgrids, the power is lowered by approximately 12.3kW (526.2 instead of 538.5kW) when the consumption is maximum.

Figure 78 until Figure 81 (Scenario 2 and 3) show that, without microgrids, the DGM must prepare himself to store a part of the energy produced by the prosumers around noon. It is a situation coming from having low consumption and maximum production from 12:00 to 13:00.
With microgrids, this situation is avoided as the EMS will use the produced power to recharge the batteries during that time. In the afternoon, the batteries will be used again to provide power to the consumption elements. This helps the DGM delivering lower amount of power with low power fluctuations.

The results of the DGM power are illustrated and analyzed in detail on Table 13. A value is negative when the DGM must provide power to the clients and positive when the DGM must store it. $percent^{increase}$ gives the percent of increase of the power with microgrids compared to the situation without microgrids.

$$percent^{increase} = \frac{P^{with\ microgrid} - P^{without\ microgrid}}{P^{without\ microgrid}} \cdot 100\ [\%]$$

Table 13 : DGM power of the tested scenarios

	Scenario 1	Scenario 2	Scenario 3
$\frac{n}{N}\,[\%]$	5	60	90
$P_{max}{}^{without\ microgrid}[kW]$	-15.7	-0.66	116.5
$P_{max}{}^{with\ microgrid}[kW]$	-19.8	-65.3	-90.2
$percent^{increase}[\%]$	26.4	$9'797.1$	-177.4
$P_{min}{}^{without\ microgrid}[kW]$	-538.5	-456.0	-417.8
$P_{min}{}^{with\ microgrid}[kW]$	-526.2	-285.3	-153.9
$percent^{increase}[\%]$	-2.28	-37.4	-63.2

Table 13 shows that the impact of microgrids on the DGM power increases with the percent of prosumers ($\frac{n}{N}$). In case of prosumers without microgrids, the maximum power to be provided is reduced at each simulation (from 538.5kW to 456.0kW and then to 417.8kW).
With microgrids, the power demand from the consumer is much lower. If the percent of prosumers is 60%, the power to be delivered par the DGM is reduced by 37.4% (285.3kW instead of 456.0kW) and by 63.2% at $\frac{n}{N} = 90\%$ (153.9kW instead of 417.8kW). This power reduction is translated into a lower supplied energy.

Table 14 : DGM energy

	Scenario 1	Scenario 2	Scenario 3
$\frac{n}{N}[\%]$	5	60	90
$E_{DNM}[kWh]$	$4'855.0$	$3'486.0$	$2'740.0$
Percent of E_{DNM} related to E_{DNM} of Scenario 1 [%]	100	71.8 (-28.2)	56.4 (-43.8)

As the percent of prosumers increases, the DGM energy is reduced. In Scenario 3, only 56.4% of the energy must be supplied to the clients (2'740kW instead of 4'855kWh → -43.6%).

Thanks to microgrids, the power balance of the prosumers is smoothed, i.e. the fluctuation of power ($\frac{\Delta P}{\Delta t}$) is moderate and the consumption looks like a sinusoidal function (Figure 81). On Table 15, $\frac{\Delta P}{\Delta t}$ indicates the DGM power fluctuations for each time step of 30min and is given in $\left[\frac{kW}{30min}\right]$.

Table 15 : DGM power fluctuations

	Scenario 1	Scenario 2	Scenario 3
$\frac{n}{N}[\%]$	5	60	90
$\frac{\Delta P}{\Delta t}_{max}$ $_{without\ microgrid}$ $\left[\frac{kW}{30min}\right]$	236.4	252.3	261.0
$\frac{\Delta P}{\Delta t}_{max}$ $_{with\ microgrid}$ $\left[\frac{kW}{30min}\right]$	223.2	93.96	23.5
$percent^{increase}[\%]$	-5.6	-62.7	-91.0
$\frac{\Delta P}{\Delta t}_{min}\vert^{without\ microgrid}$ $\left[\frac{kW}{30min}\right]$	-234.3	-227.1	-223.2
$\frac{\Delta P}{\Delta t}_{min}\vert^{with\ microgrid}$ $\left[\frac{kW}{30min}\right]$	-223.1	-93.4	-22.7
$percent^{increase}[\%]$	-4.7	-58.9	-89.8

In Scenario 1, the power fluctuation with or without microgrids is pretty much the same (reduction of 5.6 and 4.7% respectively). The higher is the percent of prosumers $\frac{n}{N}$ increases, the more the power fluctuations are reduced. In Scenario 2, $\frac{\Delta P}{\Delta t}$ goes down by approximately 60% and by 90% in Scenario 3. In this situation, the power fluctuation is divided by 10 to 11 times (from about $\pm$240kW/30min to $\pm$22kW/30min).

With the presented results above, it is possible to compare the worst and best situations (Table 16). We consider only the power the DGM must provide to the consumers (negative values).

Table 16 : Best and worst situations for a DGM

Scenario ($\frac{n}{N}[\%]$)	$P_{max}\ [kW\ ]$	$\frac{\Delta P}{\Delta t}_{max}$ $[\frac{kW}{30min}]$	$E_{DNM}[kWh]$
1, without microgrids (5)	538.5	234.3	4'855
3, with microgrids (90)	153.4	23.5	2'740
$percent^{increase}[\%]$	-71.5	-90.0	-43.5

The worst situation is Scenario 1 without microgrid, where the DGM must deliver up to 4'855 kWh of daily energy and a maximum power of 538.5kW, with dynamic power fluctuation reaching 234.3kW/30min.
In contrast, the best situation is Scenario 3 with microgrids ($\frac{n}{N} = 90\%$). The maximum power to be supplied is lower than 155kW with a power fluctuation limited to 23.5kW/30min. The daily provided energy is 2'740 kWh.

13.5 Technical and economic advantages of integrating microgrids in electric networks

With respect to the results presented above, it is worth considering the importance of integrating microgrids in electric networks, especially in the point of view of a distribution network manager. In fact, there are numerous advantages to gain from exploiting microgrids.

13.5.1 Management advantages

First, if customers announce in advance what they will consume from the grid, the DGM has a constant and known cash-flow from it. Based on the forecast consumption, he can build a strategy to supply power to the users depending on the situation.
This will help him managing in advance the elements of production and the reserve according to the amount of power to be supplied to the consumers: which production mean to use; how much power is produced and how much is kept in reserve in case of unexpected consumption. If the consumers respect what they announced within the tolerance ($|\Delta| \leq 1\%$), the DGM can even avoid situations where he must compensate for dynamic power fluctuations. Compared to today, the management budget can be drastically cut down.
With some experiences, the DGM can optimize the use of the whole system. Let's illustrate this with some examples.

- To use the means of electricity production in their optimal operating regime. A better use will lead to reduced maintenance costs.
- There will be less sudden starts/stops of these production means to compensate the unexpected power fluctuation (reduced dead time). The operating time will increase, and the income will be higher.
- To forecast and organize the reparation/maintenance phases, which will improve the flexibility of the grid for possible future improvements.

13.5.2 Secondary producers

Managing an electric grid means providing enough power to the consumers to keep the grid frequency around 50Hz, which is called frequency control. Nowadays, the DGM faces situations where the electricity demand is high, and the power fluctuation could reach unexpected values in very short time (234kW/30min in the simulation), creating difficulties to maintain the grid frequency at an acceptable range.
To achieve this goal, the production means must have the capacity to generate high power values in a short time. Sometimes, the DGM can't produce all what the customers need. Based on a defined list of requirements, the DGM recruit secondary producers, which have enough power reserves to face such situations.
The results of the simulation show that, thanks to microgrids, the management of the electric grid will be simpler and easier as the DGM must provide low power with low power fluctuation (maximum at 24kW/30min in the simulation) already known in advance. We expect that the grid frequency can be

easier to maintain around 50Hz and more secondary producers can be recruited. For the DGM, there will be more competition and more possibilities to choose between the secondary producers, which is translated into reduction of tariffs when buying or renting the power reserves.

Small reserves are needed in case:

- The DGM has to compensate the part of power he can't supply with his own production means
- If a user's consumption deviates from what was announced. The DGM can benefit from this situation as he can apply a penalty on the consumer (higher tariffs, fine …).

Even if the DGM will gain less as the power to be supplied will be lower, he will save money related to the infrastructure of the electric grid.

13.5.3 Costs of the infrastructure

An electric grid is composed from different elements, like transmission cables, converters and rectifiers. The higher the power to be transmitted is, the more expensive these elements are, especially if they are made from copper (like cables).

As microgrids will help reduce electricity demand from the grid and the power fluctuations, the requirements to be fulfilled by the infrastructure of the electric network will also be lower. By choosing components with lower requirements and optimizing the electricity transmission, it is possible to:

- reduce the costs when buying these components
- reduce the dissipated power. This is one way to increase the global efficiency of the grid.

For the DGM, a higher global efficiency is a great advantage as he will produce less power, still provide the same amount of electricity to the customers and increase his benefits.